Fall 12-17-2011

An Experimental Study of Formation of Circulation Patterns in Laminar Unsteady Driven Cavity Flows Using Particle Image Velocimeter (PIV) Techniques

Jon Farkas
University of New Orleans, jfarkas@uno.edu

an Experimental Study of Formation of Circulation Patterns in Laminar unsteady Driven Cavity Flows Using Particle Image Velocimeter (PIV) Techniques

A Thesis

Submitted to the Graduate Faculty of the
University of New Orleans
in partial fulfillment of the
requirements for the degree of

Master of Science
in
Engineering
Mechanical Engineering

by

Jon M. Farkas

B.S., Tulane University, 2004
M.S., University of New Orleans, 2011

December 2011

Acknowledgements

I would also like to highlight the contribution of my major professor Dr. K. Akyuzlu. Without his mentorship and drive, this work would never be completed. Additionally, I would like thank my laboratory mates, Manohar Chidurala and Roberto Alvarado. Manohar's guidance was indispensible and Roberto was paramount to the construction of the test setup.

Nomenclature iv
List of Figures v
List of Tables xi
Abstract xii

1. Introduction 1
2. Literature Survey 3
3. Experimental Setup 5
4. Experimental Procedures 12
    1. PIV Settings 12
    2. Experimental Procedure 13
    3. Lid Velocity Measurements 14
5. Results 16
    1. Results of Experiment 1 17
    2. Case Study of PIV Settings for Experiment 1 44
    3. Parametric Study 90
    4. Error Analysis 110
6. Conclusions 111
7. Recommendations 112

Reference 113
Vita 114

.

Nomenclature

Symbols

ArAspect ratio (h/l)

hheight of cavity

llength of cavity

Lcharacteristic length

ReReynolds number (Re= UL/ ν)

ULid speed

u Velocity component in horizontal (x) direction

vVelocity component in vertical (y) direction

xHorizontal spatial coordinate

yVertical spatial coordinate

Greek Symbol

νKinematic viscosity

List of Figures

Figure 1- Illumination of the Laser onto the Test Cavity. 6

Figure 2- Schematic of Experimental Setup Viewed From Top.....7

Figure 3- Position of Camera in Respect to Test Cavity Viewed from Above.....8

Figure 4- Pictorial View of the Test Section and Rails 9

Figure 5- Experimental Layout Showing Placement of Laser, Camera, Test Setup, and Camcorder.....9

Figure 6- Test Section Viewed From Top. 10

Figure 7- Camera and Laser Placement. 10

Figure 8- Example of Seeded Water Illuminated by the Laser.....11

Figure 9- PIV Seeding Image Experiment 1 Run 4 (Re=1250) at Time t=0.00 Seconds. 18

Figure 10- Global vector map Experiment 1 Run 4 (Re=1250) at Time t=0.00 Seconds.....19

Figure 11- PIV Seeding Image Experiment 1 Run 4 (Re=1250) at Time t=0.34 Seconds. 20

Figure 12- Global Vector Map Experiment 1 Run 4 (Re=1250) at Time t=0.34 Seconds. 21

Figure 13- PIV Seeding Image Experiment 1 Run 4 (Re=1250) at Time t=0.69 Seconds. 22

Figure 14- Global Vector Map Experiment 1 Run 4 (Re=1250) at Time t=0.69 Seconds. 23

Figure 15- Streamlines Experiment 1 Run 4 (Re=1250) at Time t=0.69 seconds. 24

Figure 16- PIV Seeding Image Experiment 1 Run 4 (Re=1250) at Time t=1.03 seconds. 25

Figure 17- Global Vector Map Experiment 1 Run 4 (Re=1250) at Time t=1.03 Seconds. 26

Figure 18- Streamlines Experiment 1 Run 4 (Re=1250) at Time t=1.03 Seconds. 27

Figure 19- PIV Seeding Image Experiment 1 Run 4 (Re=1250) at Time t=1.38 Seconds. 28

Figure 20- Global Vector Map Experiment 1 Run 4 (Re=1250) at Time t=1.38 Seconds. 29

Figure 21- Streamlines Experiment 1 Run 4 (Re=1250) at Time t=1.38 Seconds. 30

Figure 22- PIV Seeding Image Experiment 1 Run 4 (Re=1250) at Time t=1.72 Seconds. 31

Figure 23- Global Vector Map Experiment 1 Run 4 (Re=1250) at Time t=1.72 Seconds. 32

Figure 24- Streamlines Experiment 1 Run 4 (Re=1250) at Time t=1.72 Seconds. 33

Figure 25- PIV Seeding Image Experiment 1 Run 4 (Re=1250) at Time t=2.07 Seconds. 34

Figure 26- Global Vector Map Experiment 1 Run 4 (Re=1250) at Time t=2.07 Seconds. 35

Figure 27- Streamlines Experiment 1 Run 4 (Re=1250) at Time t=2.07 Seconds. 36

Figure 28- PIV Seeding Image Experiment 1 Run 4 (Re=1250) at Time t=2.41s. 37

Figure 29- Global Vector Map Experiment 1 Run 4 (Re=1250) at Time t=2.41 Seconds. 38

Figure 30- Streamlines Experiment 1 Run 4 (Re=1250) at Time t=2.41 Seconds. 39

Figure 31- Velocities (u) Along the y-y Axis (of the Circulation Center) for Experiment 1 Run 4 (Re=1250)....41

Figure 32- Velocities (v) along the x-x Axis (of the Circulation Center) for Experiment 1 Run 4 (Re=1250)....43

Figure 33- Global Vector Map for Experiment 1 Run 1 (Re=1250) at Time 0.69 Seconds. 45

Figure 34- Global Vector Map Experiment 1 Run 2 (Re=1250) at Time 0.69 Seconds. 46

Figure 35- Global Vector Map Experiment 1 Run 3 (Re=1250) at Time 0.69 Seconds. 47

Figure 36- Global Vector Map Experiment 1 Run 4 (Re=1250) at Time 0.69 Seconds Processed Using Direct Correlator. 49

Figure 37- Global Vector Map Experiment 1 Run 4 (Re=1250) at Time 0.69 Seconds Processed Using Fast Fourier Transformation Correlator. 50

Figure 38- Global Vector Map Experiment 1 Run 4 (Re=1250) at Time 0.69 Seconds Processed Using Hart Correlator. 51

Figure 39- Global Vector Map Experiment 1 Run 4 (Re=1250) at Time 0.69 Seconds Processed Using Rectangular Grid. 53

Figure 40- Global Vector Map Experiment 1 Run 4 (Re=1250) at Time 0.69 Seconds Processed Using Recursive Nyquist Grid. 54

Figure 41- Global Vector Map Experiment 1 Run 4 (Re=1250) at Time 0.69 Seconds Processed Using Gaussian Mask. 56

Figure 42- Global Vector Map Experiment 1 Run 4 (Re=1250) at Time 0.69 Seconds Processed Using Zeropad Mask. 57

Figure 43- Global Vector Map Experiment 1 Run 4 (Re=1250) at Time 0.69 Seconds Processed Using Guassian Peak. 59

Figure 44- Global Vector Map Experiment 1 Run 4 (Re=1250) at Time 0.69 Seconds Processed Using Bilinear Peak. 60

Figure 45- Global Vector Map Experiment 1 Run 4 (Re=1250) at Time 0.69 Seconds Processed Using 64 x 64 Pixel Spot Dimensions. 62

Figure 46- Global Vector Map Experiment 1 Run 4 (Re=1250) at Time 0.69 Seconds Processed Using 32 x 32 Pixel Spot Dimensions. 63

Figure 47- Global Vector Map Experiment 1 Run 4 (Re=1250) at Time 0.69 Seconds Processed Using 35% Overlay. 65

Figure 48- Global Vector Map Experiment 1 Run 4 (Re=1250) at Time 0.69 Seconds Processed Using 25% Overlay. 66

Figure 49- Global Vector Map Experiment 1 Run 4 (Re=1250) at Time 0.69 Seconds Processed Using 15% Overlay. 67

Figure 50- Global Vector Map Experiment 1 Run 4 (Re=1250) at Time 0.69 Seconds Processed Using 5% Overlay. 68

Figure 51- Global Vector Map Experiment 1 Run 5 (Re=1250) at Time t=0.00 Seconds. 70

Figure 52- Global Vector Map Experiment 1 Run 5 (Re=1250) at Time t=0.138 Seconds. 71

Figure 53- Global Vector Map Experiment 1 Run 5 (Re=1250) at Time t=0.276 Seconds. 72

Figure 54- Global Vector Map Experiment 1 Run 5 (Re=1250) at Time t=0.414 Seconds.. 73

Figure 55- Global Vector Map Experiment 1 Run 5 (Re=1250) at Time t=0.552s Seconds. 74

Figure 56- Global Vector Map Experiment 1 Run 5 (Re=1250) at Time t=0.690 Seconds. 75

Figure 57- Global Vector Map Experiment 1 Run 5 (Re=1250) at Time t=0.828 Seconds. 76

Figure 58- Global Vector Map Experiment 1 Run 5 (Re=1250) at Time t=0.996 Seconds. 77

Figure 59- Global Vector Map Experiment 1 Run 5 (Re=1250) at Time t=1.104 Seconds. 78

Figure 60- Global Vector Map Experiment 1 Run 5 (Re=1250) at Time t=1.242 Seconds. 79

Figure 61- Global Vector Map Experiment 1 Run 5 (Re=1250) at Time t=1.380 Seconds. 80

Figure 62- Global Vector Map Experiment 1 Run 5 (Re=1250) at Time t=1.518 Seconds. 81

Figure 63- Global Vector Map Experiment 1 Run 5 (Re=1250) at Time t=1.656 Seconds. 82

Figure 64- Global Vector Map Experiment 1 Run 5 (Re=1250) at Time t=1.794 Seconds. 83

Figure 65- Global Vector Map Experiment 1 Run 5 (Re=1250) at Time t=1.932 Seconds. 84

Figure 66- Global Vector Map Experiment 1 Run 5 (Re=1250) at Time t=2.070 Seconds. 85

Figure 67- Global Vector Map Experiment 1 Run 5 (Re=1250) at Time t=2.208 Seconds. 86

Figure 68- Global Vector Map Experiment 1 Run 5 (Re=1250) at Time t=2.346 Seconds. 87

Figure 69- Global Vector Map Experiment 1 Run 5 (Re=1250) at Time t=2.484 Seconds. 88

Figure 70- Global Vector Map Experiment 1 Run 5 (Re=1250) at Time t=2.622 Seconds. 89

Figure 71- Global Vector Map Experiment 2 Run 3 (Re=2530) at Time t=0.00 Seconds. 91

Figure 72- Global Vector Map Experiment 2 Run 3 (Re=2530) at Time t=0.34 Seconds. 92

Figure 73- Global Vector Map Experiment 2 Run 3 (Re=2530) at Time t=0.69 Seconds. 93

Figure 74- Global Vector Map Experiment 2 Run 3 (Re=2530) at Time t=1.03 Seconds. 94

Figure 75- Global Vector Map Experiment 2 Run 3 (Re=2530) at Time t=1.38 Seconds. 95

Figure 76- Global Vector Map Experiment 2 Run 3 (Re=2530) at Time t=1.72 Seconds. 96

Figure 77- Global Vector Map Experiment 2 Run 3 (Re=2530) at Time t=2.07 Seconds. 97

Figure 78- Global Vector Map Experiment 2 Run 3 (Re=2530) at Time t=2.41 Seconds. 98

Figure 79- Global Vector Map Experiment 3 Run 4 (Re=3030) at Time t=0 Seconds. 99

Figure 80- Global Vector Map Experiment 3 Run 4 (Re=3030) at Time t=0.34 Seconds. 100

Figure 81- Global Vector Map Experiment 3 Run 4 (Re=3030) at Time t=0.69 Seconds. 101

Figure 82- Global Vector Map Experiment 3 Run 4 (Re=3030) at Time t=1.03 Seconds. 102

Figure 83- Global Vector Map Experiment 3 Run 4 (Re=3030) at Time t=1.38 Seconds. 103

Figure 84- Global Vector Map Experiment 3 Run 4 (Re=3030) at Time t=1.72 Seconds. 104

Figure 85- Global Vector Map Experiment 3 Run 4 (Re=3030) at Time t=2.07 Seconds. 105

Figure 86- Global Vector Map Experiment 3 Run 4 (Re=3030) at Time t=2.41 Seconds 106

Figure 87- Circulation Center in Relation to Cavity Location. 109

List of Tables

Table 1- Experimental Matrix Showing Lid Velocities and Reynolds Numbers 16

Table 2- Velocities (u) Along the y-y Axis (of the Circulation Center) for Experiment 1 Run 4 (Re=1250).....40

Table 3- Velocities (v) Along the x-x Axis (of the Circulation Center) for Experiment 1 Run 4 (Re=1250).....42

Table 4- Circulation Diameter 107

Table 5- Circulation Center in Relation to Cavity Location by Time. 108

Abstract

An experimental study is conducted to determine the velocity fields, from development to steady state, in a square enclosure due to movement of a constant velocity lid using Particle Image Velocitmetry (PIV). Experiments were conducted with water, seeded with hollow glass sphere particles 10 microns in diameter, at three different lid velocities leading to Reynolds numbers in the high laminar to transitional range. The test cavity is 1 inch (25.4mm) high by 1 inch (25.4 mm) wide leading to an aspect ratio of 1.0. The depth is taken to be 5 (127mm) inches to reduce the three dimensional effects. Readings are taken from development to steady state allowing for a full spectrum of flow characteristics. PIV technique is successful in capturing the development of driven cavity flow. Circulation is shown to increase strength with time and Reynolds number. PIV capture and processing settings are determined.

Keywords: Driven Cavity Flow, Particle Image Velocimeter (PIV)

Chapter 1

Introduction

Driven cavity flow, also known as lid driven flow, is a classic problem often used in the benchmarking of computational codes. The problem contains a simple set up, a cavity with three stationary sides is filled with a fluid. Motion is induced by the movement of the fourth boundary often the top boundary or lid. The parameter governing flow region classification is the Reynolds number, Re, defined as the lid velocity U, multiplied by the characteristic length L, and divided by the kinematic viscosity ν; or $Re = UL/\nu$. In addition to its use as a comparison to numerical codes the driven cavity flow problem also has industrial applications. It can be used to model and study industrial applications including coaters used to produce paper and film melt spinning processes used to manufacture microcrystalline material [1] and continuous drying [2]. Driven cavity flow even has applications to nature such as modeling sediment bed impurities suggested by Malkus[3]. A comprehensive literature survey is presented in Chapter 2.

The objective of the thesis is to use Particle Imaging Velocimetry (PIV) to provide global velocity readings of driven cavity flow from start up development to steady state. An experimental setup is built containing a cavity and moving lid. Three experiments are conducted and velocity readings are taken using a 2-D PIV system. This work is acting as a bridge between the previous work of the University of New Orleans Cryogenics laboratory in making PIV readings of natural convection flows and future work planned for readings of mixed convection.

The experimental setup is presented in Chapter 3. The test cavity is described in terms of material used and dimensions. The lid is presented as well as the movement driving elements used. Finally, the placement of the PIV system is detailed in text and schematically.

Chapter 4 provides a more in-depth discussion of the experimental procedures. The PIV laser and capture settings are listed as well. The experimental procedures are listed step by step, and calculations of the lid velocity are explained.

Results are presented in Chapter 5. First a case study of the lowest Reynolds number experiment is presented. PIV capture and processing settings are investigated and chosen parameters are justified. Next the experiment is repeated at a higher frame rate, showing more detail of the flow formation. Finally, the results of the parametric study of flows at two higher Reynolds numbers are given. Conclusions are drawn in Chapter 6, and recommendations are made in Chapter 7.

Chapter 2

Literature Survey

Previous work published can be split into two classifications: experimental work and computational work. The majority of work published focuses on computation methods used to model driven cavity flow. Experimental work published includes steady state PIV and LDA readings, but flow development is not published. An overview of the fluid mechanics involved in driven cavity flow is given by Shankar and Deshpande [4]. Also presented in the paper is a brief overview of published experimental and computational work for 2 and 3 dimensional flows.

Few experimental studies of driven cavity flow have been published in literature. Among the first was Koseff and Street 1984, who used laser-Doppler-anemometer for velocity measurements for a cavity of aspect ratio 1[5]. They expanded upon this work to study end wall effects for aspect ratios 1, 2, and 3 using the same technique at Reynolds numbers 1000-10,000. A significant finding of their work is that at Reynolds numbers greater than 3000 the flow becomes unsteady[6]. Migeon uses particle streak technique to study the development of Taylor-Gortler-like vortices inside a square lid driven cavity in the laminar region [7]. In this experiment a vertical wall acted as the driven lid. PIV is used by Liberzon to study the effects of dilute polymers, ethylene oxide, in a driven cavity at turbulent flows [8]. The use of PIV and LDA to investigate a similar experiment, shear driven flow, is publish by O'Hern et al. in 1994 [9]. Here water is driven across the top of a square water filled cavity in order to induce motion by shear forces. The Reynolds numbers investigated are between 100 and 900. Velocity readings are

shown to be in agreement between PIV and LDA readings through most of the data, but poor near walls.

Computational work is more abundant in literature. The pioneering work is published by Ghia et al. in 1982 [10]. A coupled strongly implicit multigrid method with a uniform mesh is used to solve the Navier- Stokes equations for driven cavity flow at Reynolds numbers ranging from 1000-10,000 with a working fluid of air. This work is considered the benchmark computational publication. Erturk and Gokcol published steady 2-D simulations of incompressible driven cavity flow at high Reynolds numbers up to 21,000 are carried out using a fine mesh finite volume solver [11]. Barragy and Carey use a p-type finite element scheme to compute a stream-vorticity function solution for steady incompressible flow for Reynolds numbers up to 12,500 [12]. Additionally, Sahin and Owens use an implicit cell-vertex finite volume method coupled with the elimination of the pressure term from the momentum equation to compute both steady and unsteady solutions to the lid driven cavity for Reynolds numbers up to 10,000 for incompressible flows [13].

Chapter 3

Experimental Setup

An overview of the experimental setup is given describing the test cavity, lid, rail system, and PIV placement. A test cavity is made from Plexiglas in the dimensions of 1 inch high (25.4 mm) by 1 inch wide (25.4 mm) resulting in an aspect ratio, Ar=1.0. The length of the test section is 5 inches (127mm) to decrease the three-dimensional effect of the walls on the two dimensional flow patterns that are expected in the type of arrangement. The test cavity is elevated by two 10 inch (254 mm) Plexiglas feet. The arrangement can be seen in Figure 1. A lid of dimensions 36 inches (914.4mm) long by 5 inch (127 mm) wide, 0.25 inch (6.4 mm) thick sits on a rail system attaching to the fore and aft section of the test section. The lid is driven by a hanging mass and pulley system, allowing it to move at a constant velocity. The cavity is filled with deionized water at room temperature which has been seeded with silver-coated hollow glass spheres of average diameter of 10 μm and a density of 1300 kg/m^3

Readings are made using a 2-D PIV system manufactured by TSI. The system consists of a Solo XT dual cavity 532 nm wavelength Nd:Yag laser with a 500mm lens manufactured by New Wave, Inc., a 2048 x 2048 pixel high sensitivity CCD camera model 630059 Powerview manufactured by TSI with a 105mm lens, a TSI model 610035 LaserPulse Synchronizer, and a PC with TSI Insight 3g software for analysis. The laser is positioned normal to the test cavity length so that the beam passes through a masking slit in the support leg. It then contacts a mirror at a 45^o angle shifting the beam to pass vertically. The beam travels through a second masking filter in order to restrict the laser thickness, and finally illuminates the test section roughly in the center with respect to cavity length. This layout is shown in Figure 1. The camera is positioned

normal to the test section face and is placed at a distance where the illuminated cavity section is the focal point. Finally, the area around the face of the test section is masked to reduce reflections. The experimental setup is shown schematically in Figures 2 and 3.

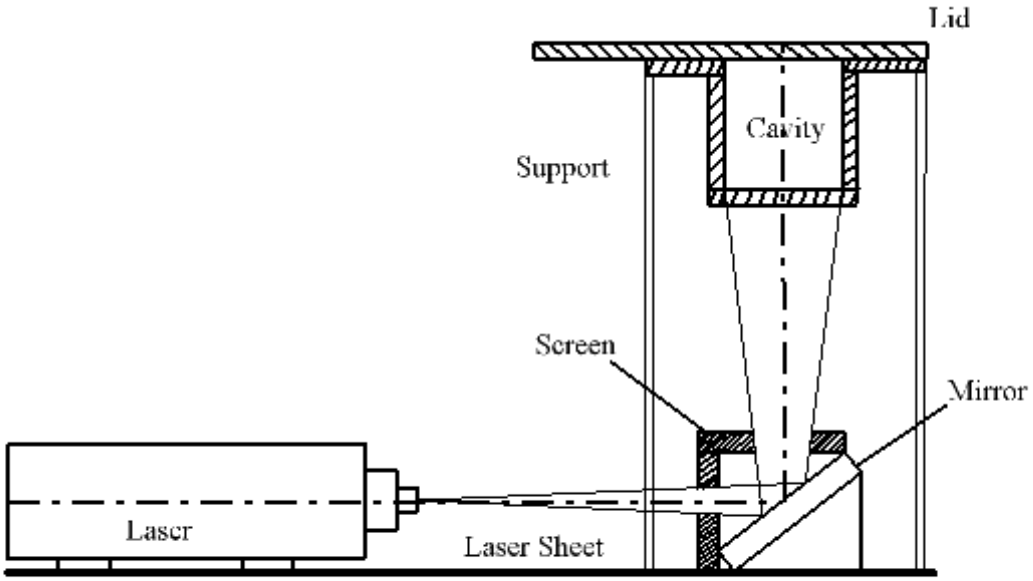

Figure 1- Illumination of the Laser onto the Test Cavity.

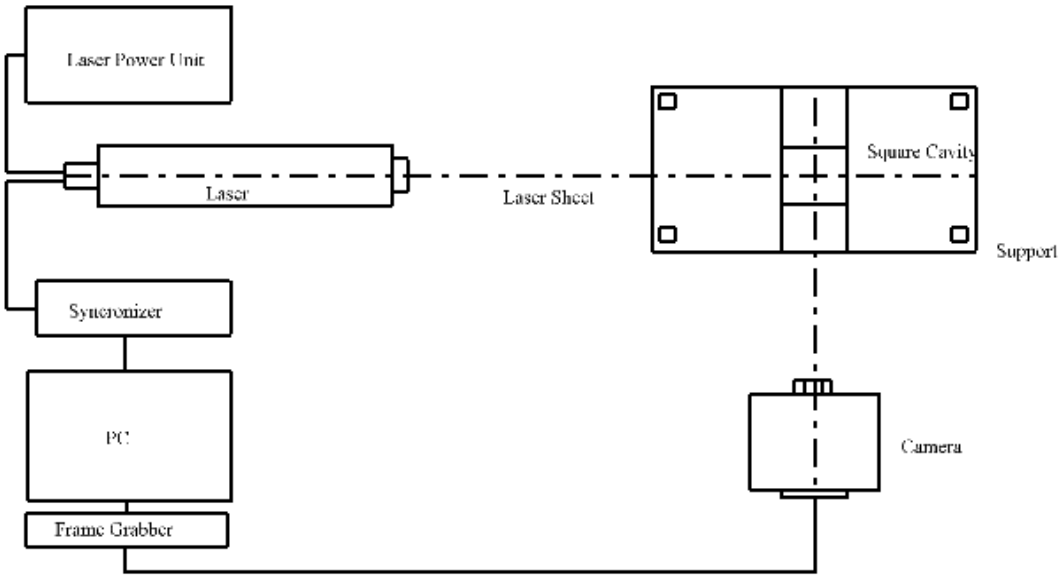

Figure 2- Schematic of Experimental Setup Viewed From Top.

.

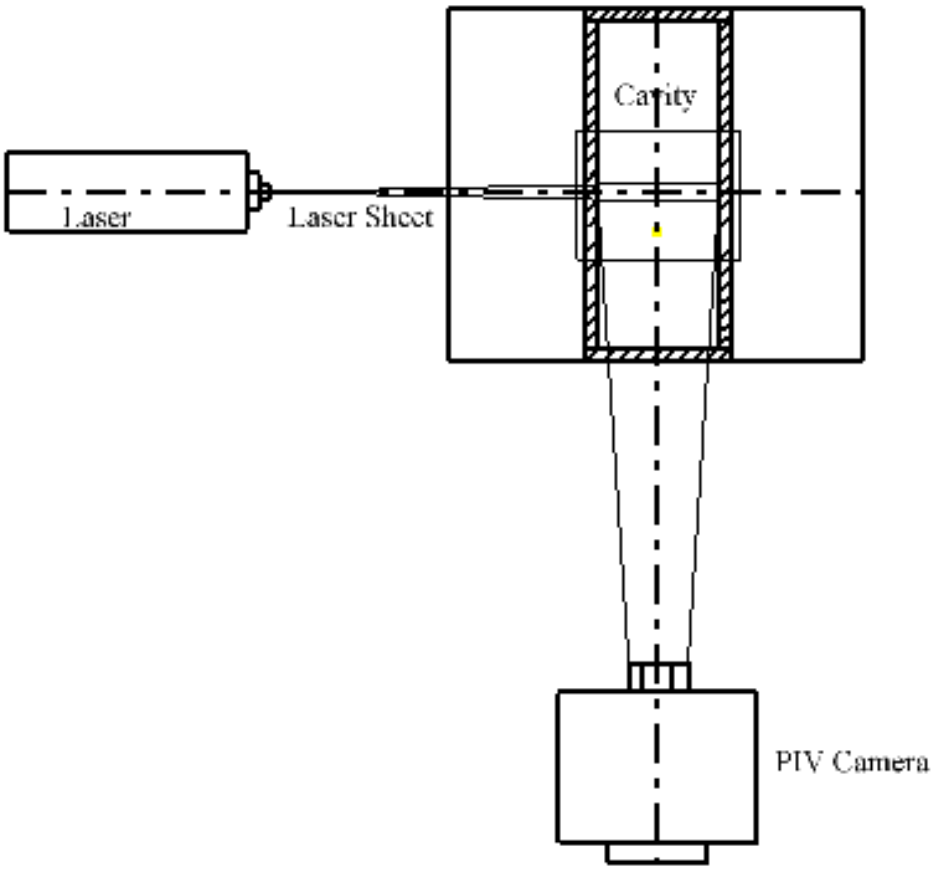

Figure 3- Position of Camera in Respect to Test Cavity Viewed from Above.

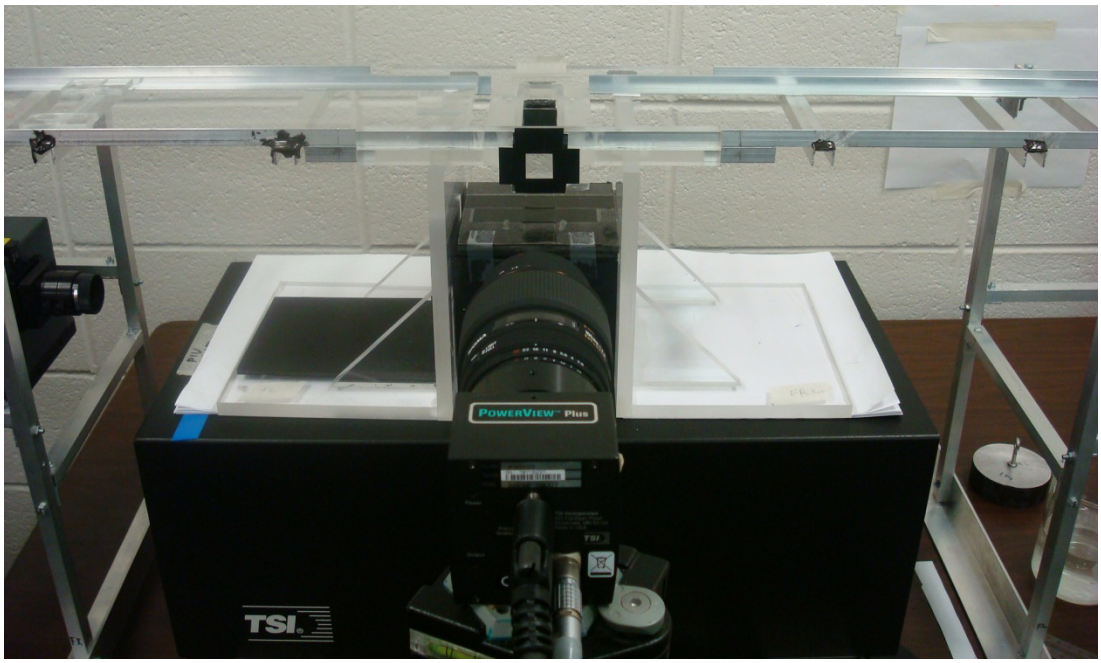

Figure 4- Pictorial View of the Test Section and Rails.

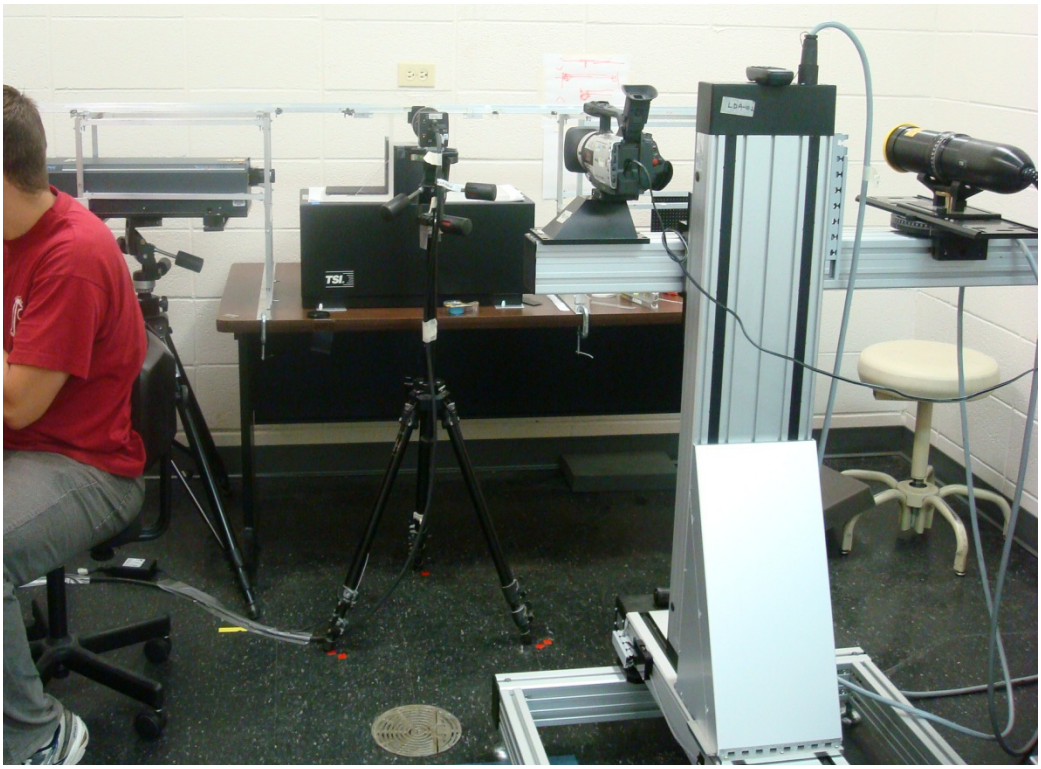

Figure 5- Experimental Layout Showing Placement of Laser, Camera, Test Setup, and Camcorder.

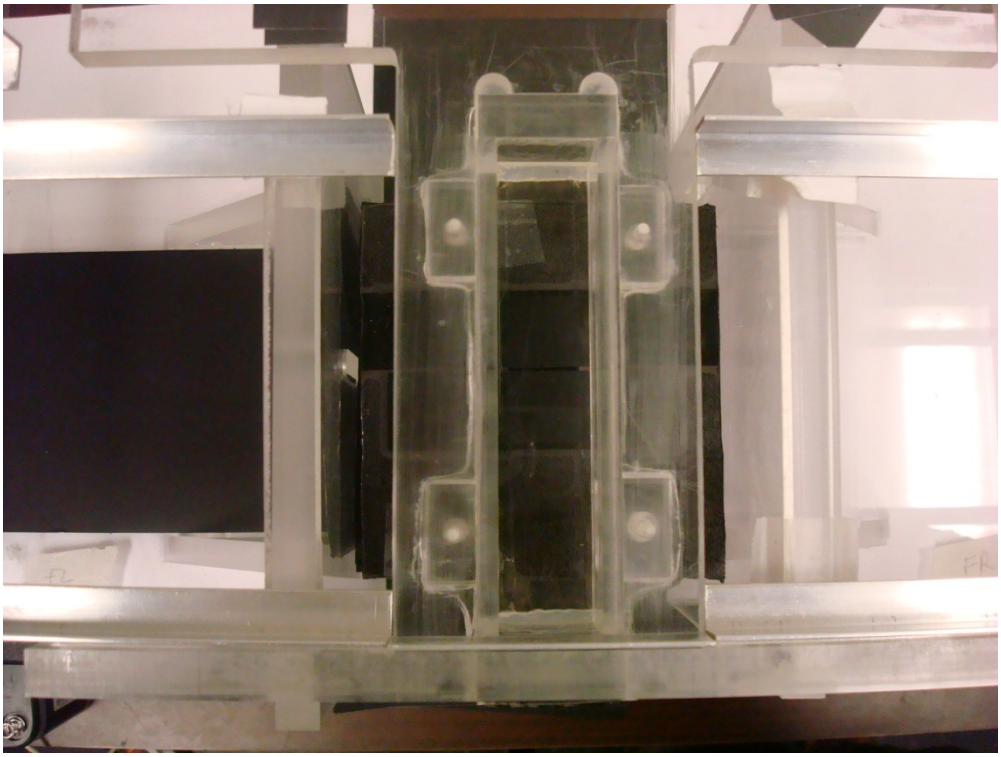

Figure 6- Test Section Viewed From Top.

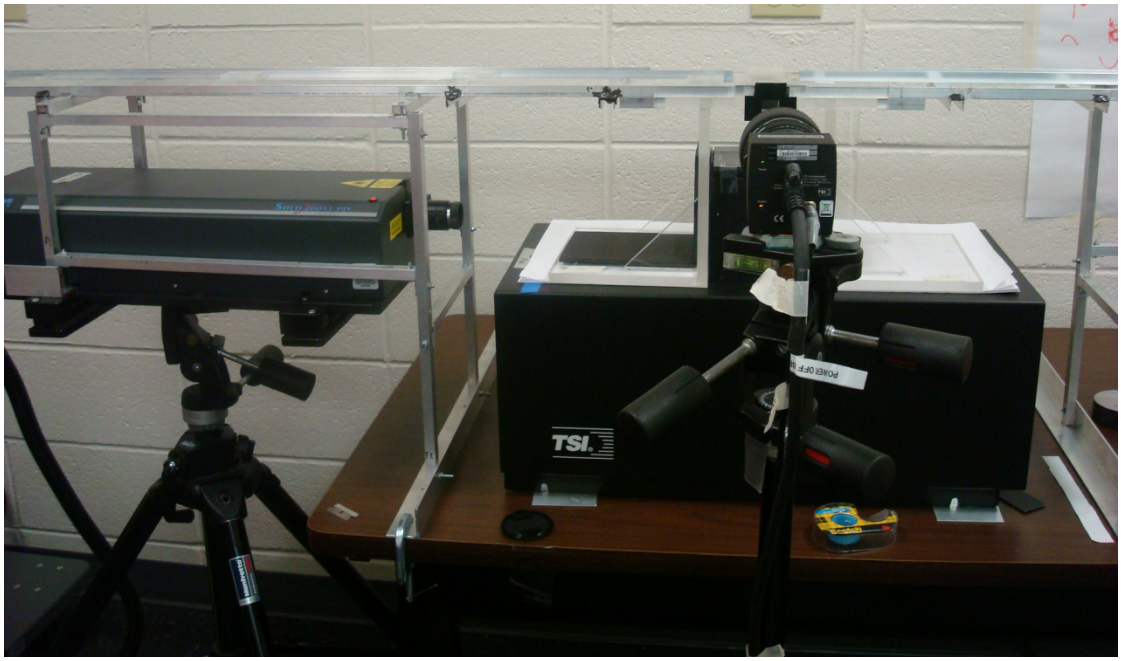

Figure 7- Camera and Laser Placement.

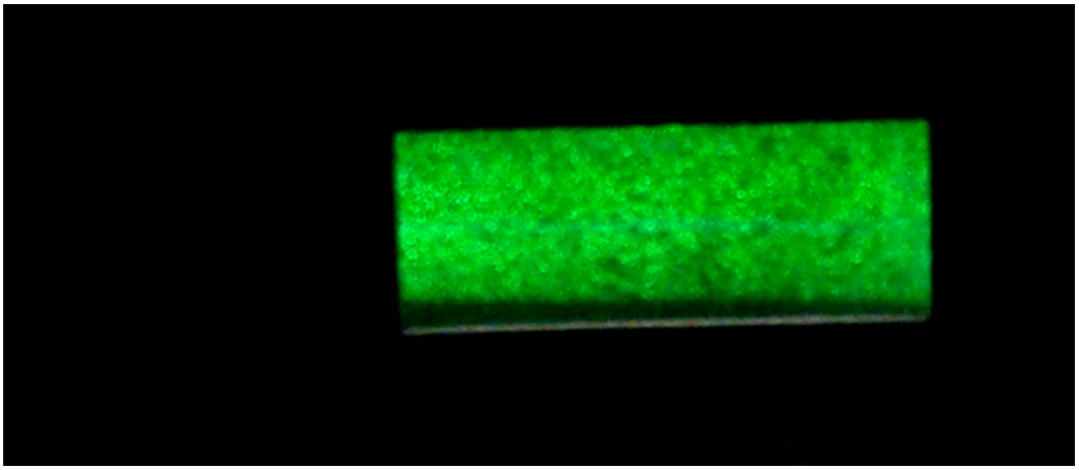

Figure 8- Example of Seeded Water Illuminated by the Laser.

Chapter 4

Experimental Procedures

The procedure of running the experiment is important to ensure that the experiments are able to be repeated. In section 4.1 the settings of the PIV system are described. In section 4.2 the procedures for running the experiment are listed. In section 4.3 the procedures for determining the lid velocity are explained.

4.1 PIV Settings

Capturing usable readings is governed by many options in the PIV system. The justification for chosen parameters is shown in Chapter 6, here the parameter values are stated. As stated in Chapter 3 the PIV system is composed of a laser emitting a thin laser sheet illuminating the flow being studied, a high sensitivity CCD and a PC with Insight 3G software to govern the capture settings and image processing. For the experiments the laser is set to high power and an energy level of 90 (units are not given) at the laser power unit. The laser is also set to be triggered by the synchronizer. Within the Insight 3G software the laser energy is set to 200 for laser A and 195 for laser B (units not given). Furthermore the laser beam passes through a mask on the cavity support and a second mask on top of the mirror in order to reduce the laser width to a very thin sheet.The image capture settings are set to straddle image, giving dual framed images, a delta t, the time separating laser pulses, at 1800 μs, with a camera exposure time of 2000 μs. The frame rate of the camera is set to 2.90 hz. The images capture mode is set to synchronized, meaning the captures and laser pulsing will be governed and synchronized by the synchronizer, and sequence, meaning a sequence of images will be taken. The number of captures in the sequence is varied according to lid speed so extraneous images are not captured after the lid has stopped moving. After capturing the experiment, the frames are masked to remove image areas

not of interest to the flow. The images are then processed with the software using a Hart's correlation, a Nyquist Grid, and a Guassian Peak engine. The images are processed with an interrogation area of 64 x 64 pixels and an overlay of 15%, these values are justified in Chapter 6. These values can be elaborated on in the Insight operations manual [14]. Additional Post-processing though present as a software option is not applied to the images.

4.2 Experimental Procedure

1. Power on PC, synchronizer and laser. Remove camera lens cover, open laser shutter cover.

2. Open Insight software, set capture settings to those listed in section 4.1.

3. Focus camera to area of laser light plane.

4. Place a ruler in the cavity at the section of laser light plane. Capture image and use for spatial calibration.

5. Position lid so the front edge is approximately 3 cm past the aft edge of the test cavity. Using construction paper for clearance, align lid to the front rail. While holding lid, hang fore and aft masses on pulleys.

6. Through small hole in lid, fill test cavity with seeded water until water is touching lid without any air pockets.

7. Begin PIV capture by pressing "capture" in Insight software. Release lid. When capture is completed save images.

8. Mask images in software so only cavity is processed.

9. Process images.

The lid is started from a zero velocity and is quickly accelerated to a constant velocity. The lid is positioned so its front edge is approximately 3 cm past the aft edge of the test cavity. Water with seeding is added to the cavity until it is touching the lid. On the fore end of the lid a counterweight is suspended from a pulley at the end of the rail system. At the aft end masses of higher weight are suspended from a pulley at the end of the rail system. The lid is moved by allowing the aft masses to fall free pulling the lid forward. Movement is stopped before the lid completely passes the cavity.

4.2 Measuring Lid Velocity

1. Attach ruler to rail just aft of test section.

2. Affix marker flags to lid.

3. Position lid so the front edge is approximately 3 cm past the aft edge of the test cavity. Using construction paper for clearance, align lid to the front rail. While holding lid, hang fore and aft masses on pulleys.

4. Through small hole in lid, fill test cavity with seeded water until water is touching lid without any air pockets.

5. Release lid.

6. Using a 32 bit camcorder, focused on the ruler, record experiment.

7. Analyze playback frame by frame. Find when marker flag enters and passes ruler. Use the camcorders time stamp to determine time.

8. Knowing the time and the distance the marker flag traveled determine velocity by divided distance by time.

The lid velocity is determined by attaching a ruler next to the aft section of the test cavity on the rail. Marker flags are affixed to the lid; the experiments are ran without taking PIV measurements and recorded with a 32 bit camera recorder. The playback is then analyzed to see where the marker flag enters and leaves the ruler and the corresponding time stamp for the frames is noted and used to measure velocities with a simple distance divided by time calculation.

Chapter 5

Results

The results are presented for the three experiments as shown in the experimental matrix Table 1. In section 5.1 of the results presents a case study of speed Experiment 1 (Re= 1250), section 5.2 investigates how PIV timing settings and processing settings were determined to yield optimal results. The experiment is then repeated with a larger frame rate in order to show greater detail of the unsteady formation of the driven cavity flow. In section 5.3 of the results of the parametric study for Experiments 2 (Re=2530) and Experiment 3 (Re=3030) are presented and properties of the circulation are given.

Table 1- Experimental Matrix Showing Lid Velocities and Reynolds Numbers

Experiment	Lid Velocity, U (m/s)	Reynolds Number, Re	Run Number	Delta t, Δt (s)	Capture Rate (hz)
1	0.05	1250	1	0.0060	2.90
			2	0.0050	2.90
			3	0.0018	2.90
			4	0.0018	2.90
			5	0.0018	7.25
2	0.10	2530	1	0.0018	2.90
			2	0.0018	2.90
			3	0.0018	2.90
			4	0.0018	2.90
3	0.12	3030	1	0.0018	2.90
			2	0.0018	2.90
			3	0.0018	2.90
			4	0.0018	2.90

5.1 Experiment 1 Run 4 (Re=1250)

The results of Experiment 1 Run 4 (Re=1250) are presented in Figures 9-30 below. The experiments are captured with a delta t of 1800 μs and processed with the following settings: Harts correlation, no mask, Gaussian Peak, Nyquist grid, an interrogation area of 64 x 64, and an overlay of 15 %. PIV images are shown, followed by the global velocity vector plot, and finally streamlines for the time step (streamlines are not given for time steps t=0.00 seconds or t=0.34 seconds). The centerline velocities at steady state are then given for the horizontal and vertical axises in Figures 31-32. The justification of these settings is shown section 5.2 as well as a repetition of the experiment at a higher frame rate.

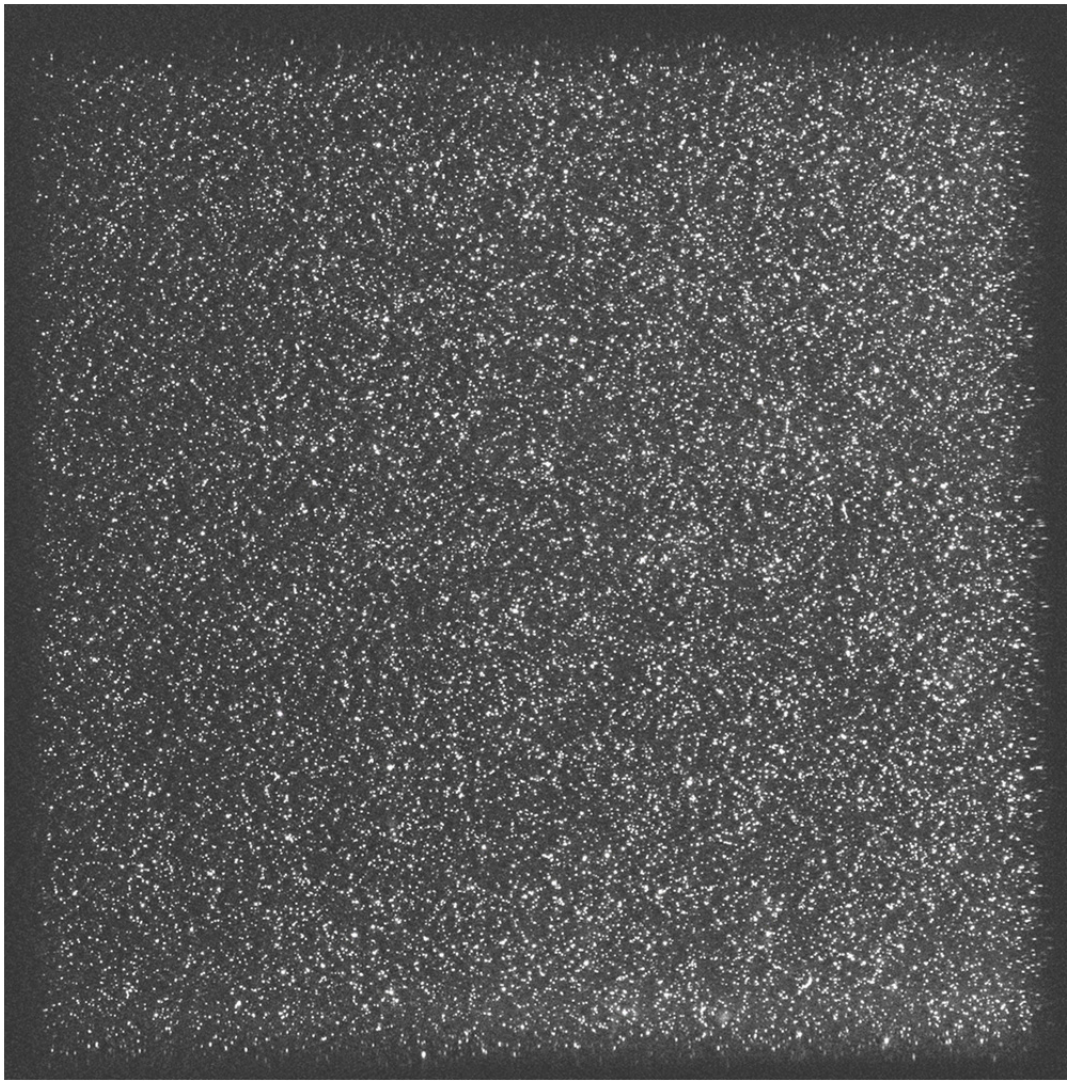

Figure 9- PIV Seeding Image Experiment 1 Run 4 (Re=1250) at Time t=0.00 Seconds.

Uniform seeding is seen in Figure 9 as no lid motion has occurred.

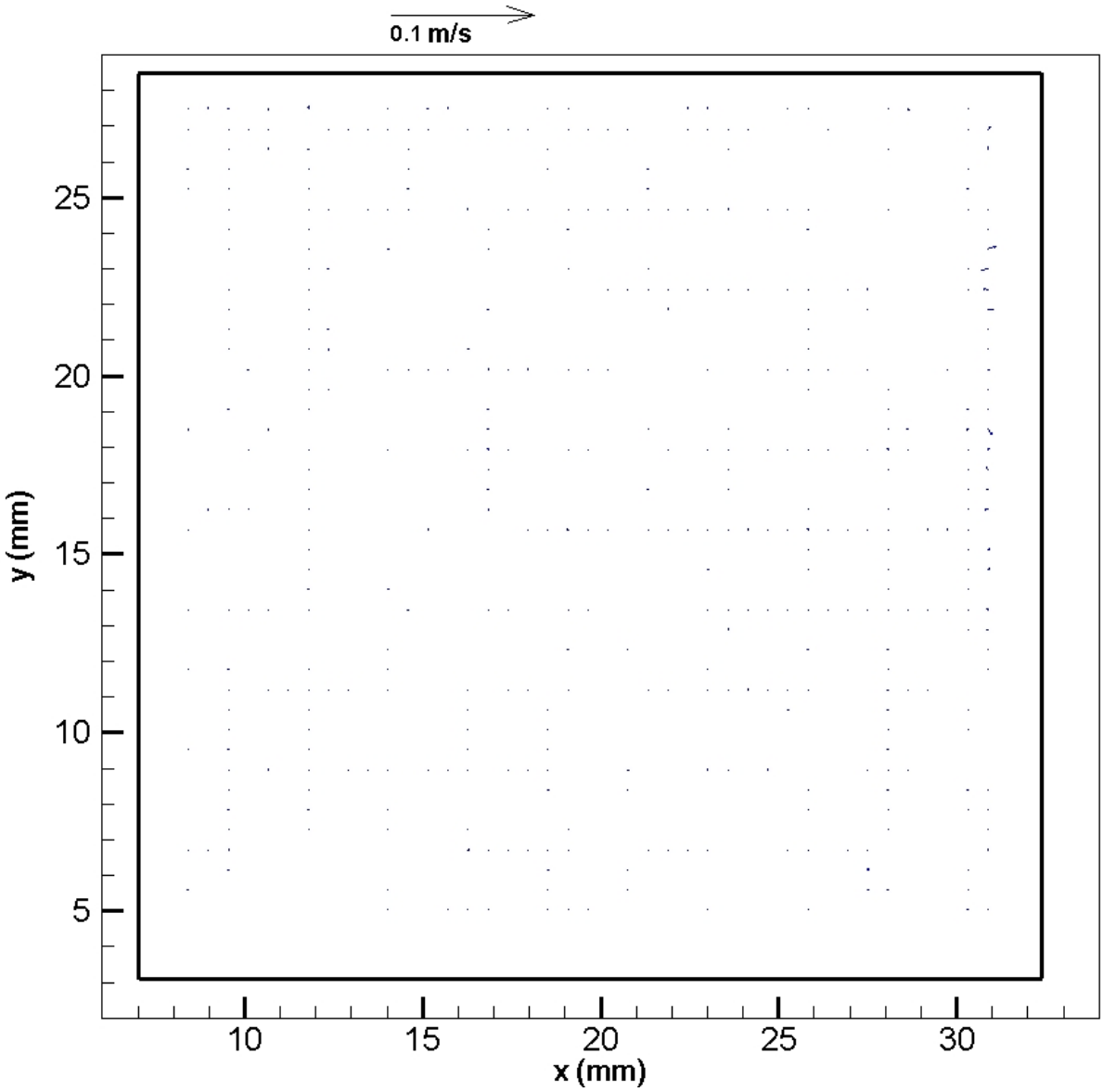

Figure 10- Global vector map Experiment 1 Run 4 (Re=1250) at Time t=0.00 Seconds.

As expected no velocity vectors are seen in Fig. 10 as lid motion has not occurred.

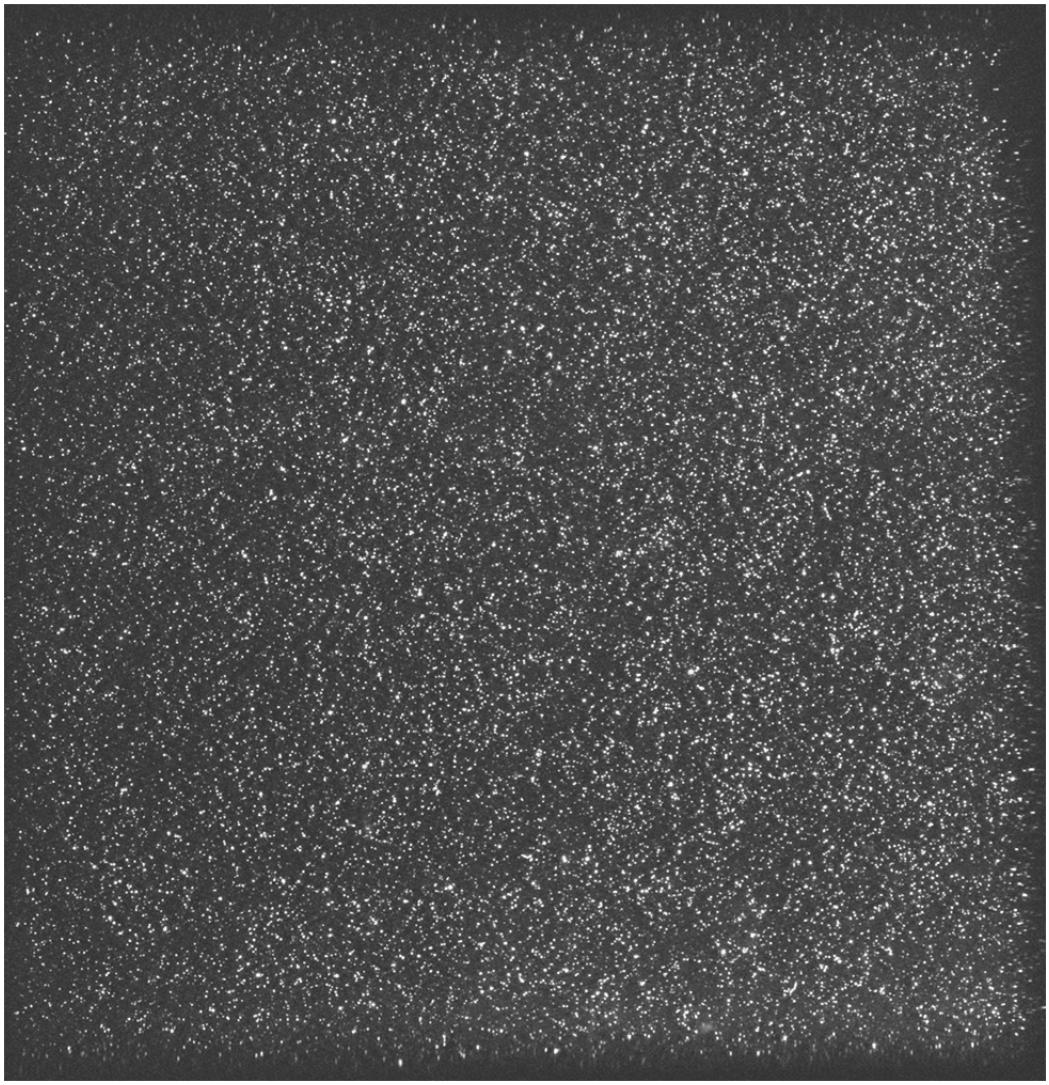

Figure 11- PIV Seeding Image Experiment 1 Run 4 (Re=1250) at Time t=0.34 Seconds.

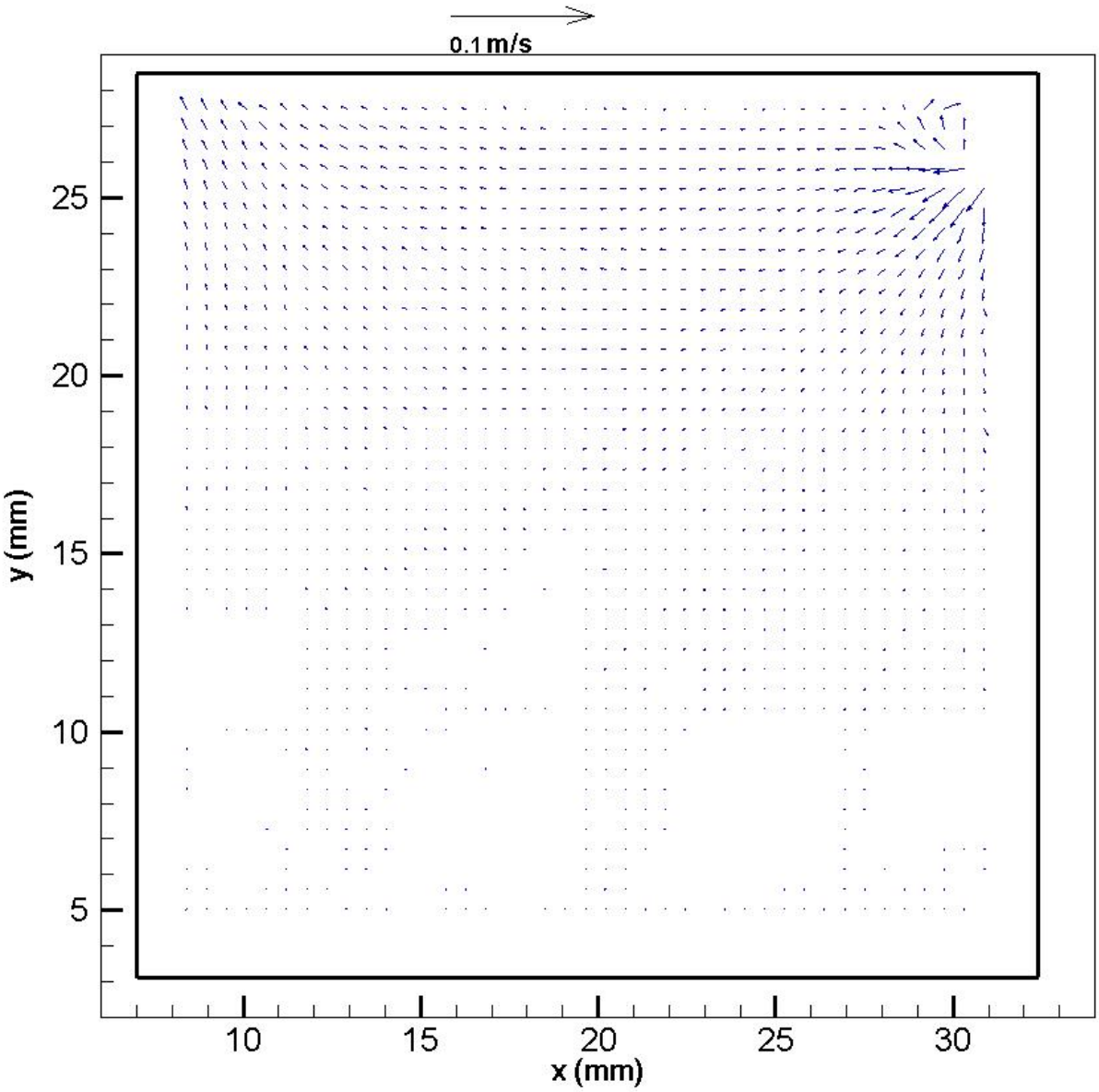

Figure 12- Global Vector Map Experiment 1 Run 4 (Re=1250) at Time t=0.34 Seconds.

In Fig. 12 motion has begun, the circulation is starting to develop at the upper right, downstream lid, of the cell.

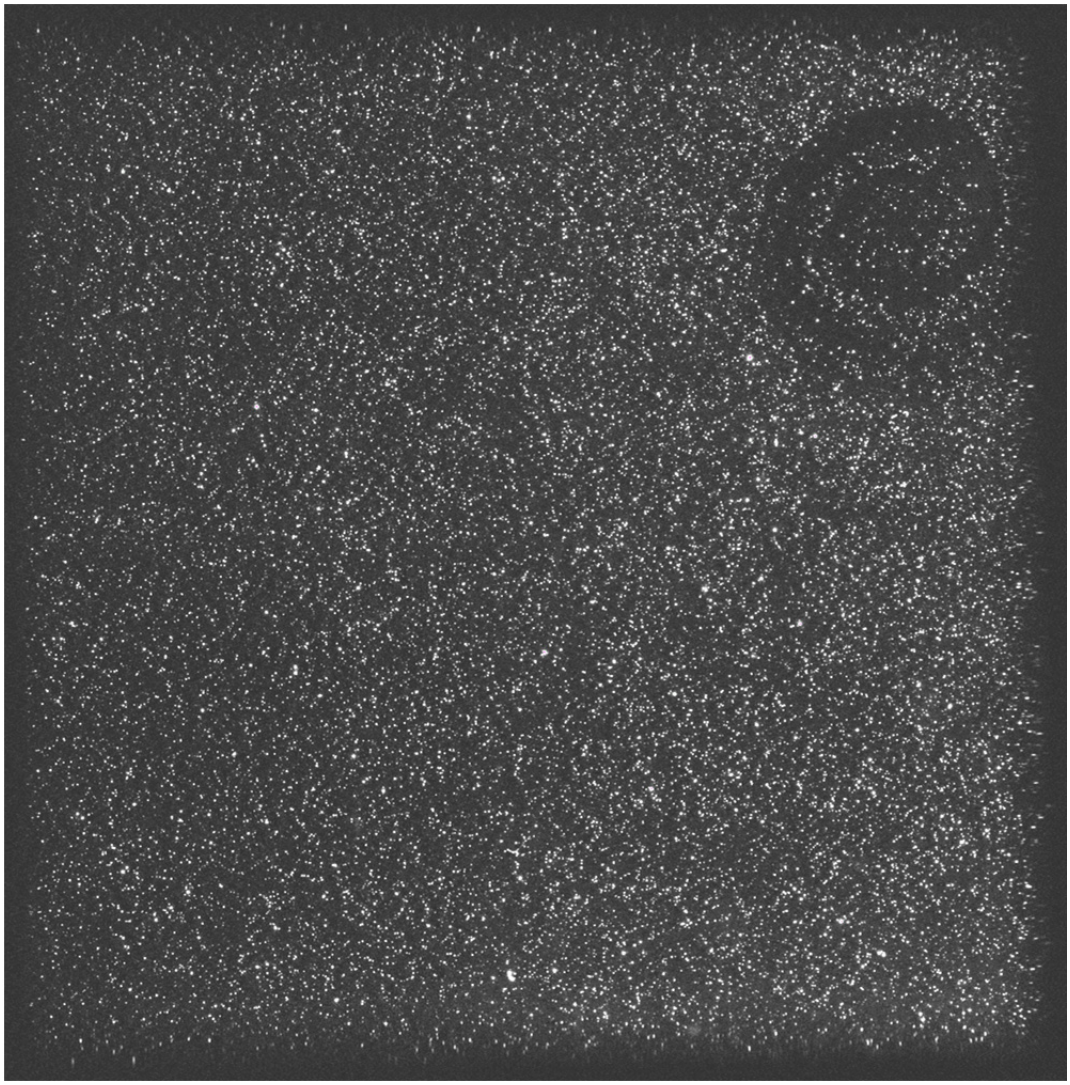

Figure 13- PIV Seeding Image Experiment 1 Run 4 (Re=1250) at Time t=0.69 Seconds.

In Fig. 13. the circulation at the top right of the cell becomes apparent visually as the seeding material is displaced by lid motion.

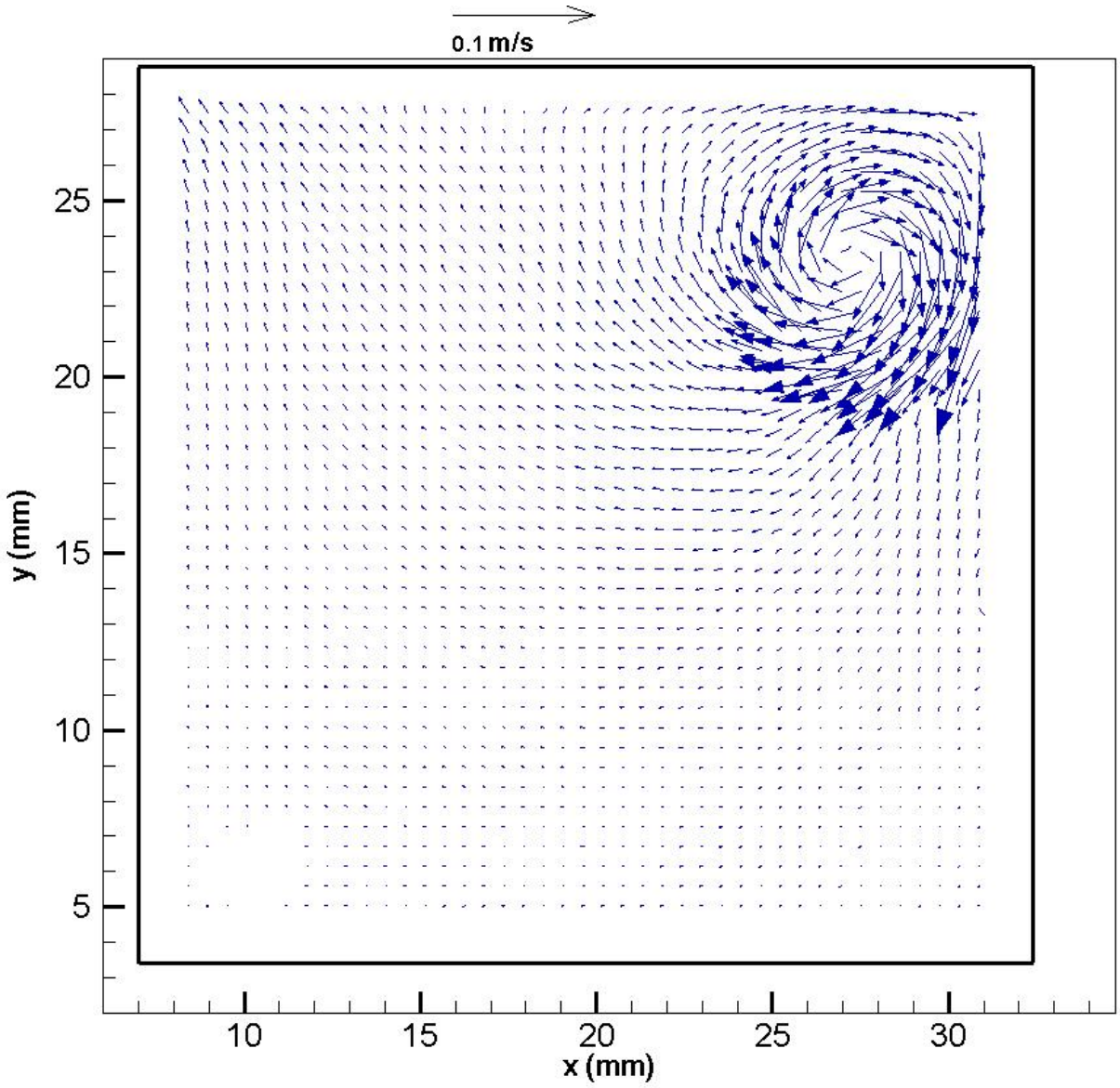

Figure 14- Global Vector Map Experiment 1 Run 4 (Re=1250) at Time t=0.69 Seconds.

As expected the circulation strength has increased in Fig. 14. The center of circulation has also moved diagonally toward the center of the cell as the motion has pushed the circulation away from the wall.

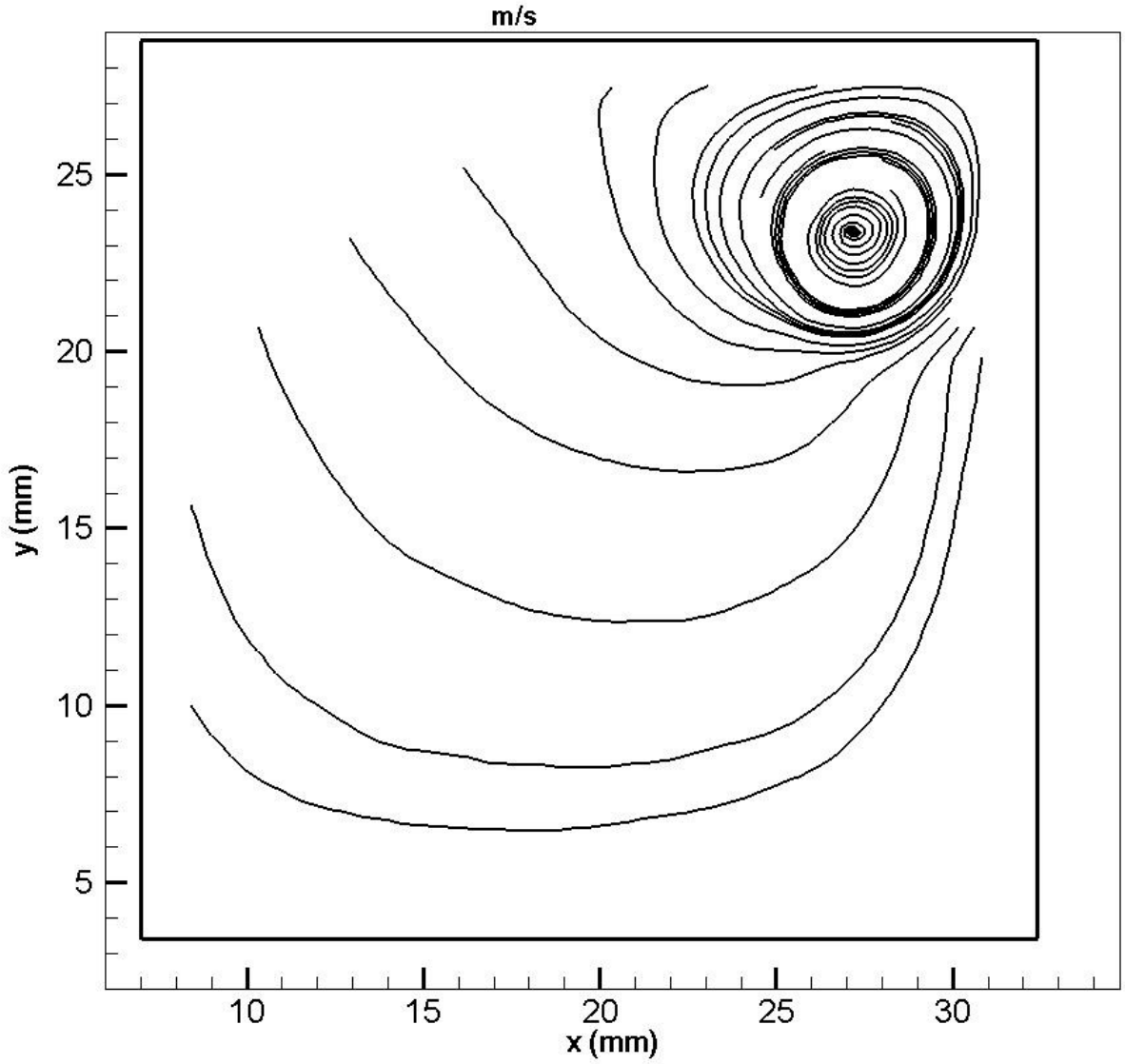

Figure 15- Streamlines Experiment 1 Run 4 (Re=1250) at Time t=0.69 seconds.

In Fig. 15. the circulation is more apparent in the streamlines concentrated at the top right of the cell as expected.

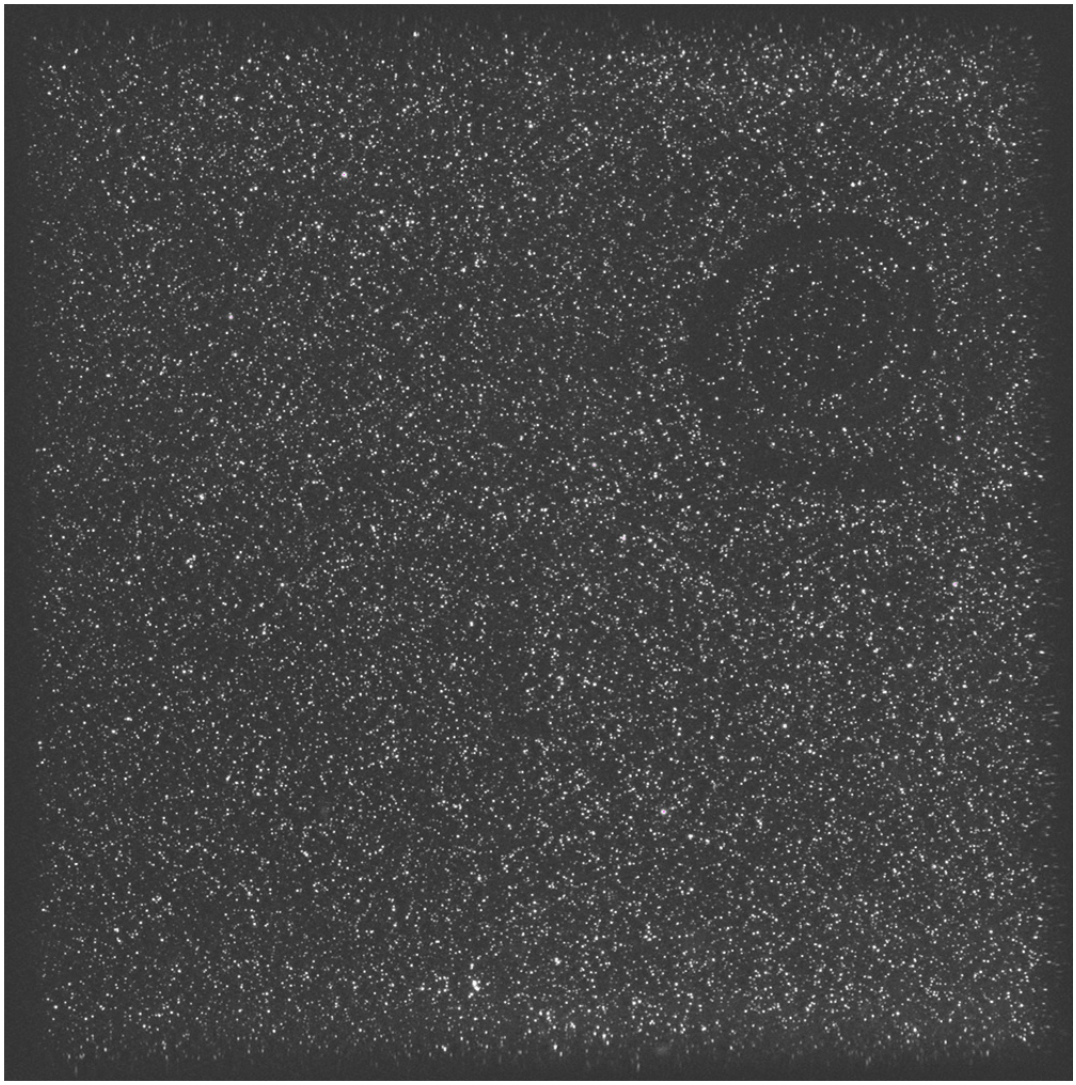

Figure 16- PIV Seeding Image Experiment 1 Run 4 (Re=1250) at Time t=1.03 seconds.

From the seeding shown in the PIV Fig. 16 the movement of the circulation toward the center of the cell is apparent with a visual comparison to the previous PIV image (Fig. 13).

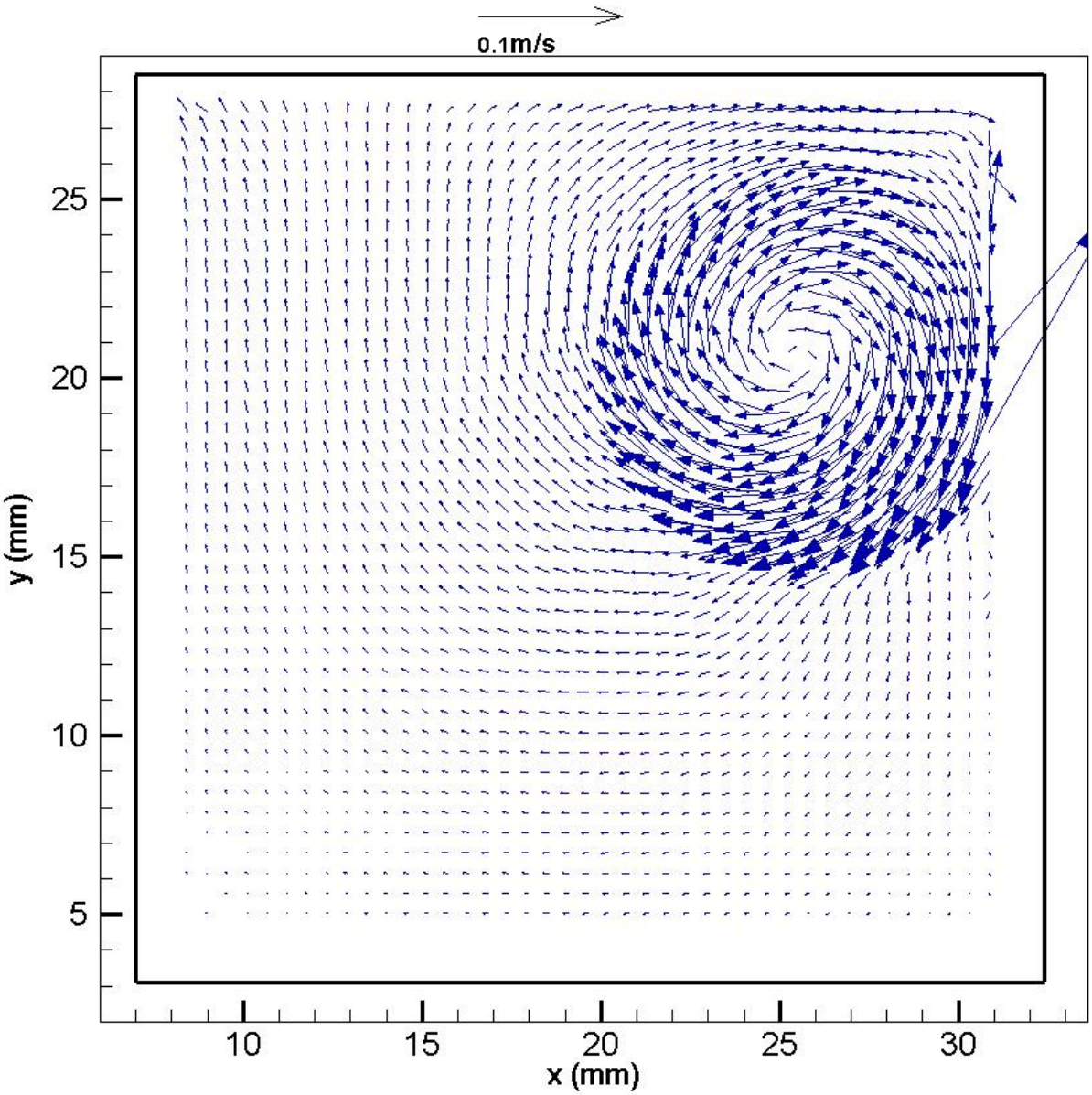

Figure 17- Global Vector Map Experiment 1 Run 4 (Re=1250) at Time t=1.03 Seconds.

As expected the strength of the circulation has increased from the previous time step, as shown in Fig. 17. The diameter has grown and it continues to move toward the center of the cell.

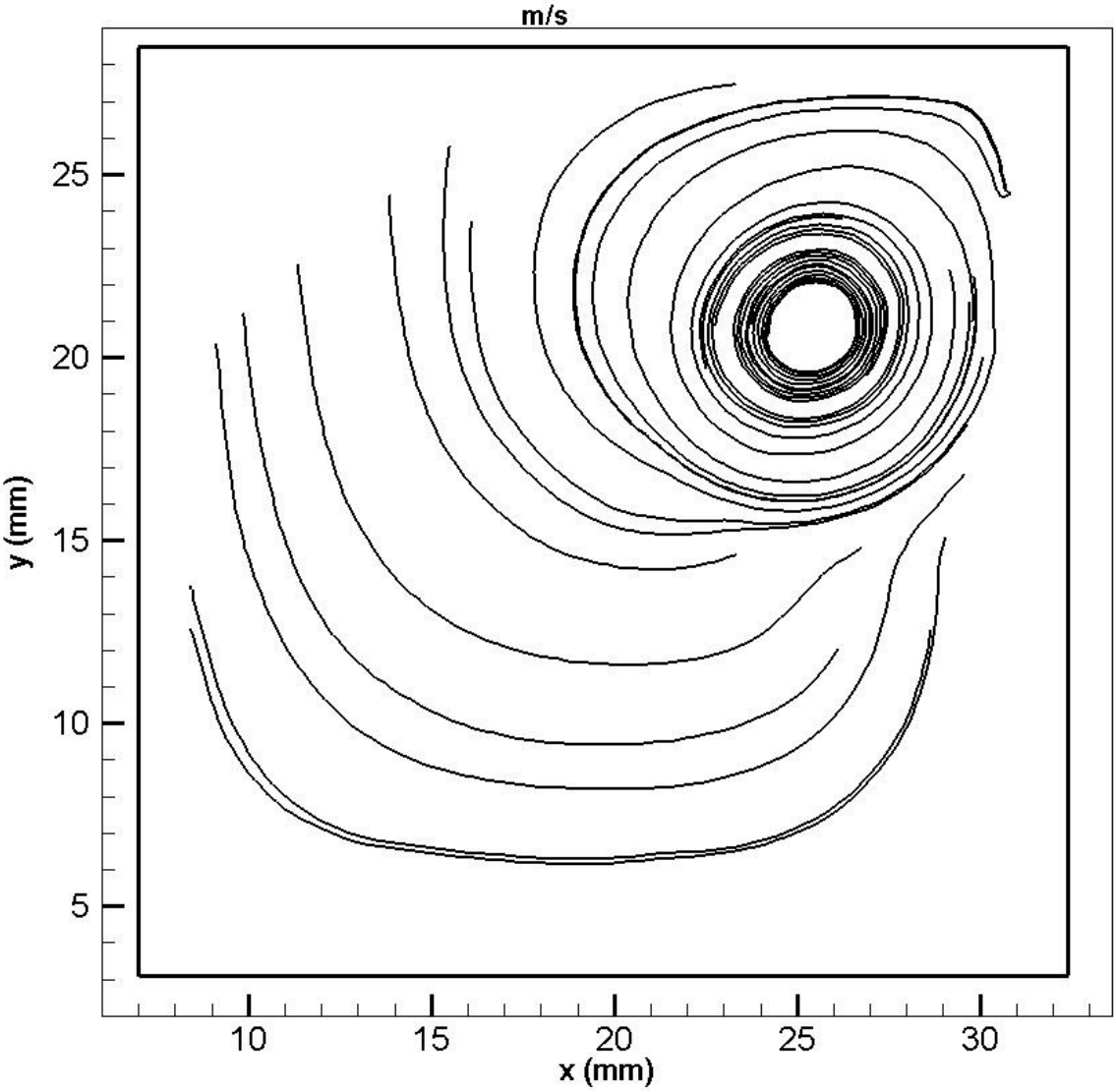

Figure 18- Streamlines Experiment 1 Run 4 (Re=1250) at Time t=1.03 Seconds.

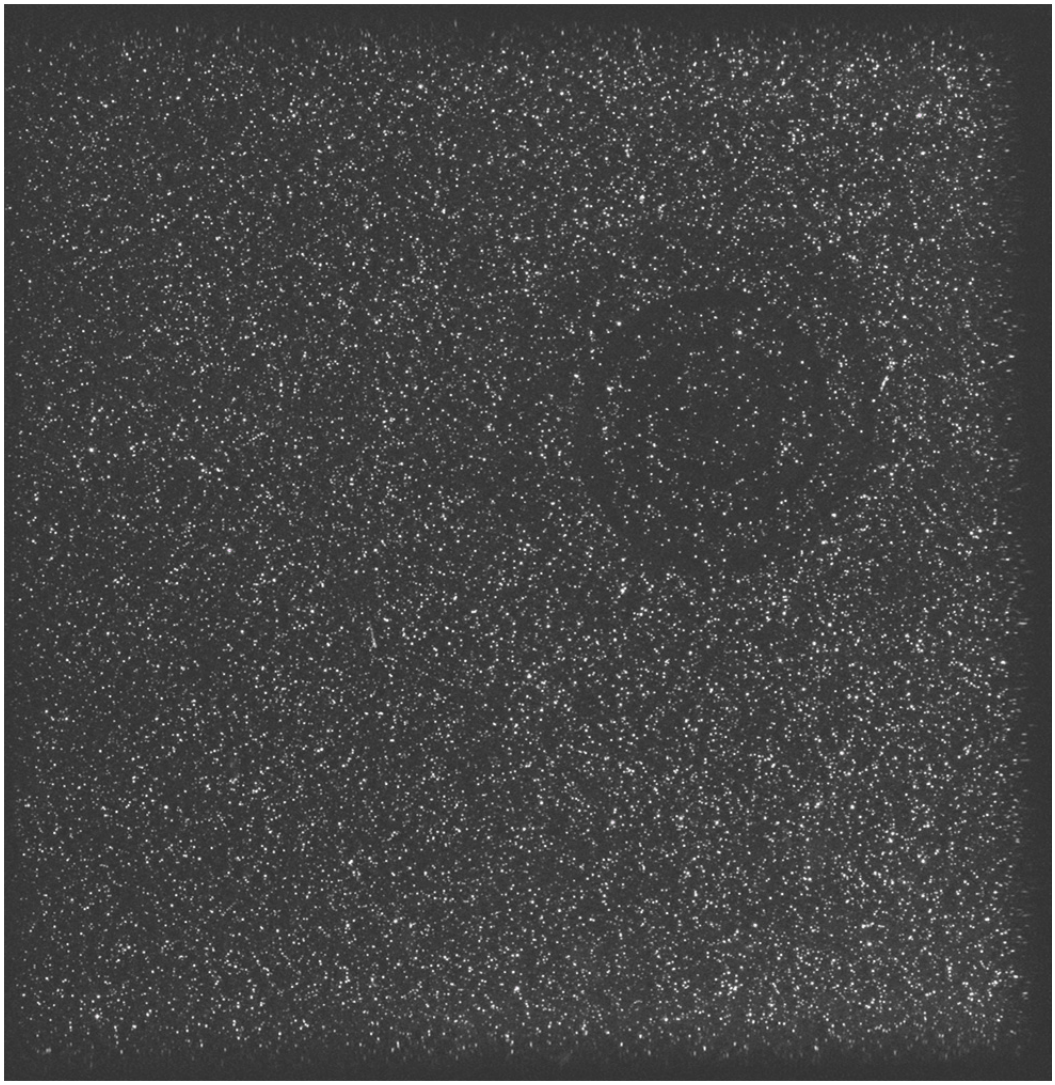

Figure 19- PIV Seeding Image Experiment 1 Run 4 (Re=1250) at Time t=1.38 Seconds.

Again, with a visual inspection of the PIV seeding in Fig. 19 the circulation movement toward the center of the cell cavity can be seen.

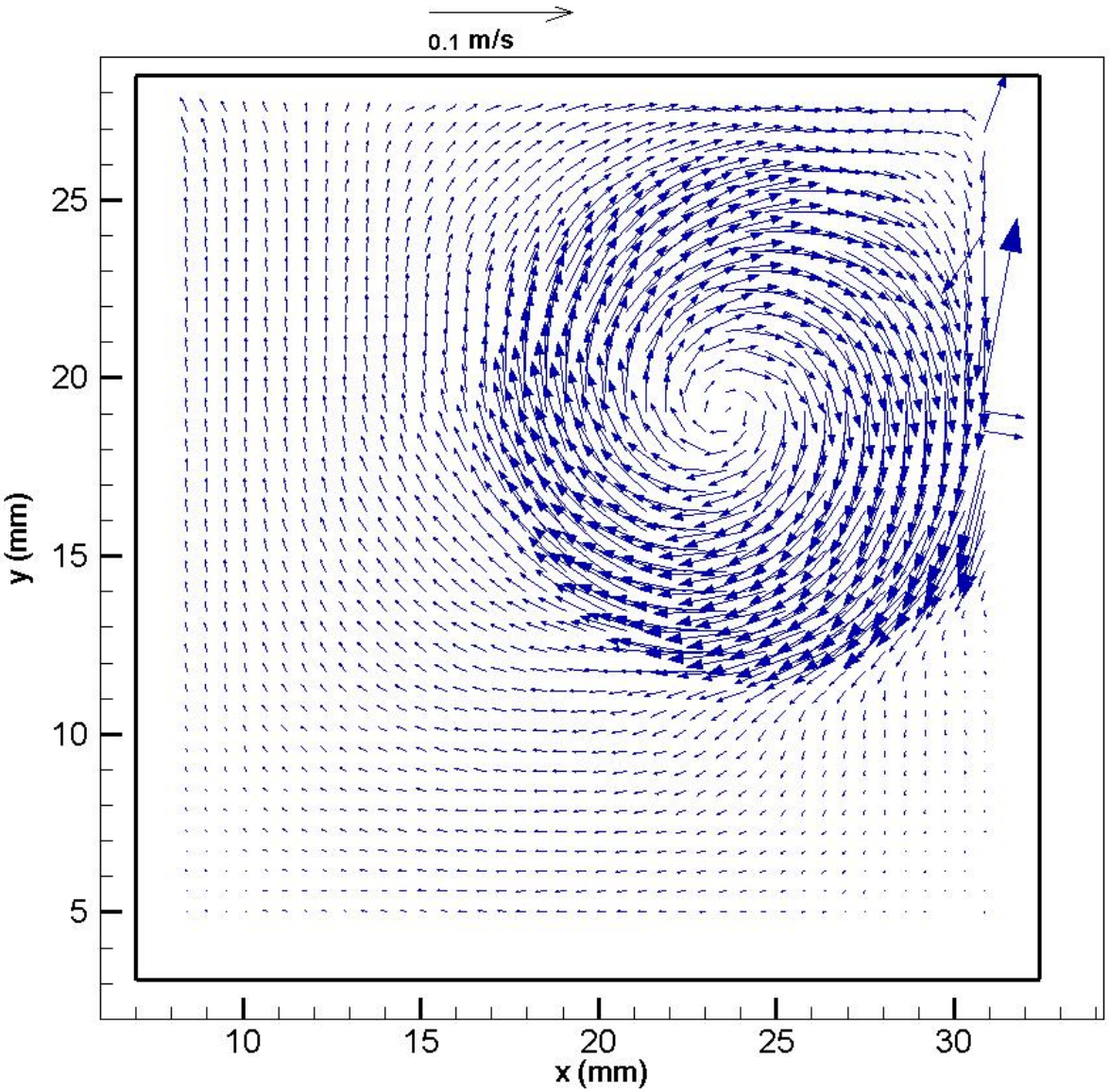

Figure 20- Global Vector Map Experiment 1 Run 4 (Re=1250) at Time t=1.38 Seconds.

Continuing the expected trend, Fig. 20 shows that circulation diameter continues to grow from the previous time step. The diagonally movement toward the center of the cell continues as well.

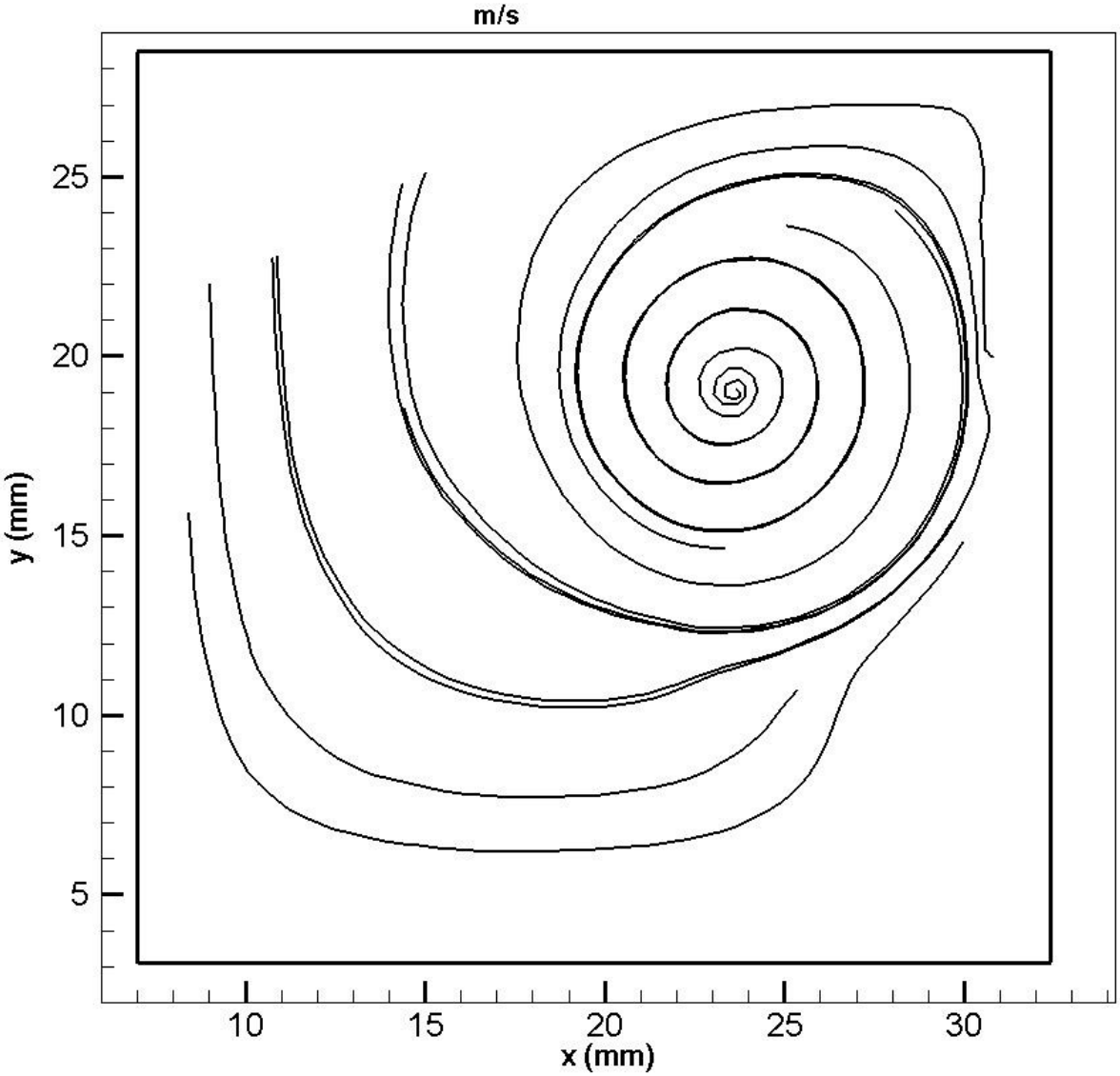

Figure 21- Streamlines Experiment 1 Run 4 (Re=1250) at Time t=1.38 Seconds.

An inspection of the streamlines of Fig. 21 validates the observations drawn from Fig. 20.

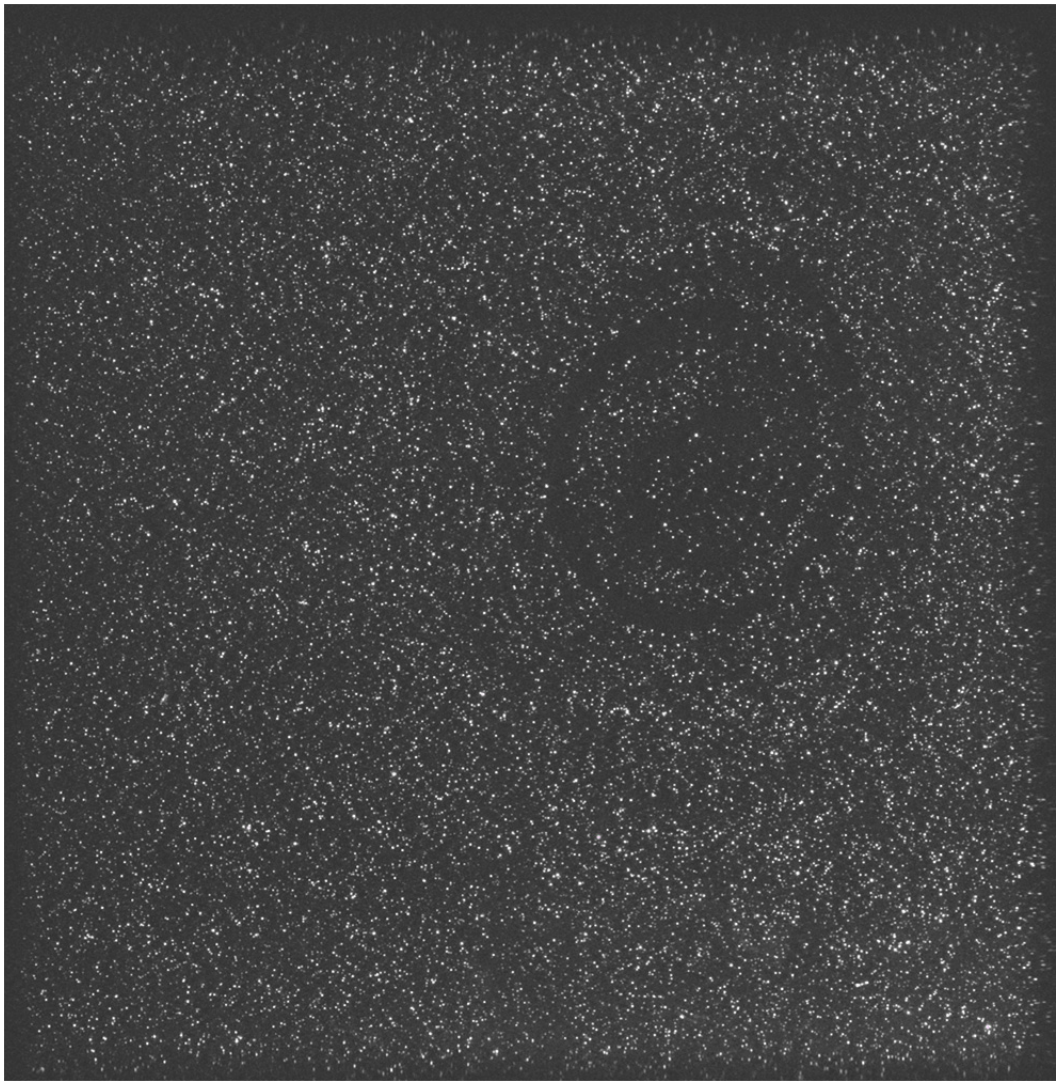

Figure 22- PIV Seeding Image Experiment 1 Run 4 (Re=1250) at Time t=1.72 Seconds.

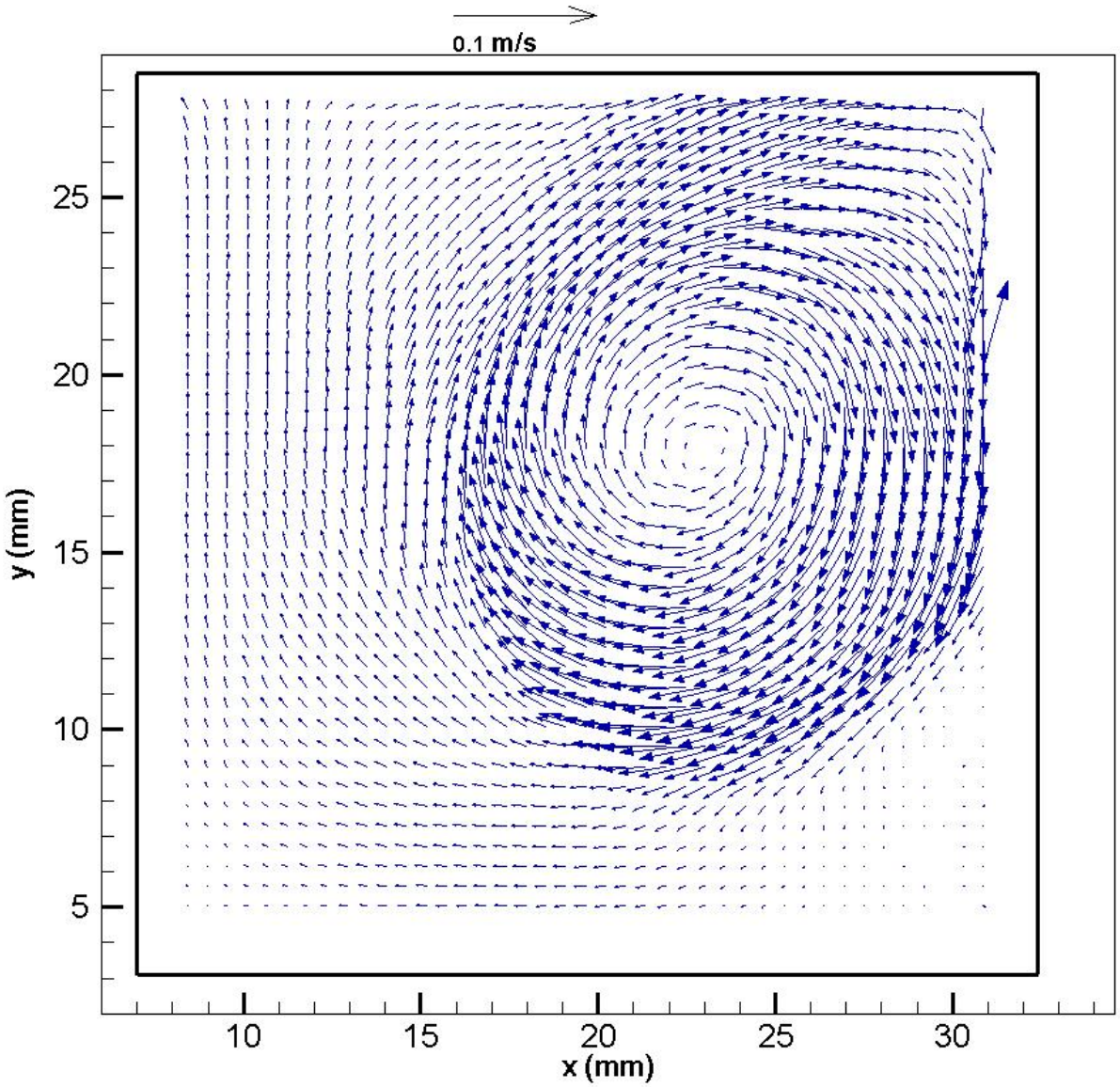

Figure 23- Global Vector Map Experiment 1 Run 4 (Re=1250) at Time t=1.72 Seconds.

Again as expected the circulation diameter continues to increase. This can be seen easily in Fig. 23. The circulation center continues to travel to the center of the cell as seen in Fig. 23 or by a visual inspection of the seeding in Fig. 22.

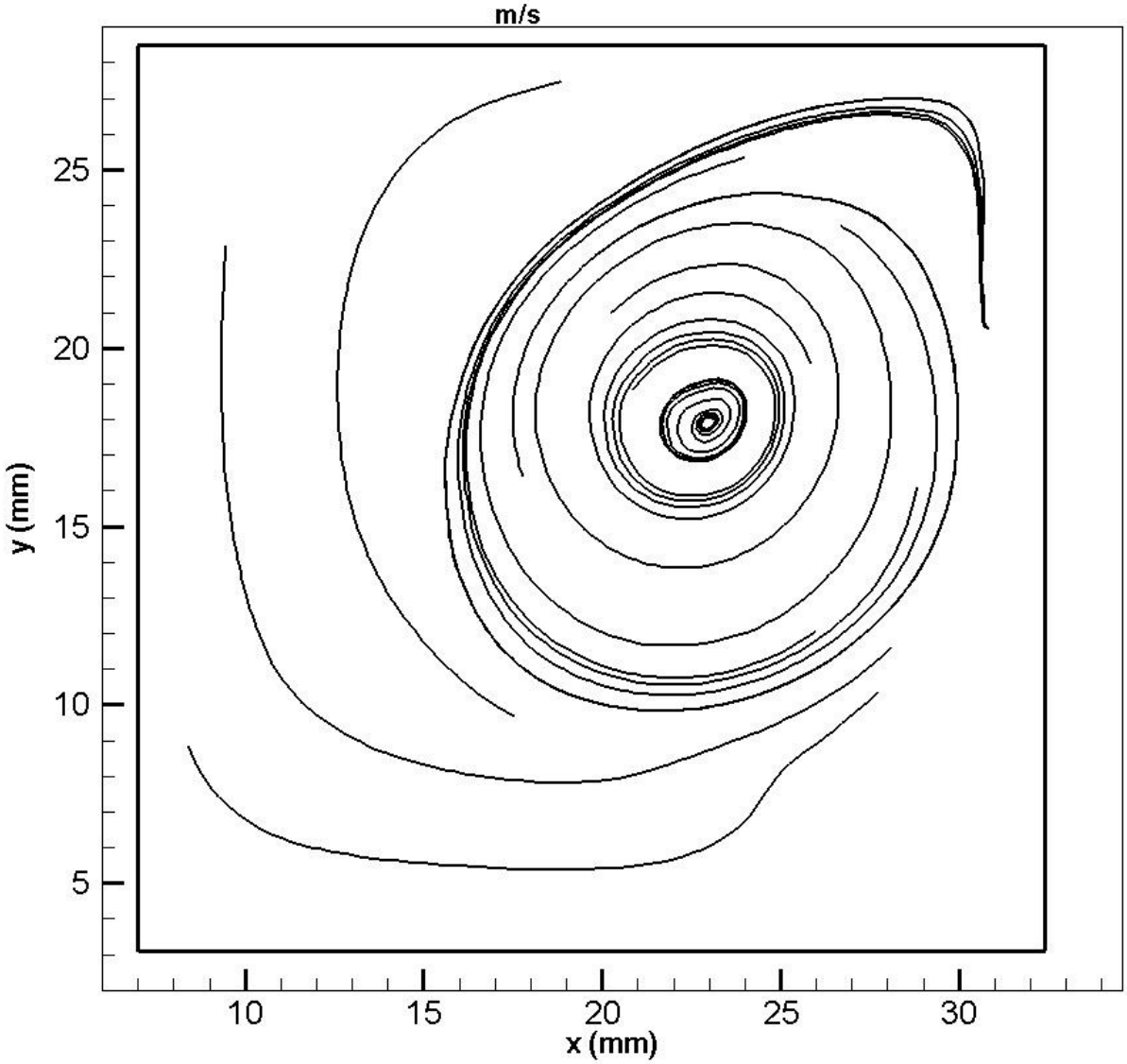

Figure 24- Streamlines Experiment 1 Run 4 (Re=1250) at Time t=1.72 Seconds.

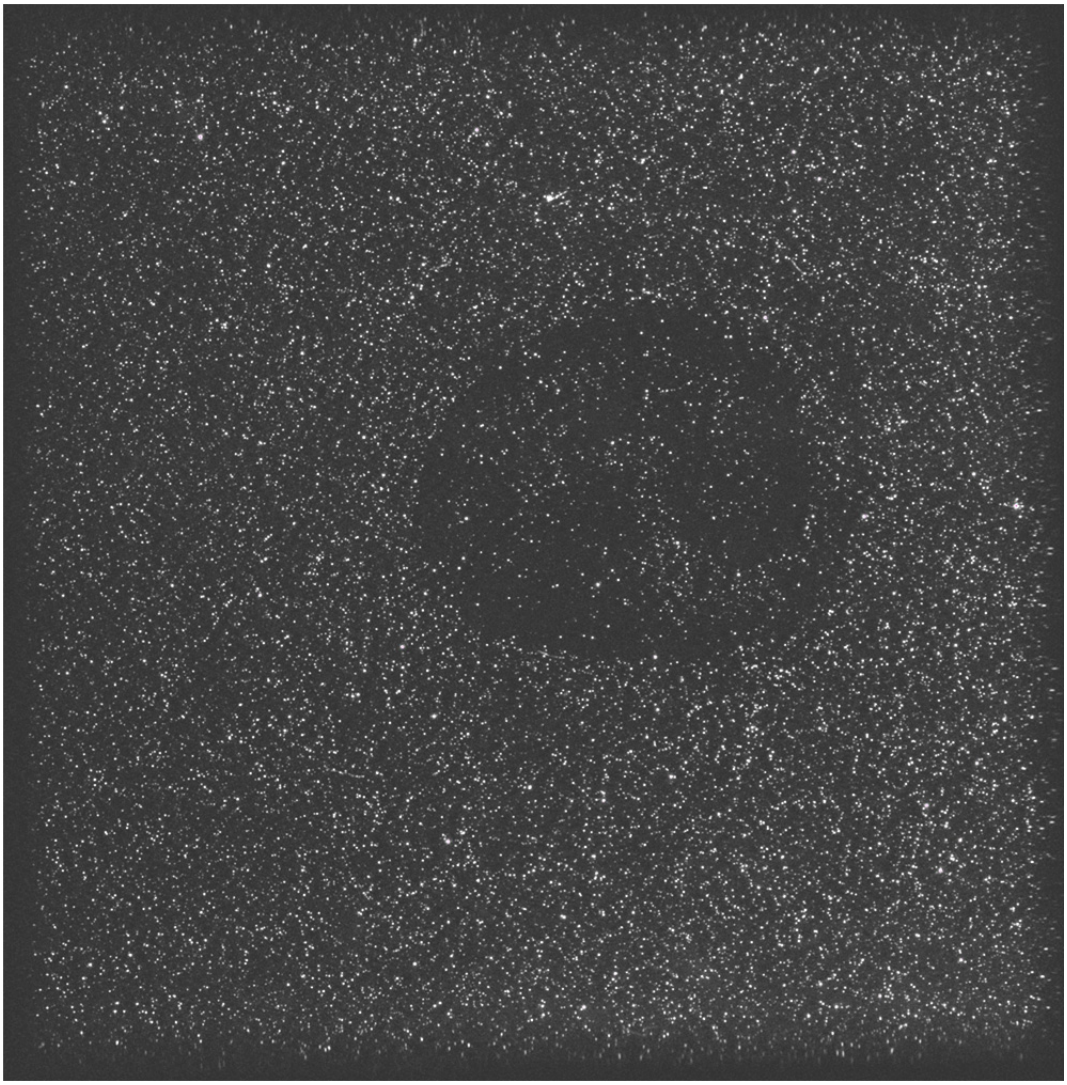

Figure 25- PIV Seeding Image Experiment 1 Run 4 (Re=1250) at Time t=2.07 Seconds.

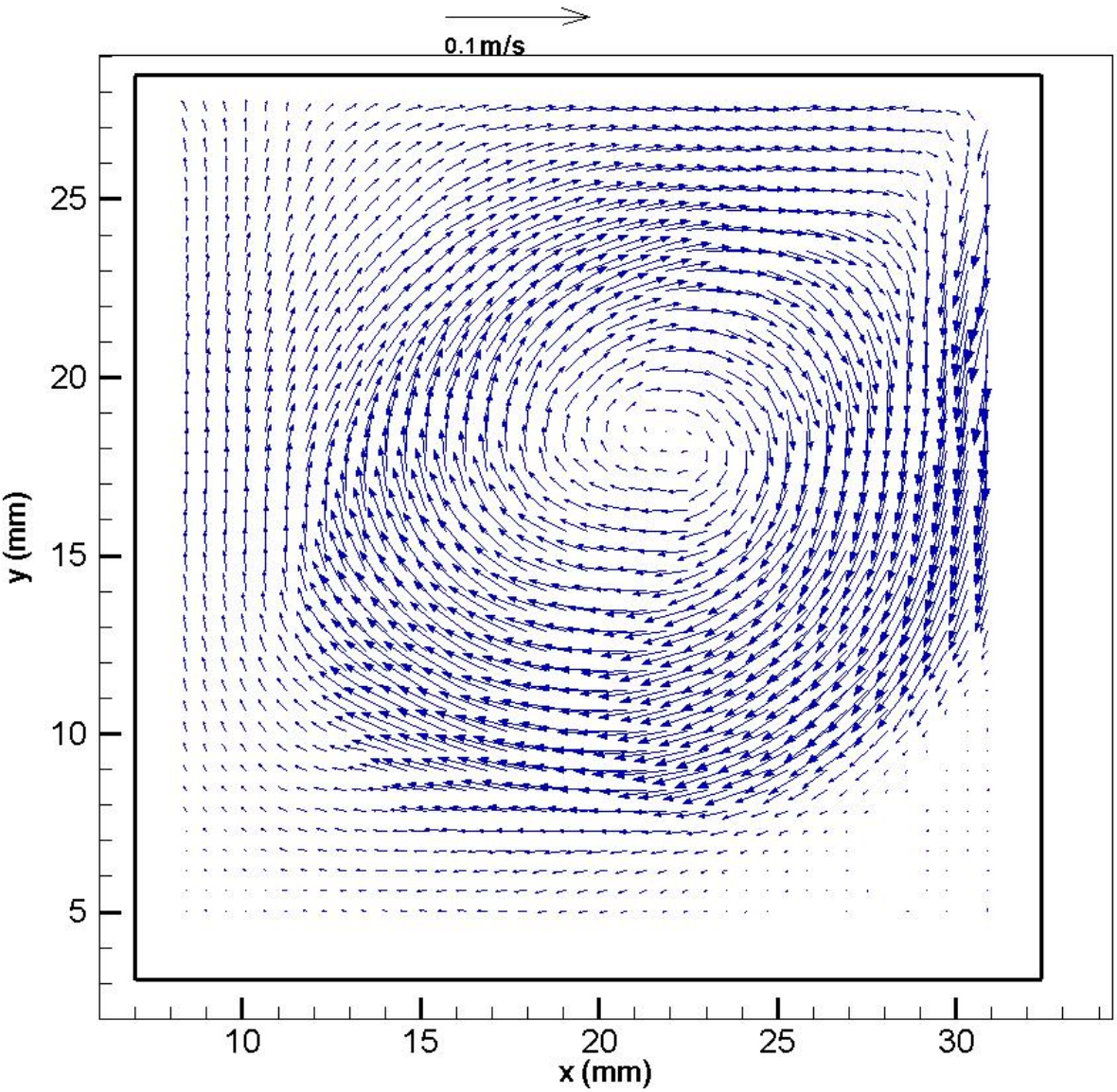

Figure 26- Global Vector Map Experiment 1 Run 4 (Re=1250) at Time t=2.07 Seconds.

In Fig. 26 it is seen that the circulation diameter has increased enough to almost engulf the whole cell.

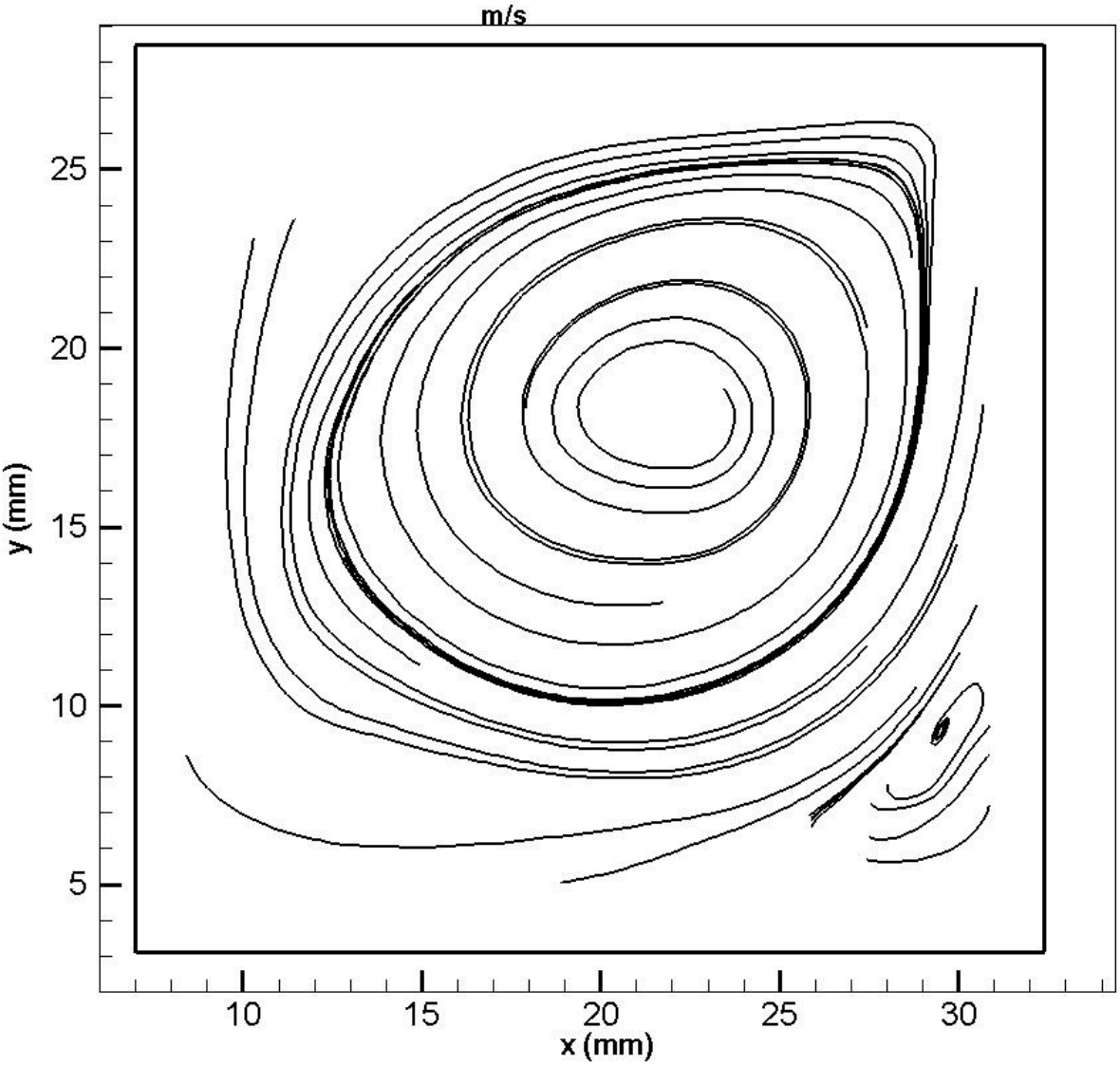

Figure 27- Streamlines Experiment 1 Run 4 (Re=1250) at Time t=2.07 Seconds.

In Fig. 27 the appearance of a downstream secondary is detected in the streamlines. This is predicted by the theory.

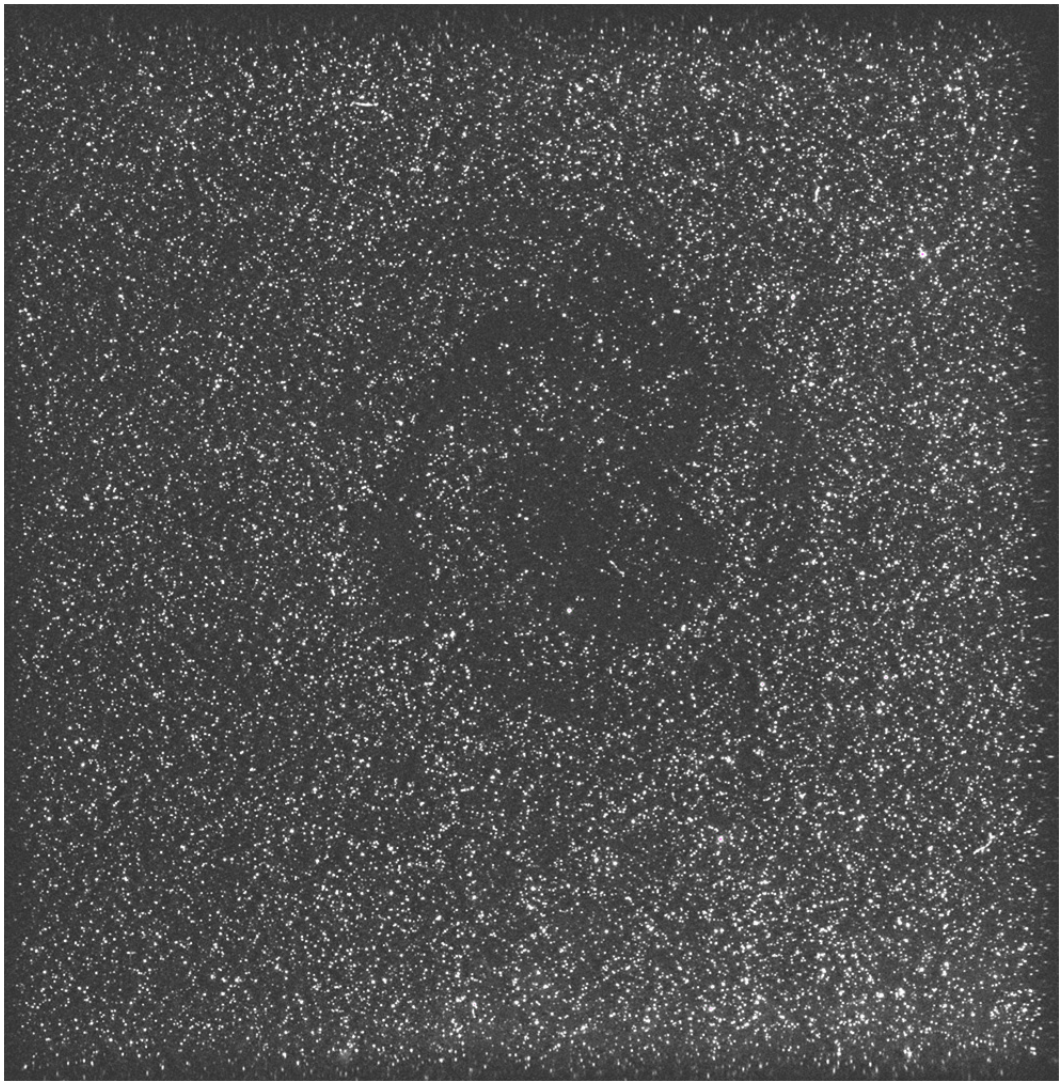

Figure 28- PIV Seeding Image Experiment 1 Run 4 (Re=1250) at Time t=2.41s.

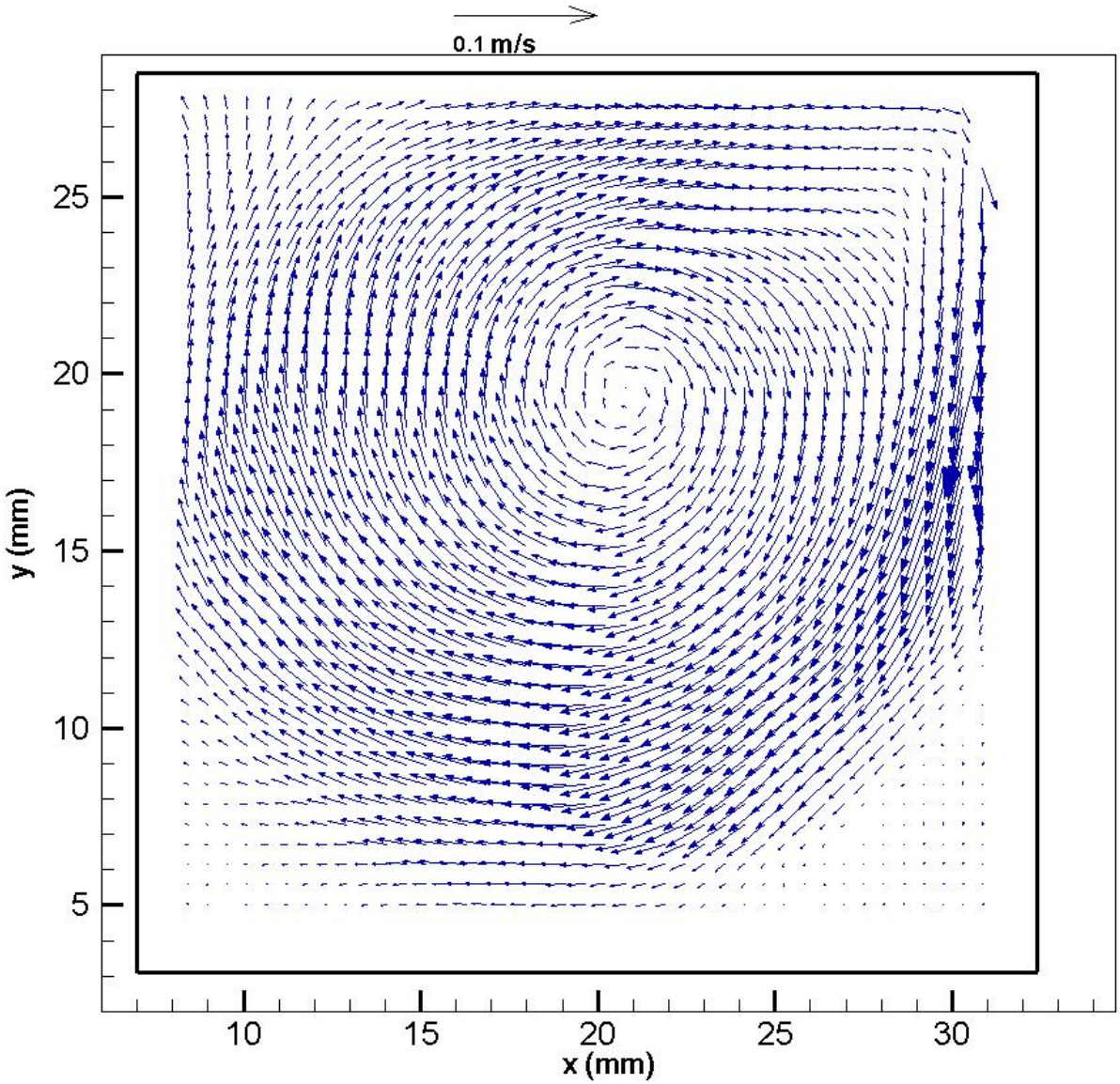

Figure 29- Global Vector Map Experiment 1 Run 4 (Re=1250) at Time t=2.41 Seconds.

In Fig. 29 steady state has been achieved in the cell. The time is 2.41 seconds after the initial movement of the lid. The circulation has engulfed the whole cell it's center is not quite at the center of the cavity, but very close. The downstream secondary eddy becomes more apparent in Fig. 30.

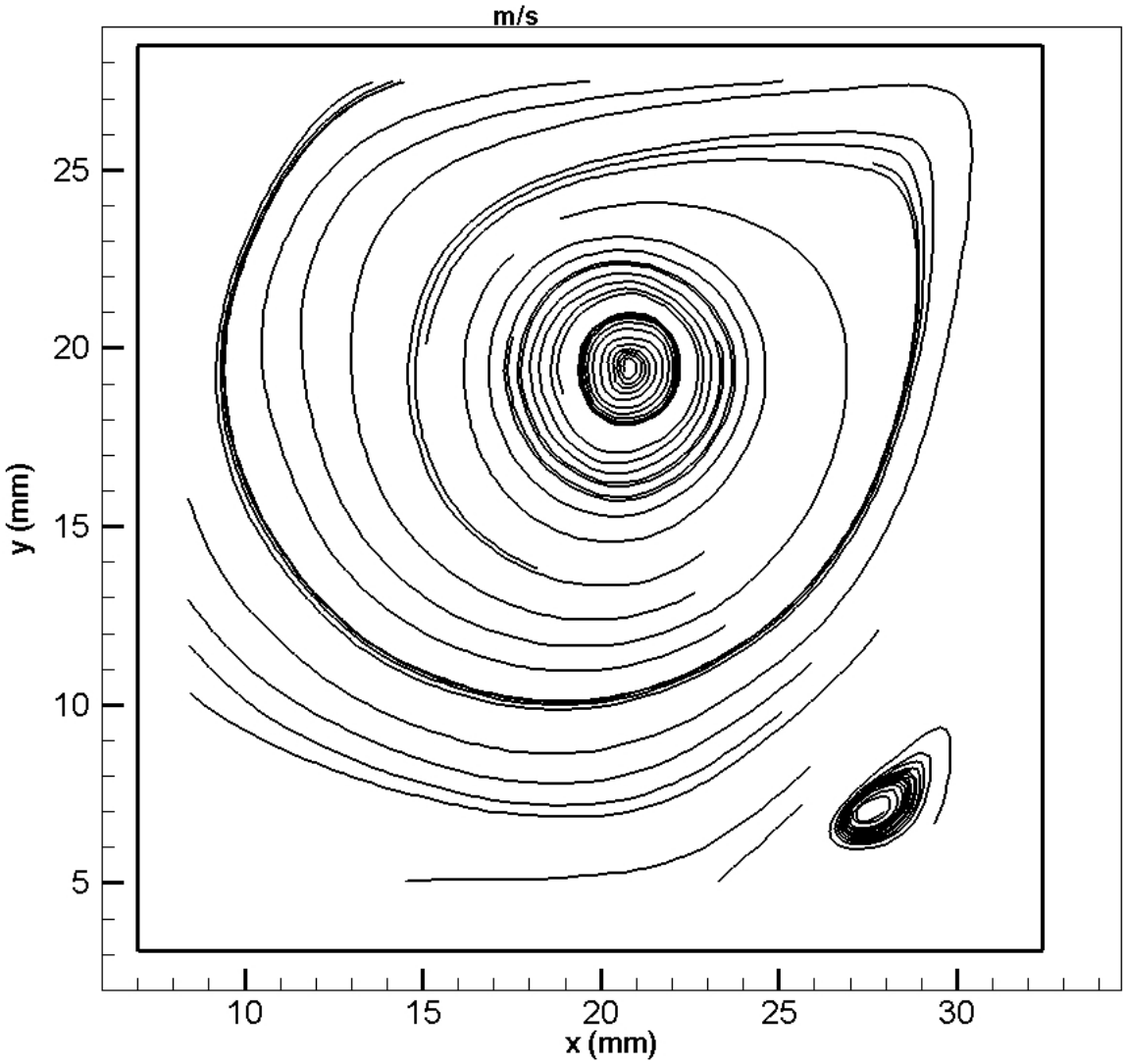

Figure 30- Streamlines Experiment 1 Run 4 (Re=1250) at Time t=2.41 Seconds.

Table 2- Velocities (u) Along the y-y Axis (of the Circulation Center) for Experiment 1 Run 4 (Re=1250)

y (m)	u (m/s)
0.028	0.05
0.027287	0.027134
0.02646	0.027517
0.025633	0.028852
0.024807	0.028897
0.02398	0.028022
0.023154	0.026761
0.022327	0.023531
0.021501	0.017158
0.020674	0.009667
0.019847	0.003761
0.019021	-0.00289
0.018194	-0.00895
0.017368	-0.01269
0.016541	-0.01747
0.015715	-0.02051
0.014888	-0.02269
0.014061	-0.02577
0.013235	-0.02677
0.012408	-0.02884
0.011582	-0.0302
0.010755	-0.03186
0.009929	-0.03231
0.009102	-0.03213
0.008275	-0.0316
0.007449	-0.02958
0.006622	-0.01984
0.005796	-0.01163
0.005	0
0.028	0.05

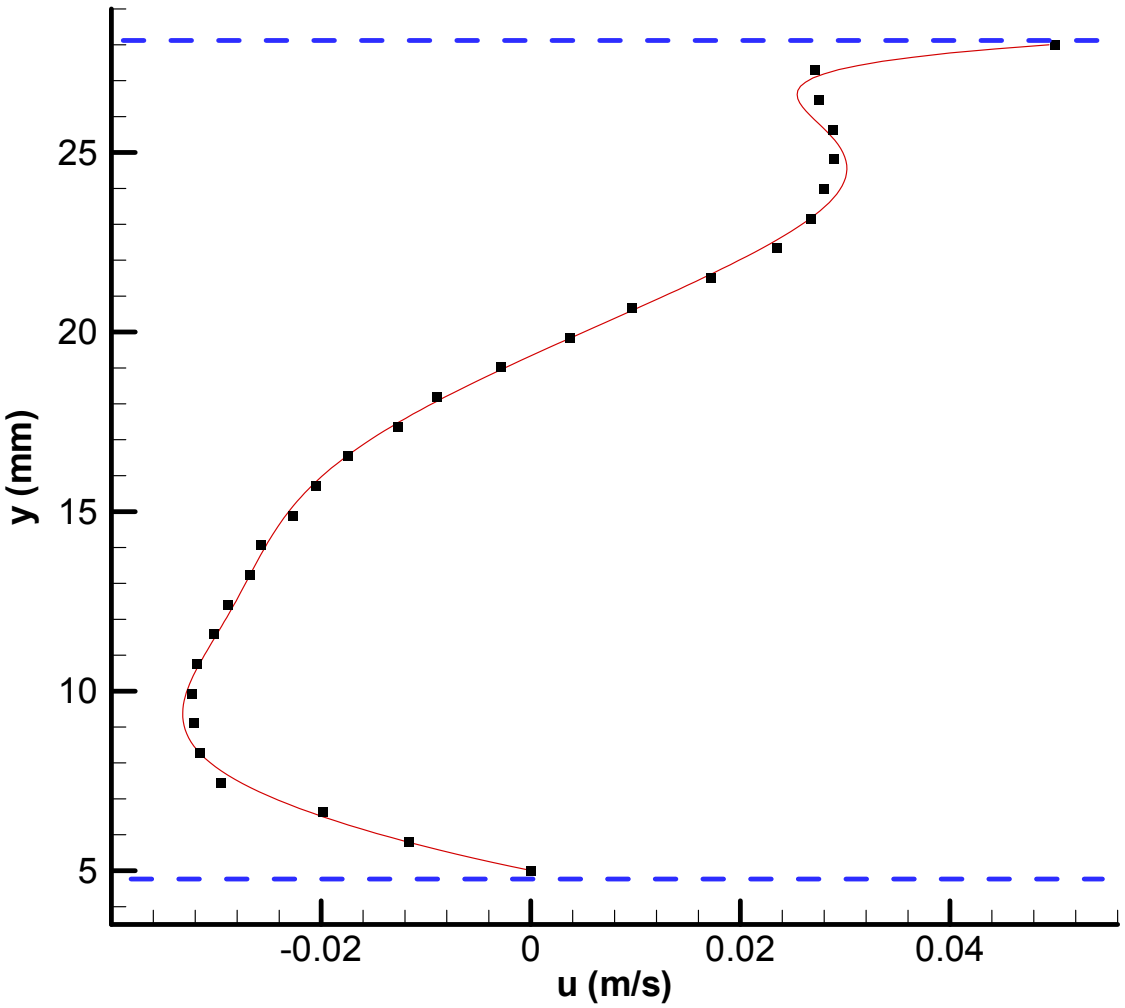

Figure 31- Velocities (u) Along the y-y Axis (of the Circulation Center) for Experiment 1 Run 4 (Re=1250)

In Fig. 31 the distribution of the u velocities measured by PIV readings follow the trend predicted by theory. The sudden decrease in velocity magnitude around y = 27 mm is predicted by Eturk et al. [13]

Table 3- Velocities (v) Along the x-x Axis (of the Circulation Center) for Experiment 1 Run 4 (Re=1250)

x (m)	v (m/s)
0.031	0
0.03062	-0.05507
0.029797	-0.04652
0.028974	-0.03307
0.028151	-0.02363
0.027329	-0.02243
0.026506	-0.02345
0.025683	-0.02335
0.02486	-0.0226
0.024038	-0.02091
0.023215	-0.01917
0.022392	-0.0145
0.021569	-0.00864
0.020747	0.000387
0.019924	0.008406
0.019101	0.013489
0.018278	0.019238
0.017455	0.023486
0.016633	0.02668
0.01581	0.028114
0.014987	0.028415
0.014164	0.028152
0.013342	0.028315
0.012519	0.029369
0.011696	0.030235
0.010873	0.029795
0.010051	0.028052
0.009228	0.023841
0.008	0
0.031	0

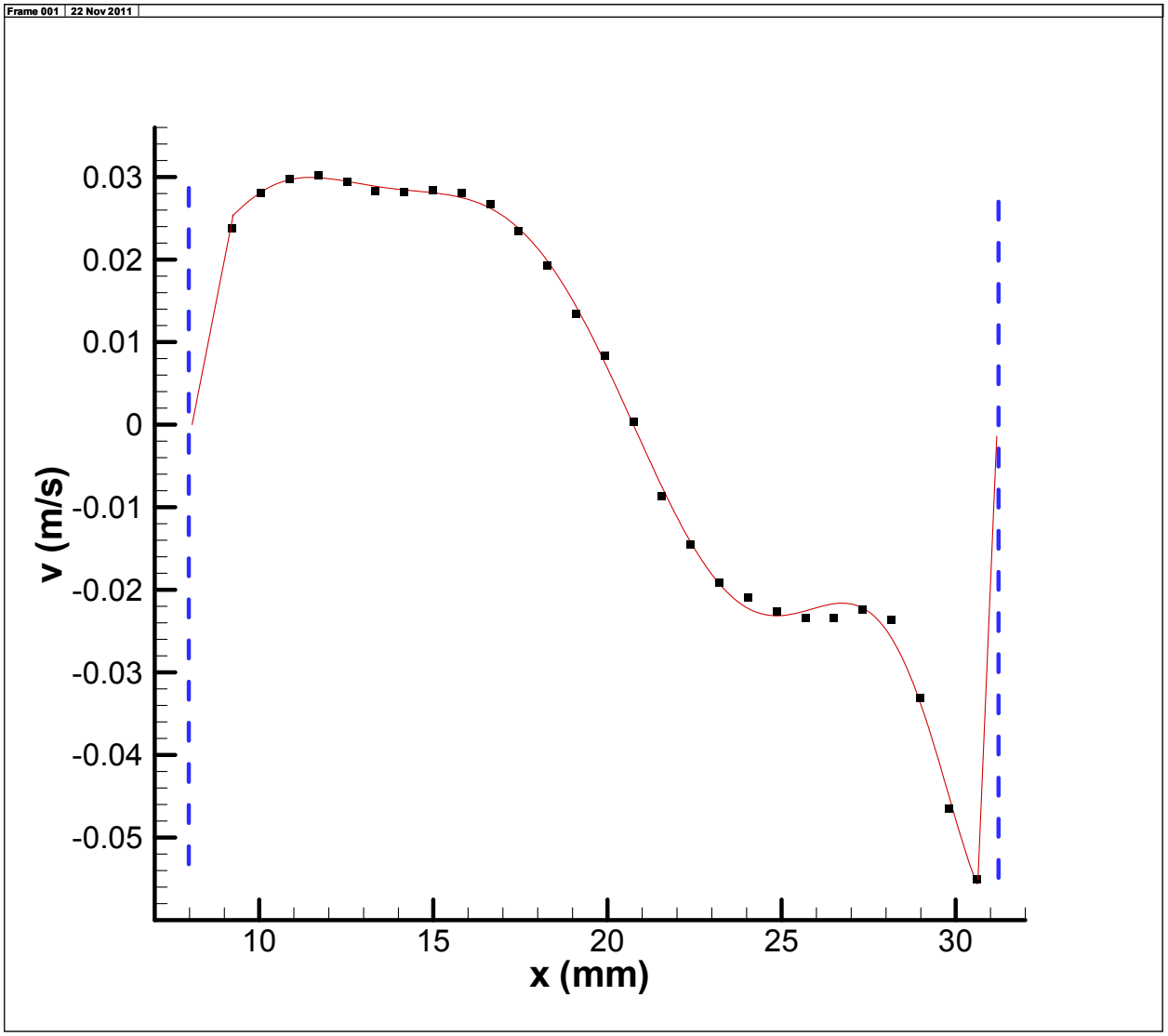

Figure 32- Velocities (v) along the x-x Axis (of the Circulation Center) for Experiment 1 Run 4 (Re=1250)

In Fig. 32 the distribution of the v velocities measured by PIV readings follow the trend predicted by theory.

5.2 Case study of PIV settings for Experiment 1

The lowest Reynolds number experiment is used to determine the capture and processing settings yielding optimal results of global velocity readings. The case study is broken in to two parts; first PIV capture settings are examined and second the processing options offered by the Insight software are presented. With respect to PIV capture settings the timing between laser pulses A and B, known as delta t, is the variable which determines if the capture will yield usable data results. If the delta t is set to high the seeding particles read by the software will have moved too far between frames A and B for the software to yield a useful data analysis. If it is set too low the seeding particles will not have traveled enough distance for the software to capture movement. Times investigated were 6000 μs delta t shown in Fig 33., 5000 μs delta t shown Fig. 34, and 1800 μs delta t shown in fig 35. The formation of the higher velocity circulation proved to be a sensitive area of capture and was used as the reference reading area.

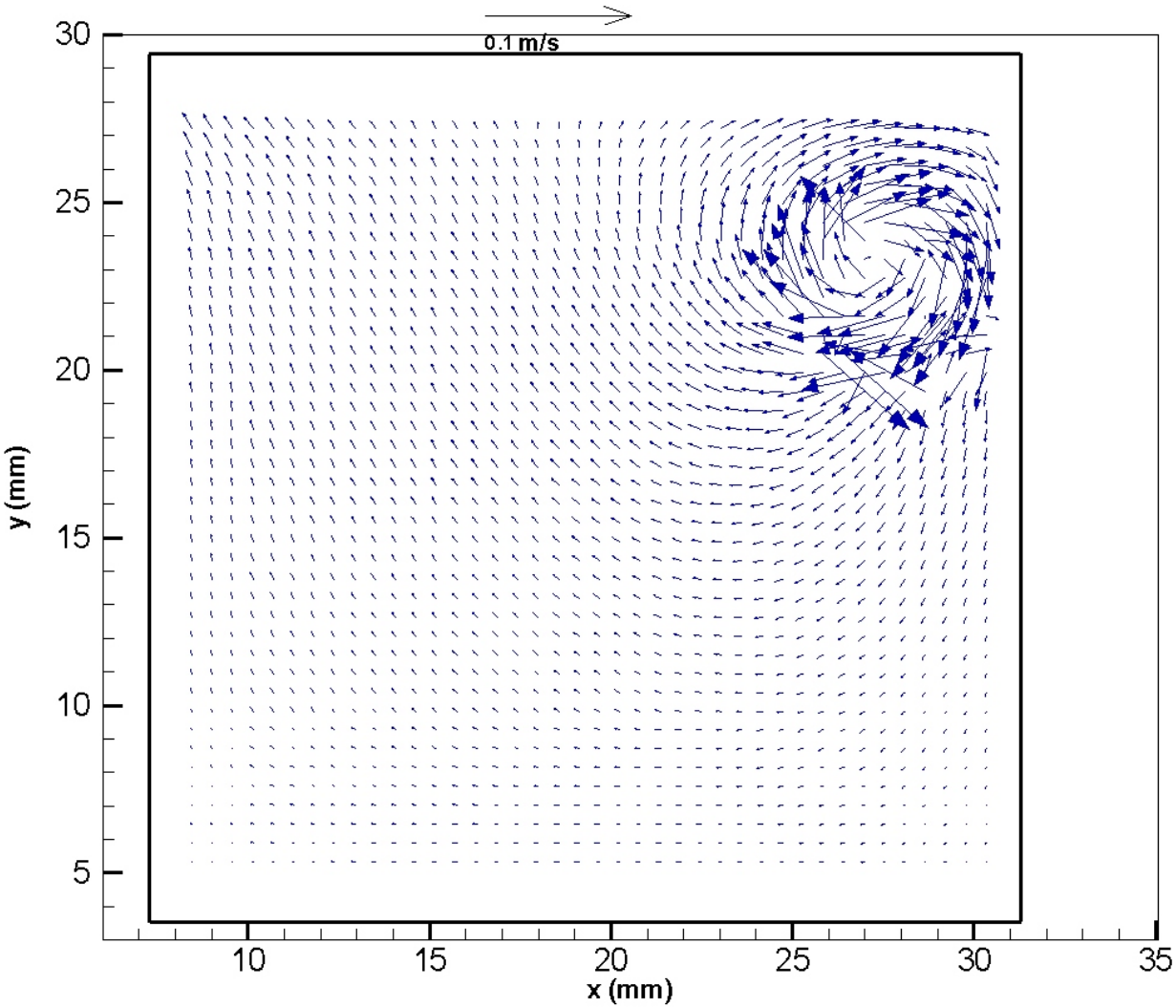

Figure 33- Global Vector Map for Experiment 1 Run 1 (Re=1250) at Time 0.69 Seconds.

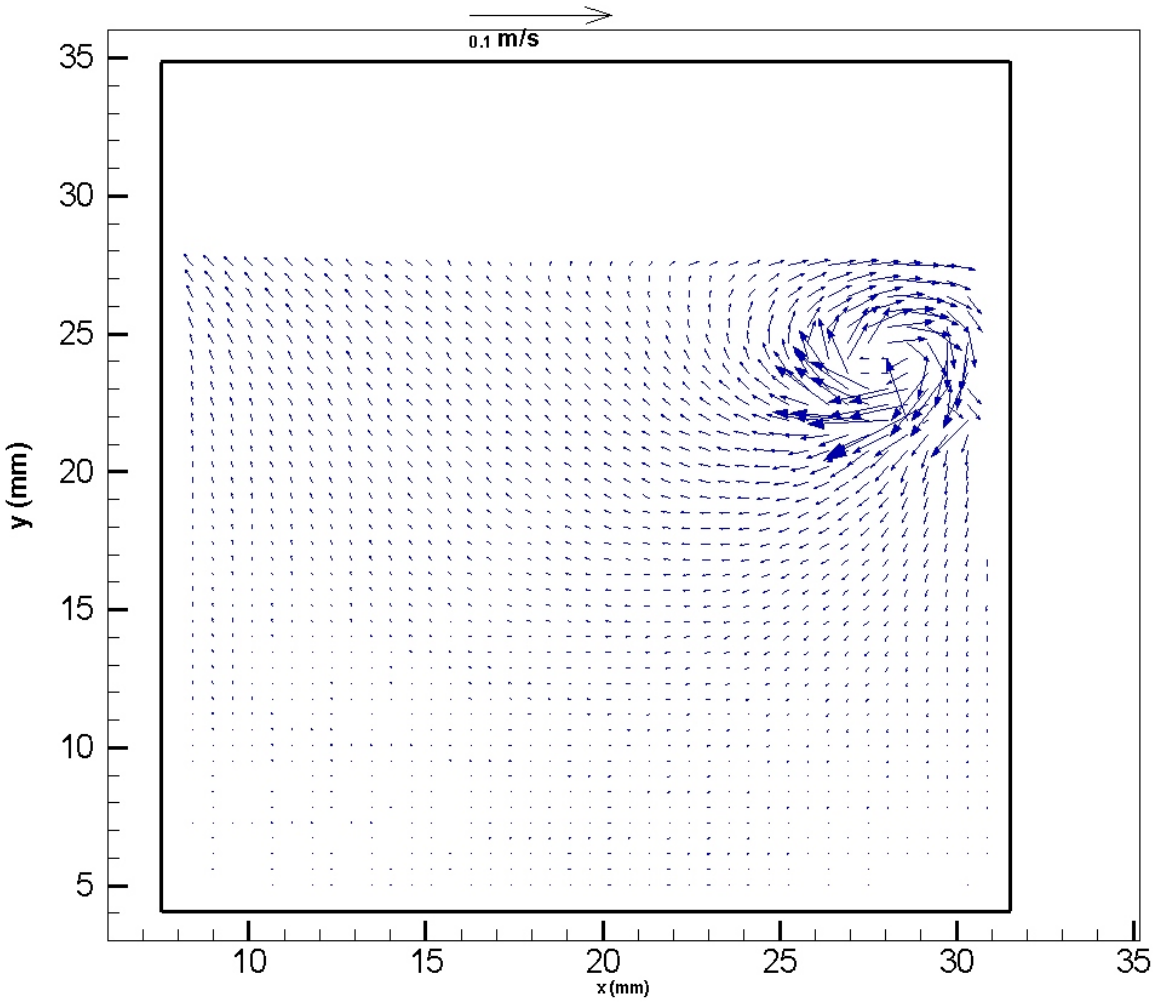

Figure 34- Global Vector Map Experiment 1 Run 2 (Re=1250) at Time 0.69 Seconds.

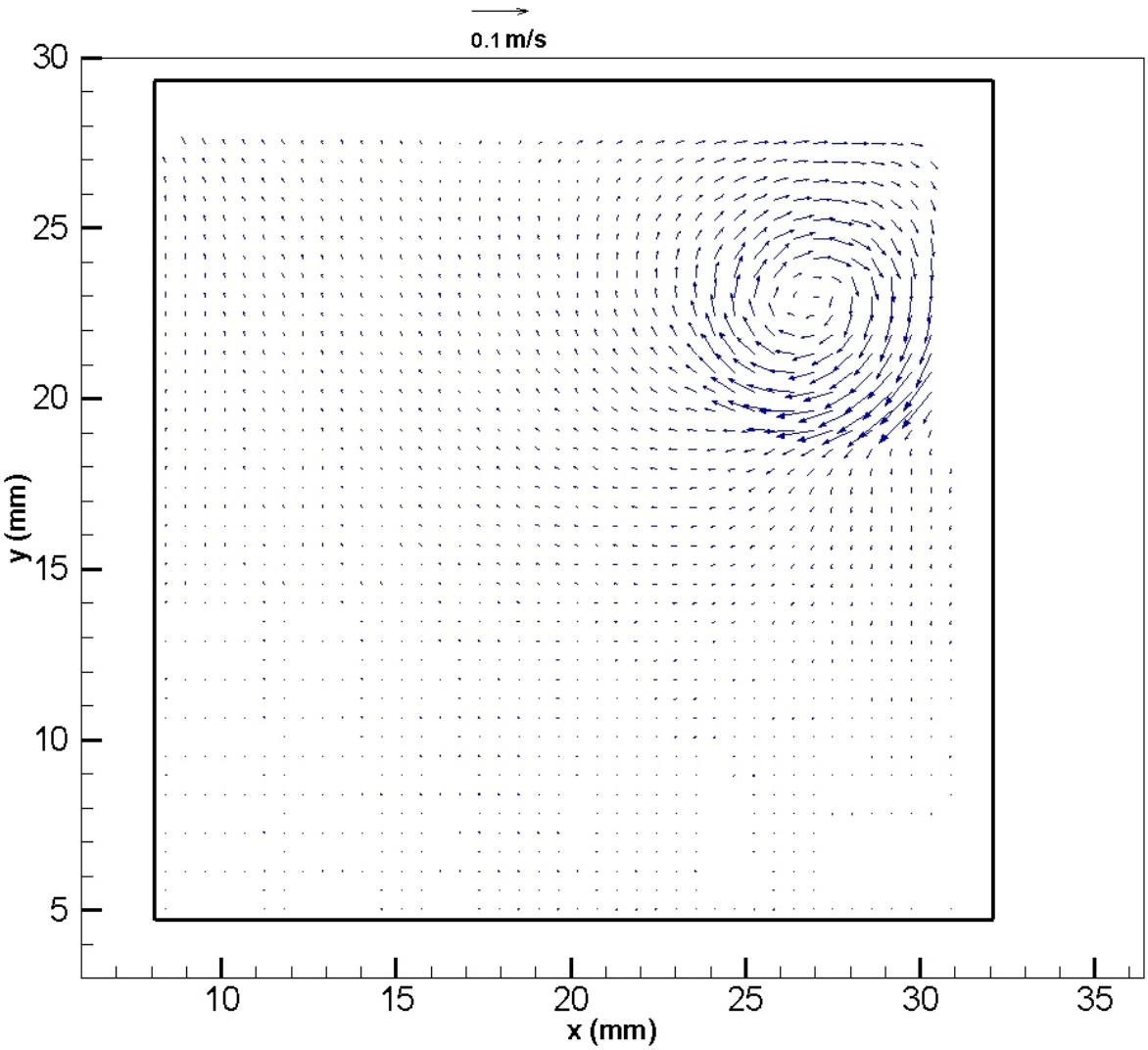

Figure 35- Global Vector Map Experiment 1 Run 3 (Re=1250) at Time 0.69 Seconds.

Comparing Figure 33-35 it can be seen that the higher value of delta t leads to poor readings in the circulation area. A timing of 1800 us delta t yields the best laser pulse separation for the velocity ranges of the experiments and is set as a fixed value for the remaining experiments.

The second part of the case study was to determine the processor settings. Processing of the data is performed by comparing image pairings of A and B frames using the Insight software. Processor settings variables are correlation engine, grid engine, spot mask engine, peak engine, interrogation area and percent overlay. The first setting investigated was the use of correlation engines: Direct Correlator shown in Fig. 36, Fast Fourier Transformation Correlator shown in Fig. 37, or Hart Correlator shown in Fig. 38. [Correlation engines are algorithms that sum the particle image matches at all displacements with in the displacement range] All correlations were performed with the same interrogation areas, 64 by 64 pixel, and the same overlay 35%, the same grid engine Nyquist Grid, no mask for spot engine masking, and Guassian Peak for the Peak engine.

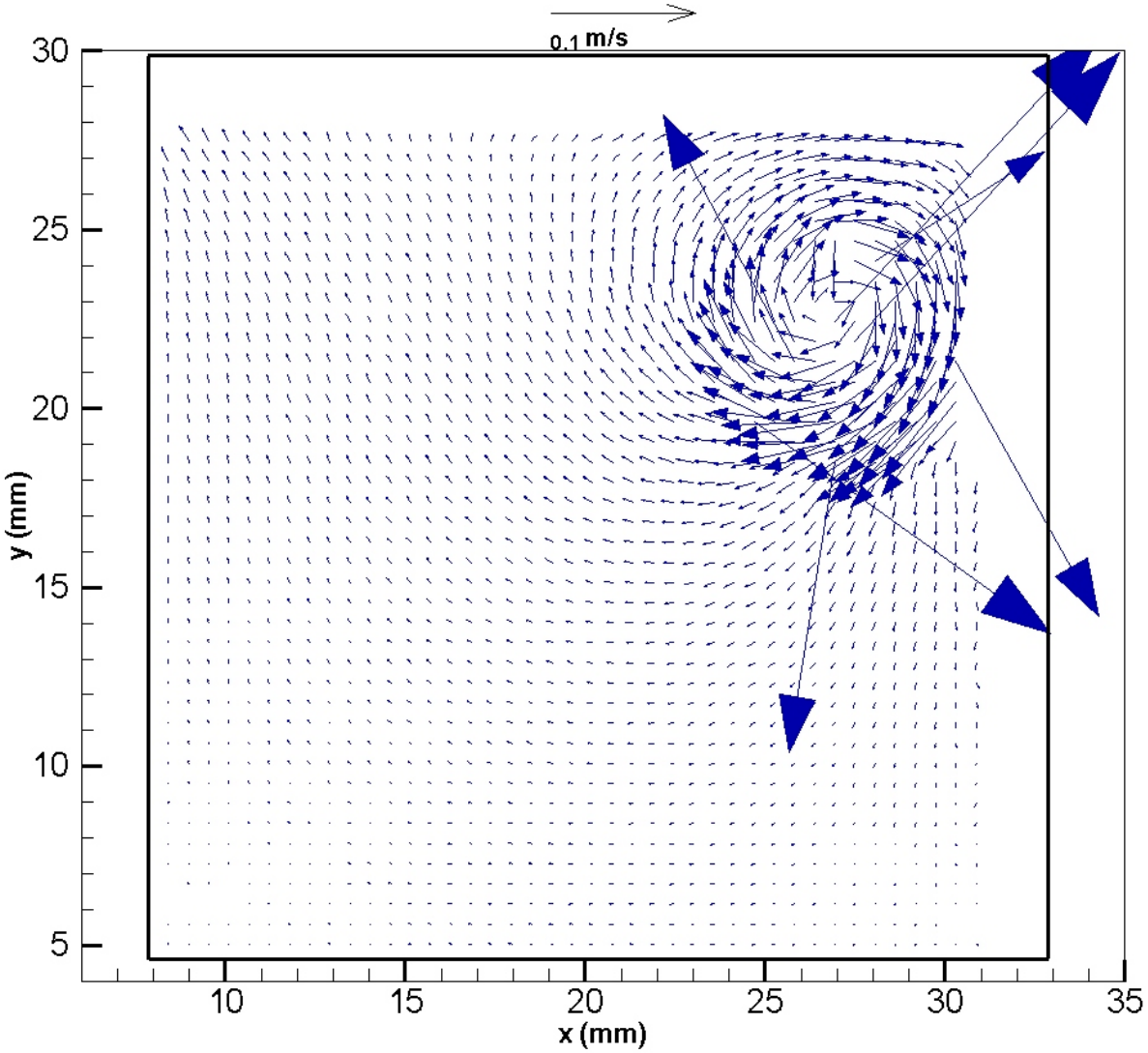

Figure 36- Global Vector Map Experiment 1 Run 4 (Re=1250) at Time 0.69 Seconds Processed Using Direct Correlator.

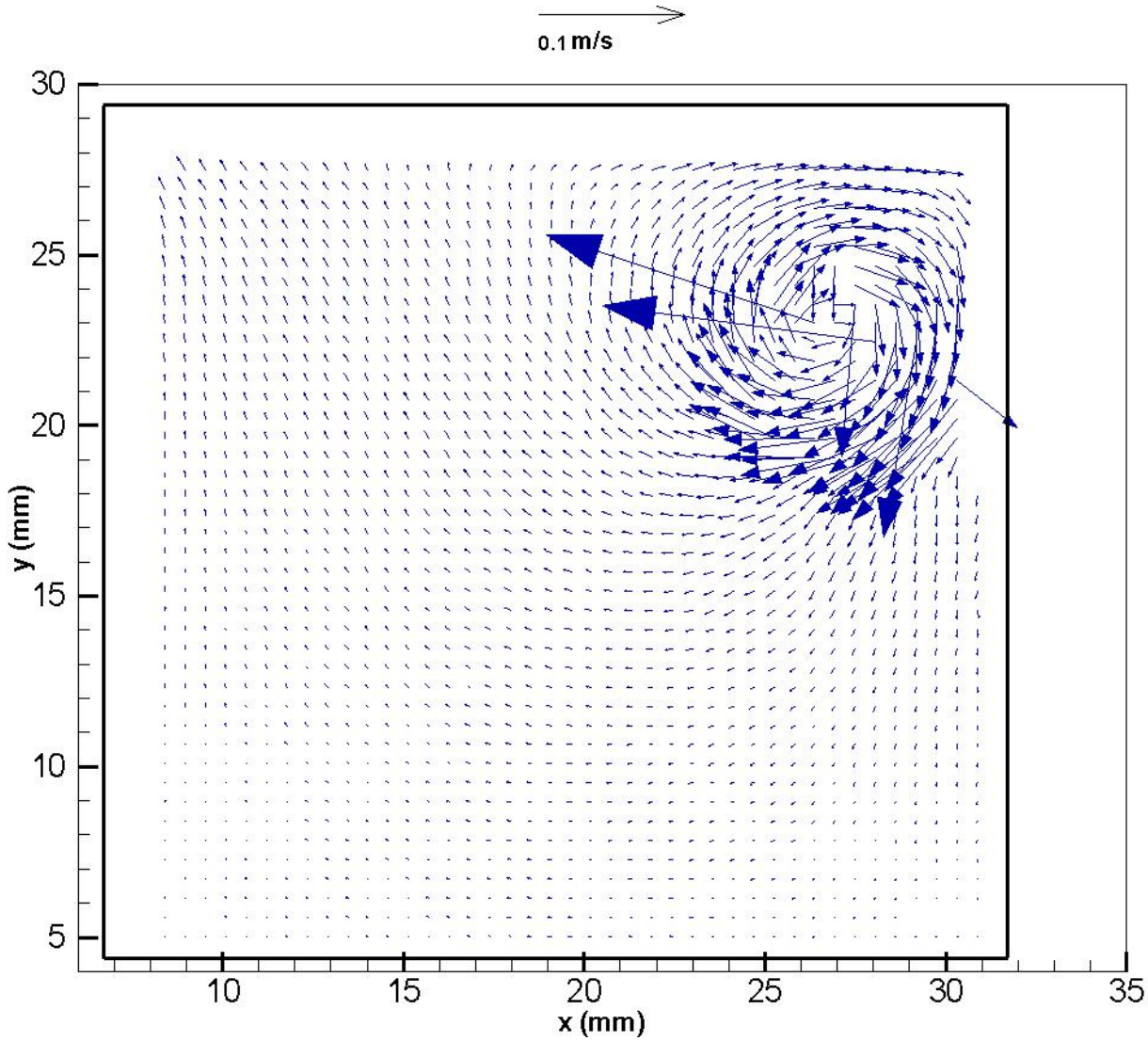

Figure 37- Global Vector Map Experiment 1 Run 4 (Re=1250) at Time 0.69 Seconds Processed Using Fast Fourier Transformation Correlator.

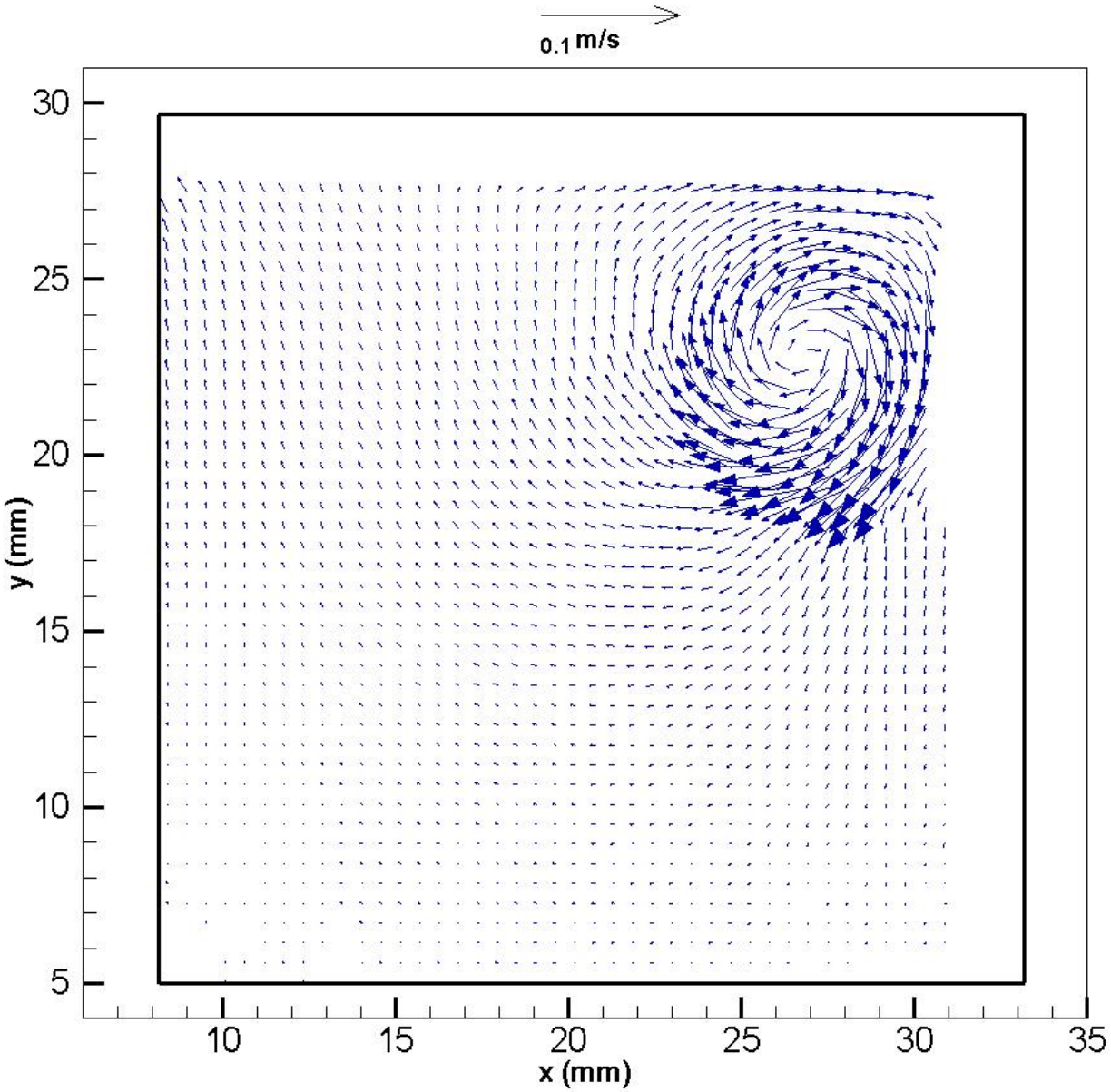

Figure 38- Global Vector Map Experiment 1 Run 4 (Re=1250) at Time 0.69 Seconds Processed Using Hart Correlator.

A visual inspection of the Figs. 36-38 shows that Harts Correlation is the proper choice for the correlation engine, as the other correlation engines yielded incorrect vectors. Next the grid engine was evaluated for optimal results. The grid engine breaks the input images into smaller spots for processing. As stated Nyquist Grid was used as the constant setting for the correlation engine evaluation, so Rectangular grid and Recursive Nyquist Grid are shown in Fig. 39 and Fig 40 respectively. Again All correlations were performed with the same spot dimensions, 64 by 64 pixels, the same overlay 35%, no mask for spot engine masking, and Guassian Peak for the Peak engine.

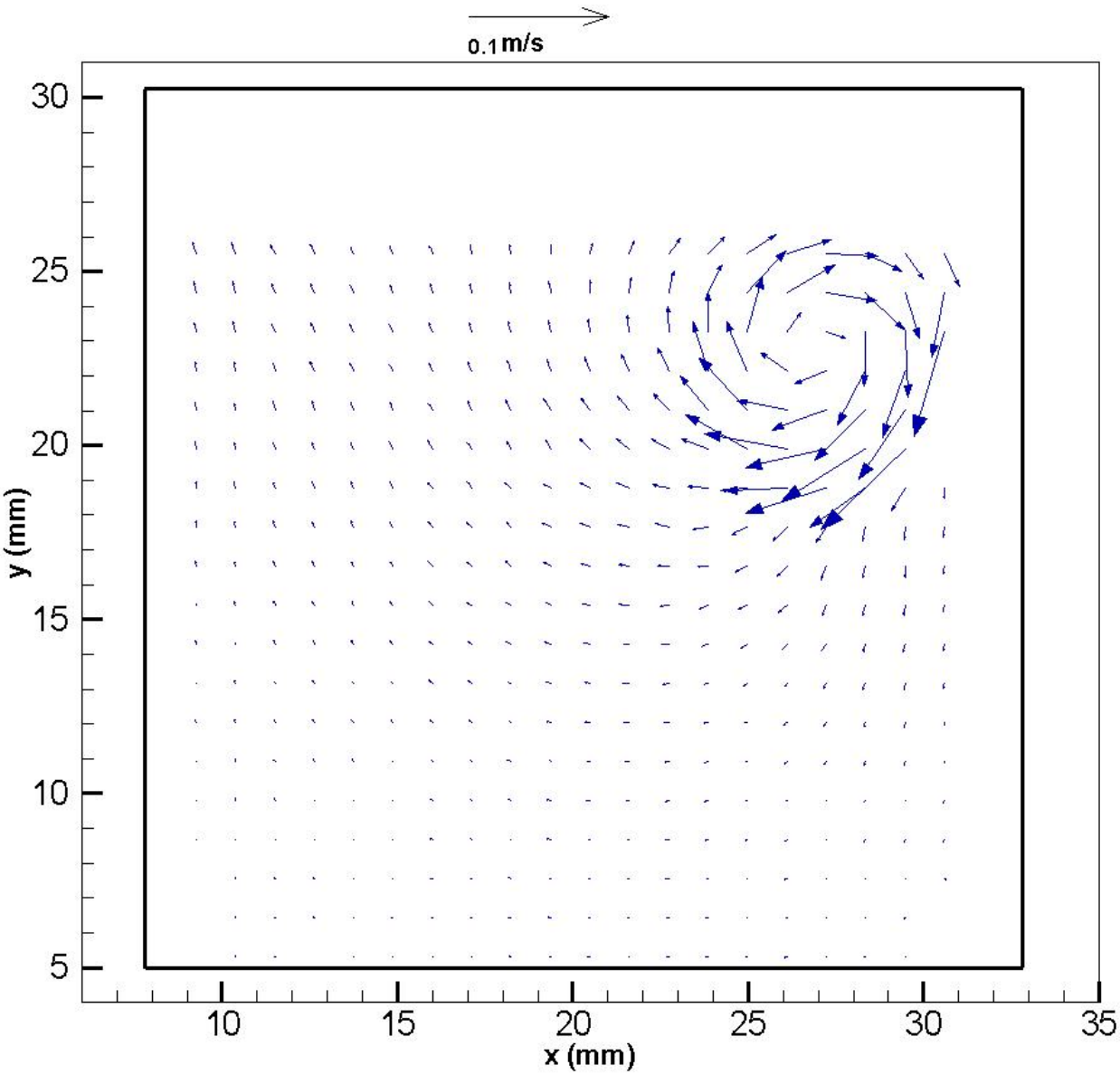

Figure 39- Global Vector Map Experiment 1 Run 4 (Re=1250) at Time 0.69 Seconds Processed Using Rectangular Grid.

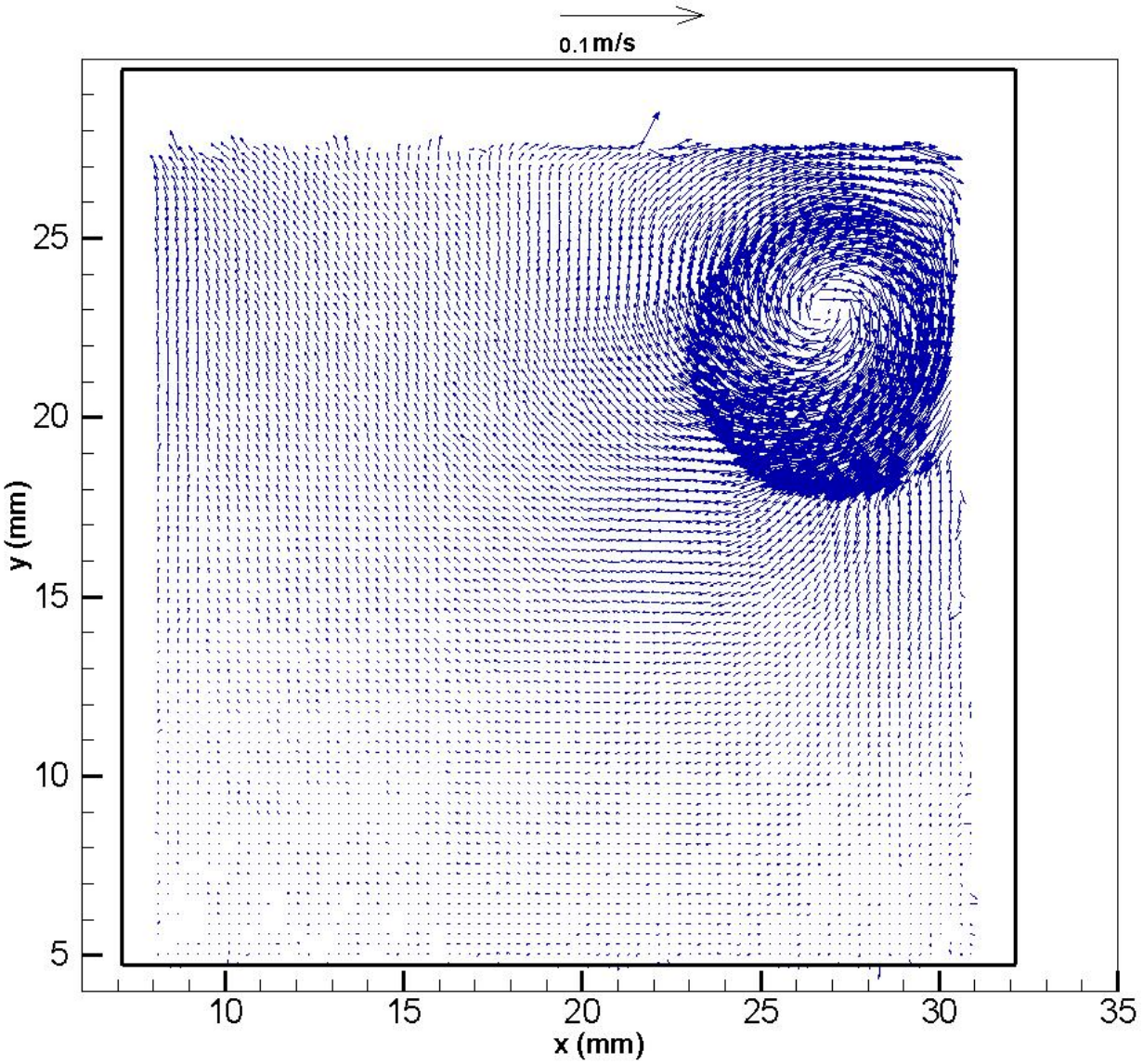

Figure 40- Global Vector Map Experiment 1 Run 4 (Re=1250) at Time 0.69 Seconds Processed Using Recursive Nyquist Grid.

Again based on a visual inspection of the results Nyquist Grid was chosen for the grid engine. The rectangular grid engine of Fig. 39 removed to much information, and the recursive Nyquist Grid added too much as seen in Fig. 40. With Hart Correlator and Nyquist grid fixed as correlation engine and grid engine respectively, the next setting investigated was the spot engine mask. The spot mask engine conditions the image spots created by the grid engine. Three options are available for spot engine mask; no mask, Guassian mask, or zeropad mask. No mask was used as the fixed value in the previous investigations, Guassian mask shown in Fig. 41 and zeropad mask in Fig. 42. Again spot dimensions are 64 x 64 pixels, 35% overlay, and Gaussian Peak engine.

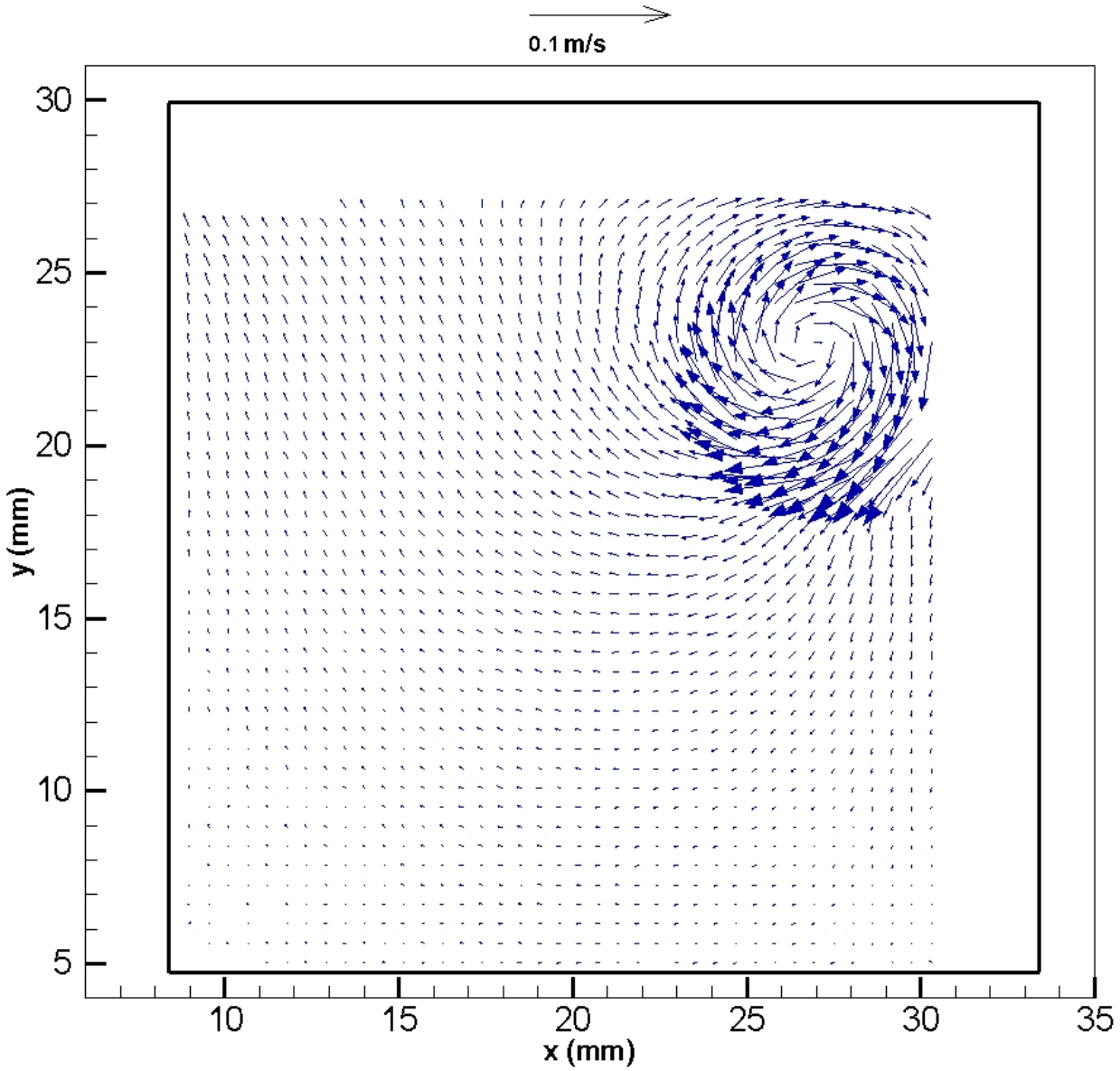

Figure 41- Global Vector Map Experiment 1 Run 4 (Re=1250) at Time 0.69 Seconds Processed Using Gaussian Mask.

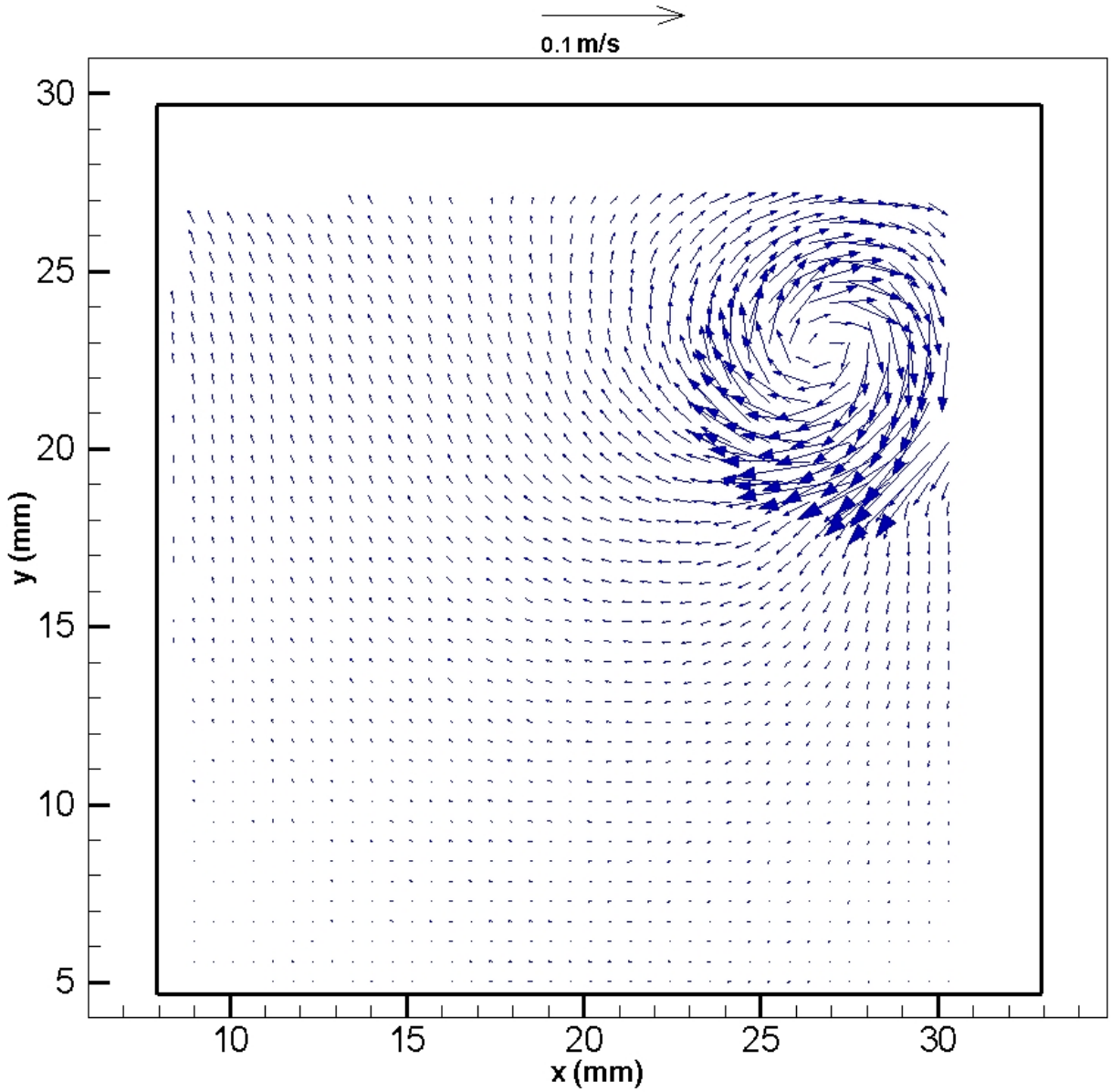

Figure 42- Global Vector Map Experiment 1 Run 4 (Re=1250) at Time 0.69 Seconds Processed Using Zeropad Mask.

Figs. 41 and 42 show thatGaussian and zeropad masks removed some of the near wall vectors so No mask was choosen for spot mask engine. The final PIV engine setting investigated was the peak engine, a validation method comparing peak velocity to neighborhood velocities. The options are Guassian Peak shown in Fig 43, the fixed value used in previous investigations, and bilinear peak shown in Fig 44. Spot dimensions remain 64 x 64 pixels and overlay remains 35%.

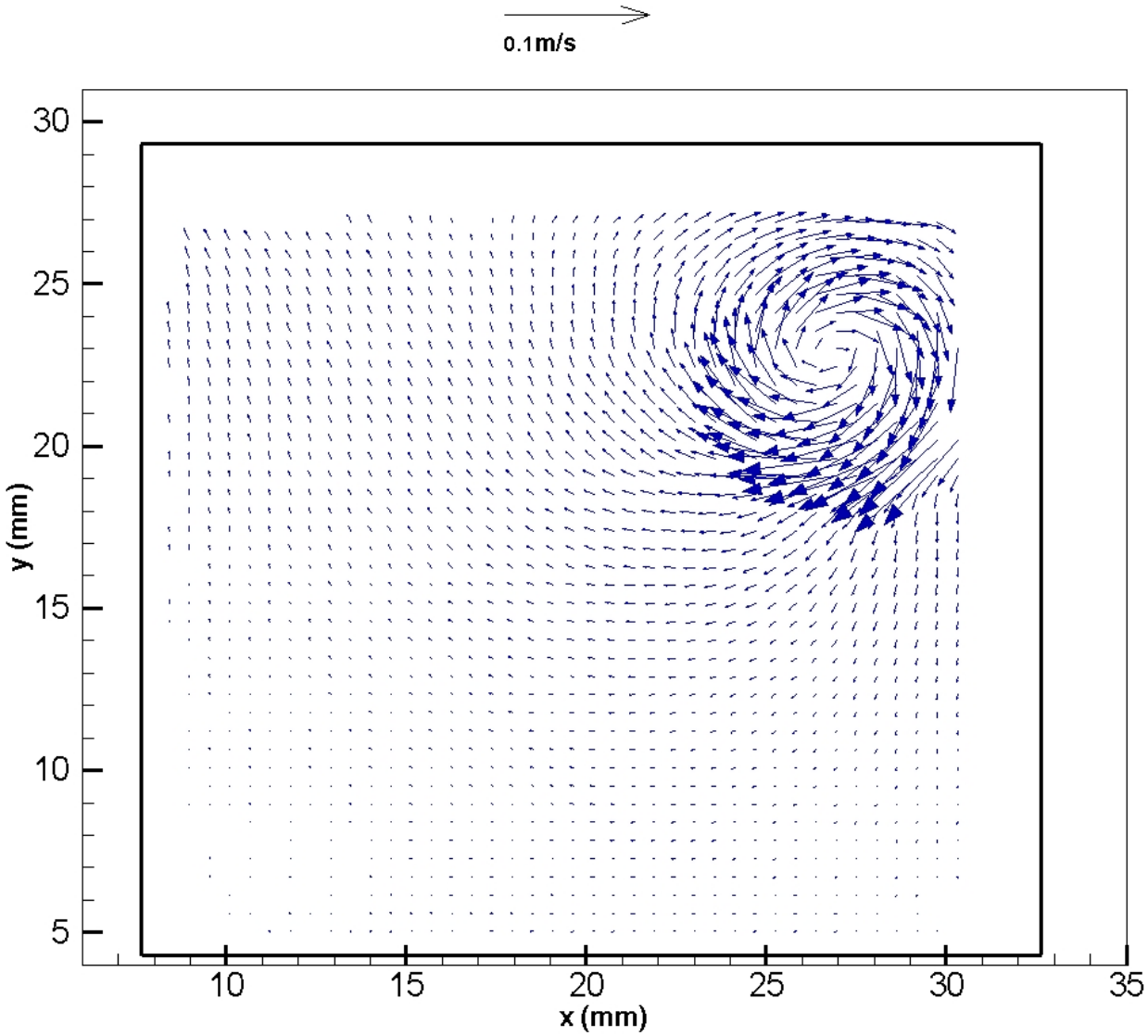

Figure 43- Global Vector Map Experiment 1 Run 4 (Re=1250) at Time 0.69 Seconds Processed Using Guassian Peak.

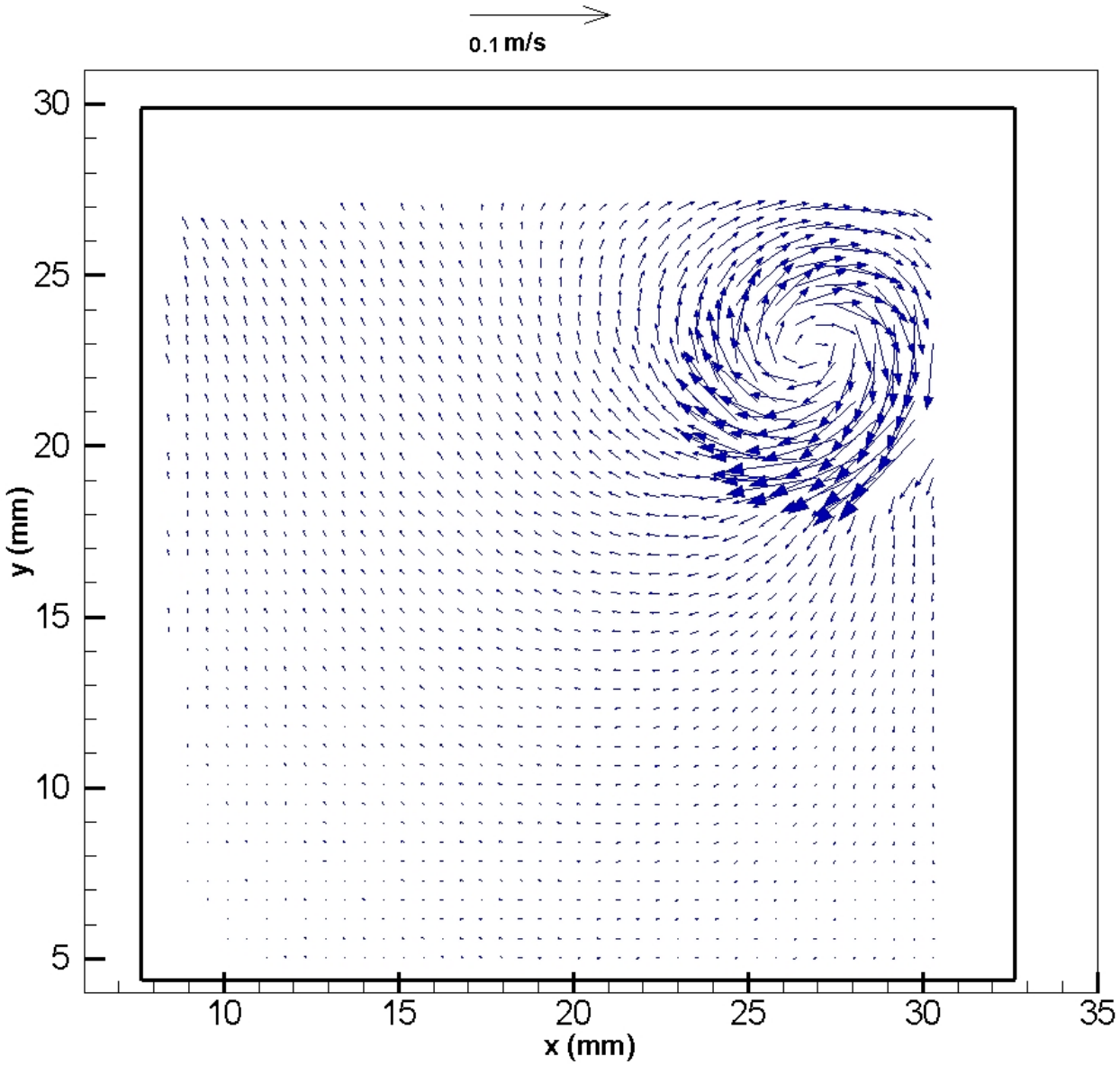

Figure 44- Global Vector Map Experiment 1 Run 4 (Re=1250) at Time 0.69 Seconds Processed Using Bilinear Peak.

Guassian peak was chosen as bilinear peak removed some vectors in the circulation as shown in Fig. 44. The PIV processor engine values are now fixed with Hart Correlatror for correlation engine, no mask for spot mask engine, Nyquist Grid for grid engine, and Guassian peak for peak engine. The spot dimensions also know as interrogation area is now investigated. This is the size of the area in which spots, or seeding particles, will be compared. A spot dimesion of 64 by 64 pixels, which was used as the fixed value for the plugin engine settings and can be seen in fig 45, and 32 by 32 pixels as shown in fig 46.

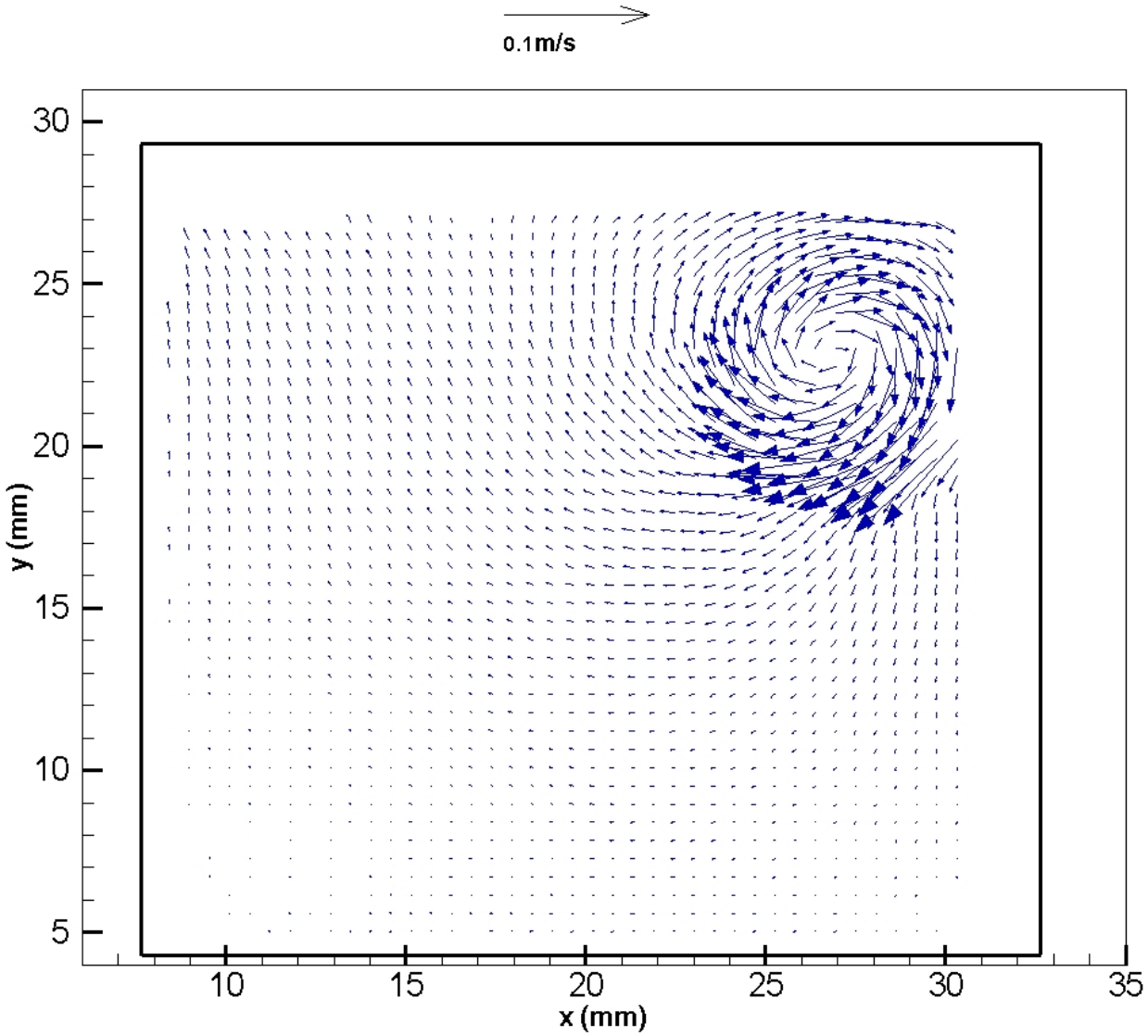

Figure 45- Global Vector Map Experiment 1 Run 4 (Re=1250) at Time 0.69 Seconds Processed Using 64 x 64 Pixel Spot Dimensions.

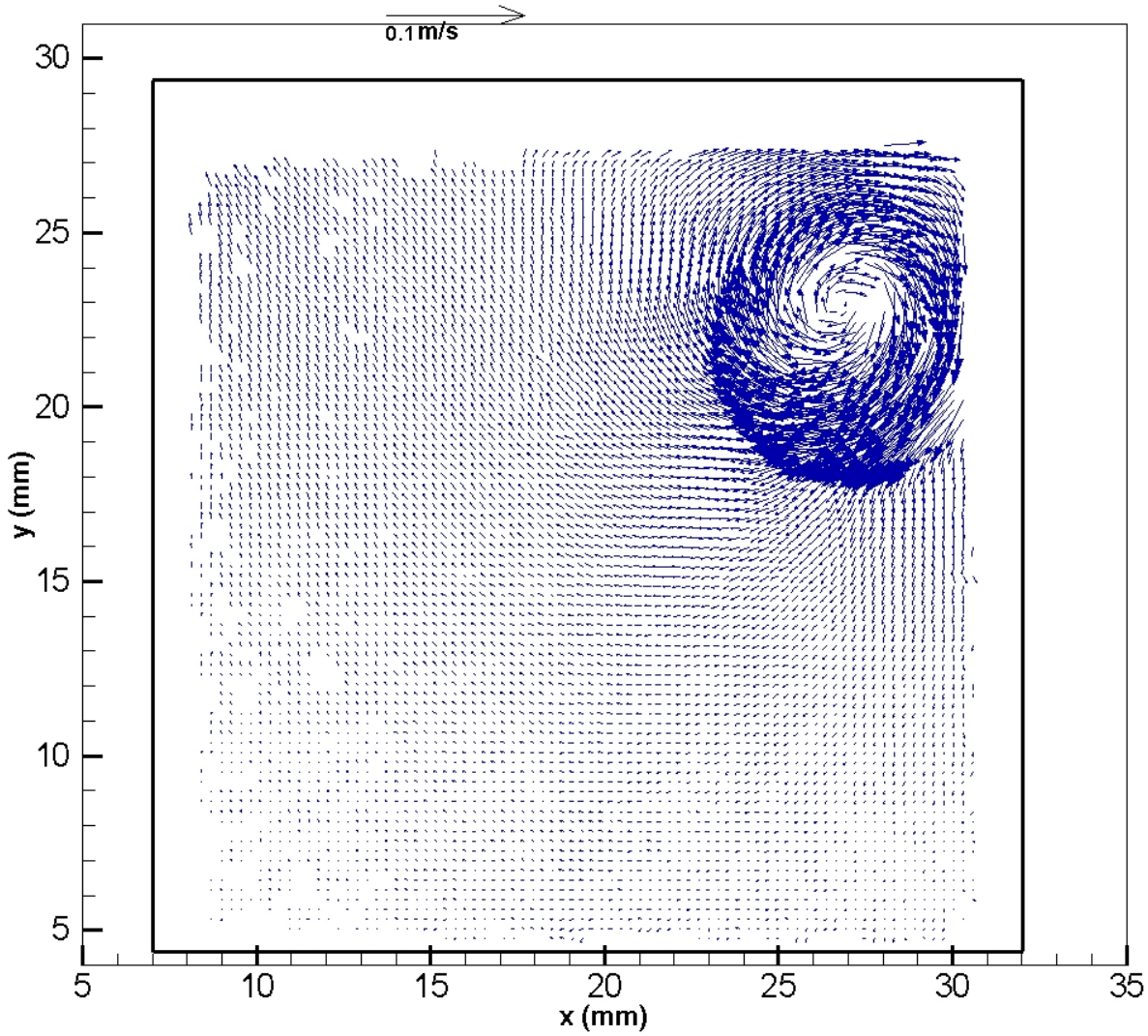

Figure 46- Global Vector Map Experiment 1 Run 4 (Re=1250) at Time 0.69 Seconds Processed Using 32 x 32 Pixel Spot Dimensions.

Spot dimensions when fixed at 32 x 32 pixels as the lower setting gave too much information as seen in Fig. 46. The final value investigated was the over lay, or the amount the interrogation area will be overlaid with the next interrogation area. The range of possible values is 0.01% to 50%, with a lower value being preferred. As a value of 35% was fixed during the previous parameter investigations, a higher value is not studied. Values shown are 35% in fig 47, 25% in fig 48, 15%in fig. 49 and 5% in fig 50.

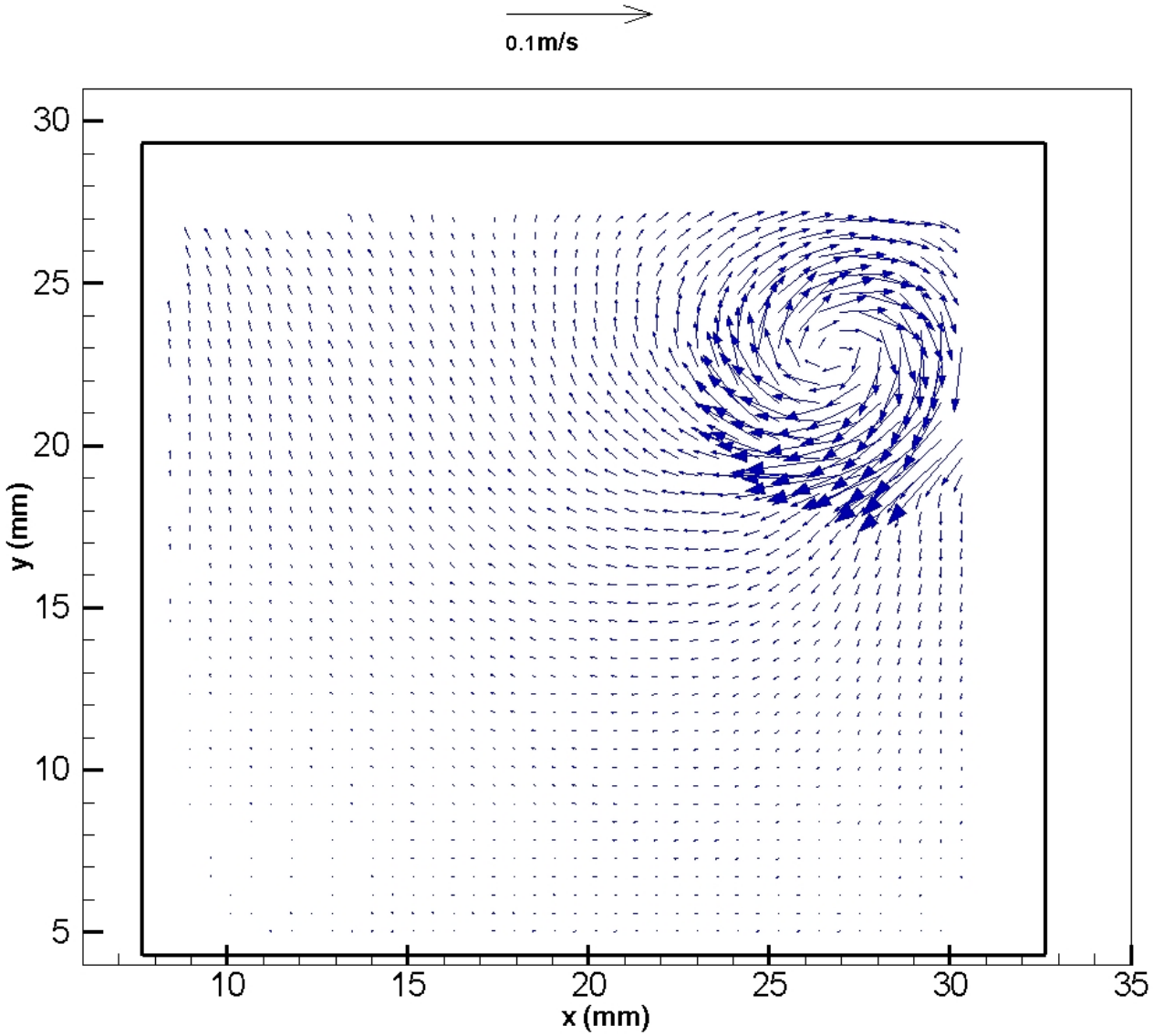

Figure 47- Global Vector Map Experiment 1 Run 4 (Re=1250) at Time 0.69 Seconds Processed Using 35% Overlay.

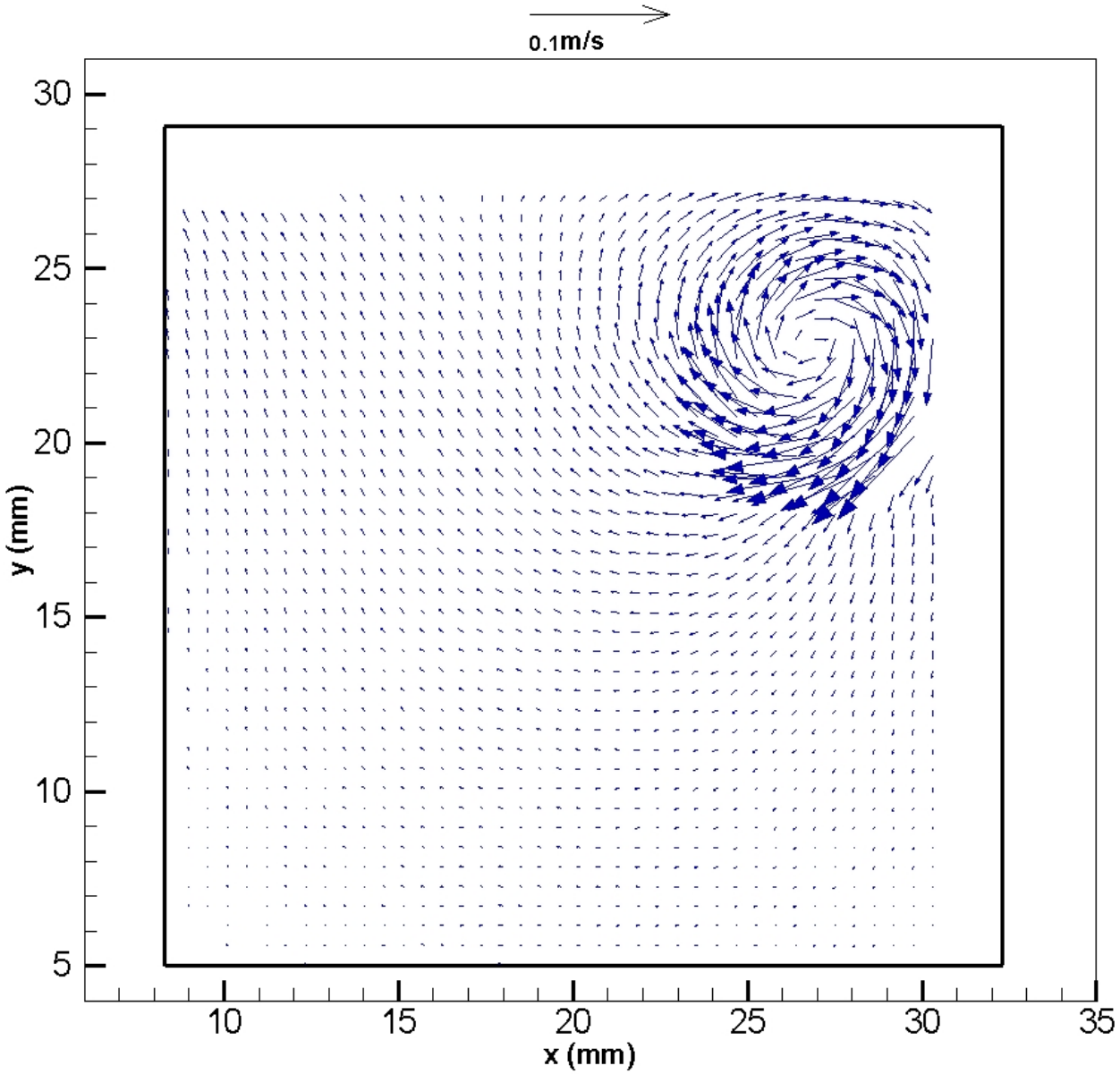

Figure 48- Global Vector Map Experiment 1 Run 4 (Re=1250) at Time 0.69 Seconds Processed Using 25% Overlay.

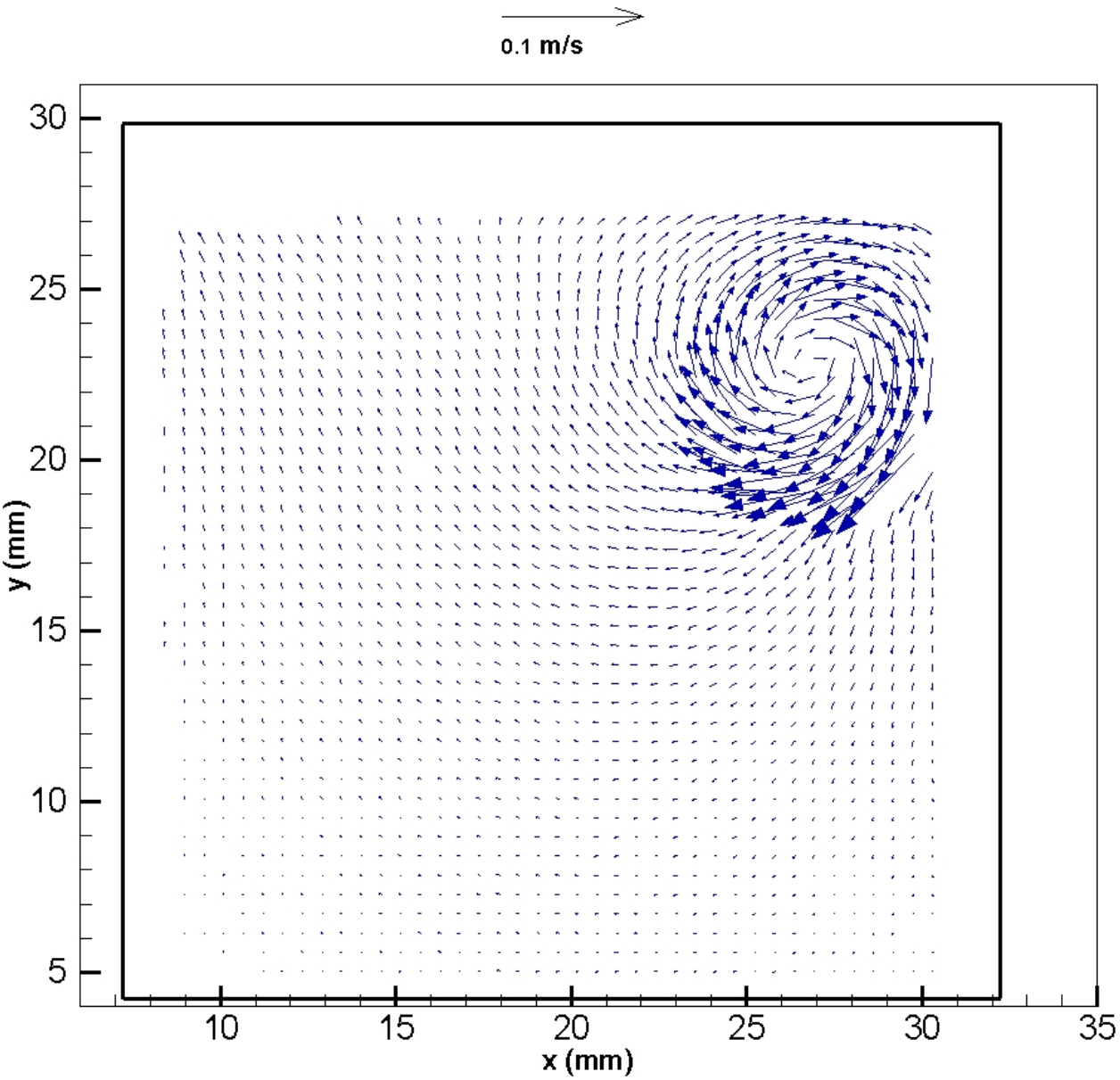

Figure 49- Global Vector Map Experiment 1 Run 4 (Re=1250) at Time 0.69 Seconds Processed Using 15% Overlay.

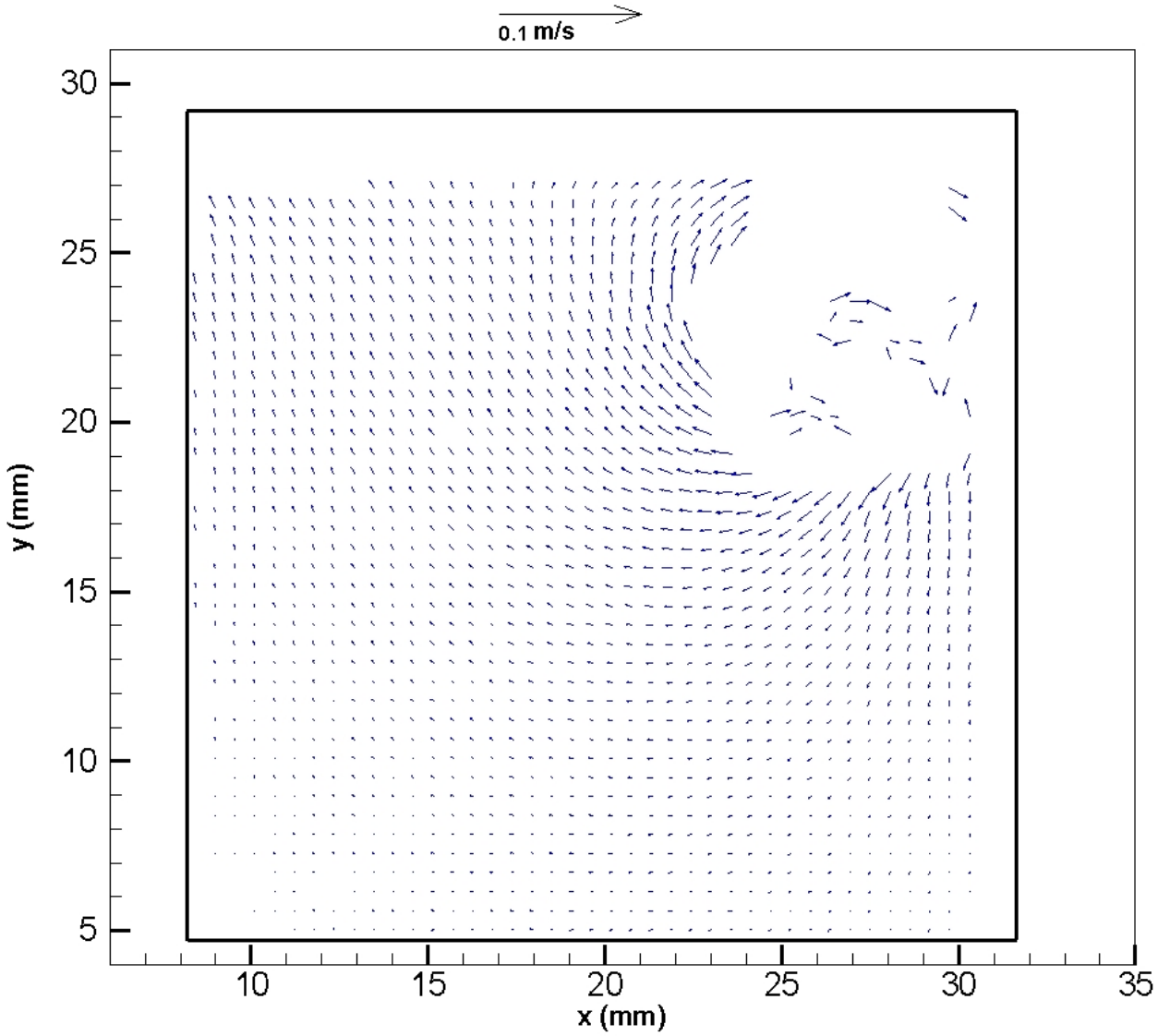

Figure 50- Global Vector Map Experiment 1 Run 4 (Re=1250) at Time 0.69 Seconds Processed Using 5% Overlay.

Studying Figures 48-50 the overlay was chosen to be 15% as it proves to be the lowest overlay that will not remove vectors. The case study led to the PIV capture setting to be set at a repetition rate of 2.90hz, a delta t of 1800 us, and 2000us PIV exposure time. The processor settings are fixed at Hart correlator for correlation engine, Nyquist grid for grid engine, no mask for spot engine mask, bilinear peak for peak engine, 64 x 64 pixel interrogation area with 15% overlay. All further plots are presented with these settings.

The experiment is then repeated at a higher frame rate in Run 5 to show the development in more detail. This is shown in the following figures 51- 70.

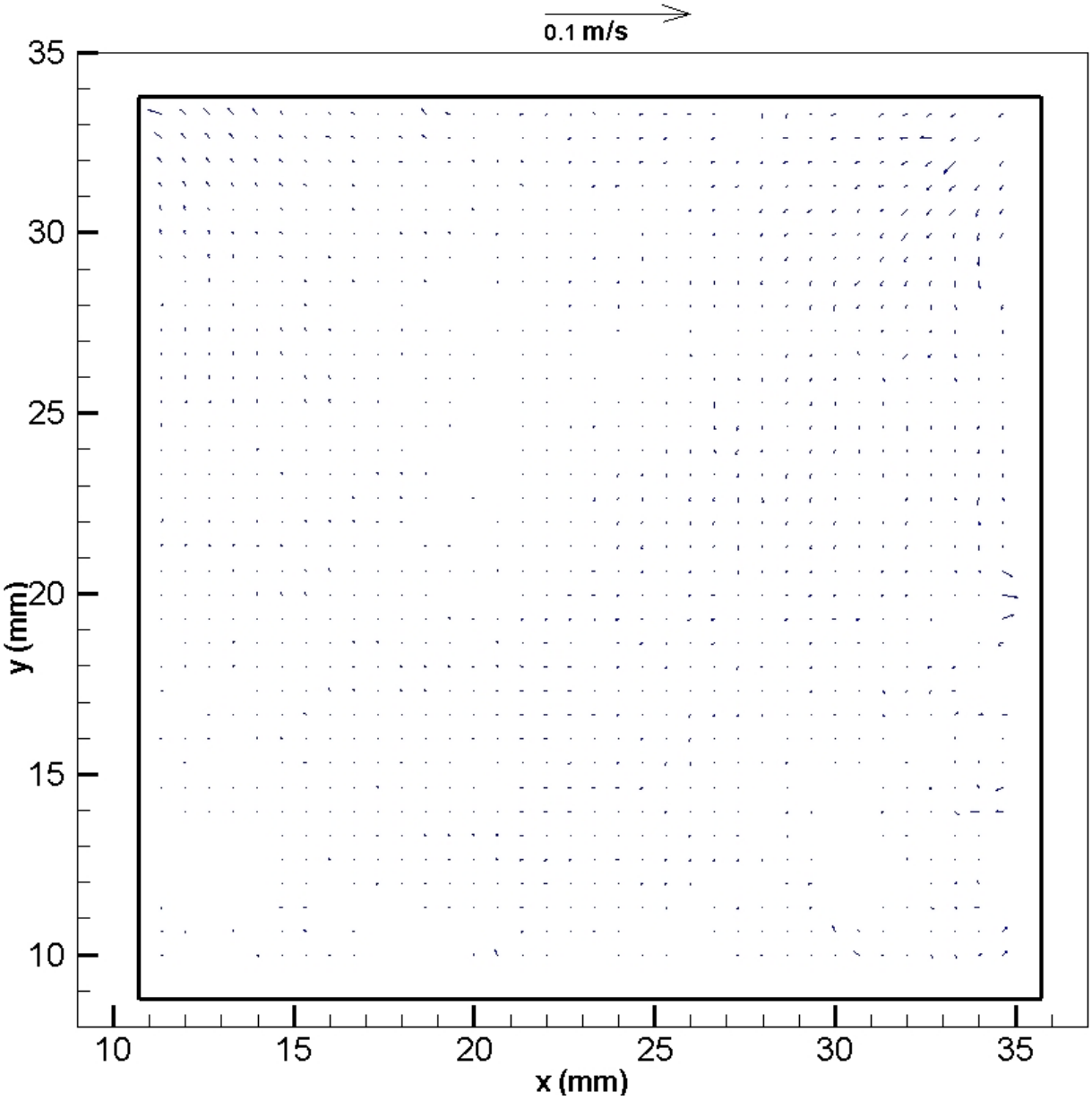

Figure 51- Global Vector Map Experiment 1 Run 5 (Re=1250) at Time t=0 Seconds.

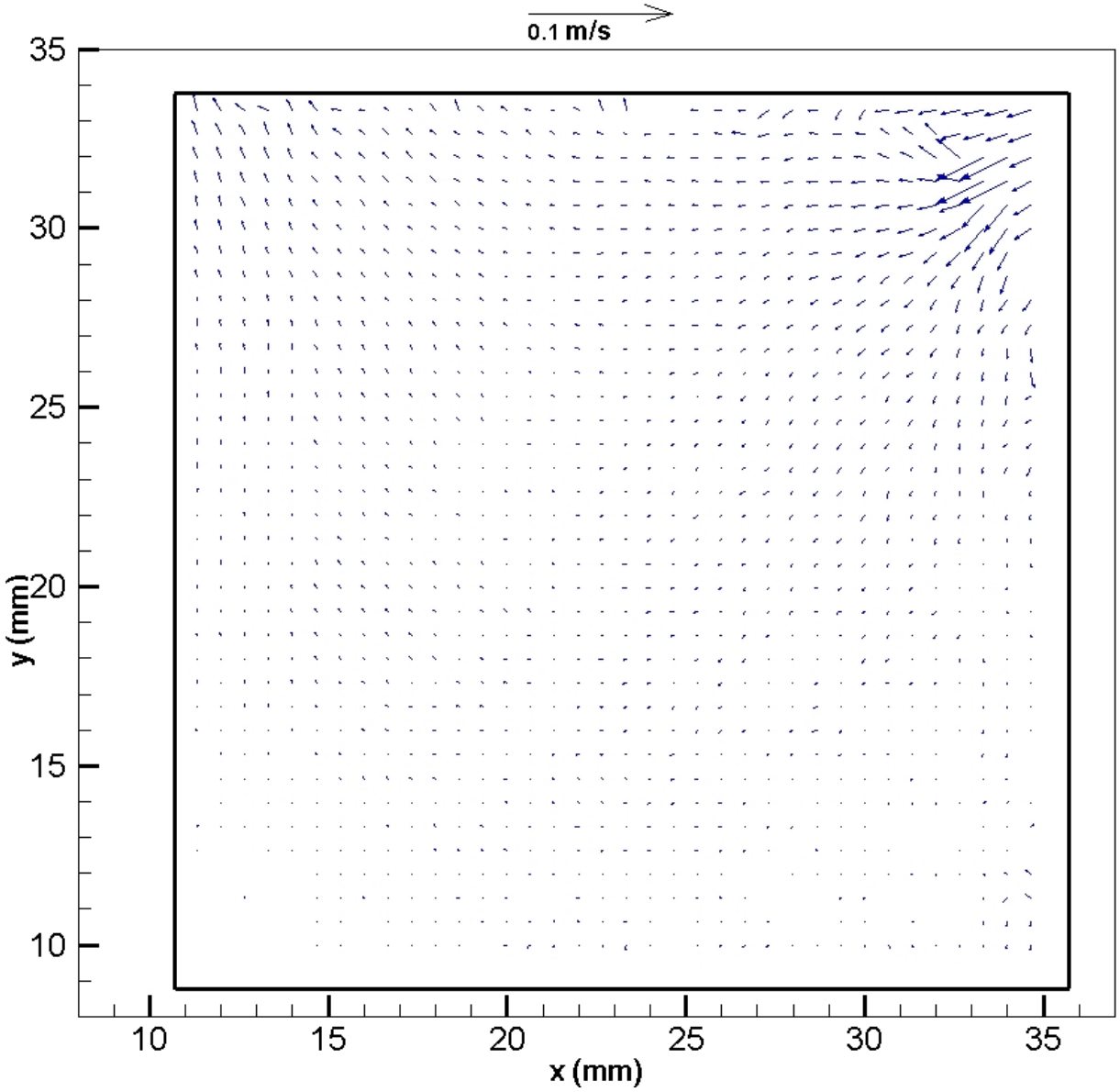

Figure 52- Global Vector Map Experiment 1 Run 5 (Re=1250) at Time t=0.138 Seconds.

In Fig. 52 the top right of the cavity is beginning to become excited and movement is starting to develop.

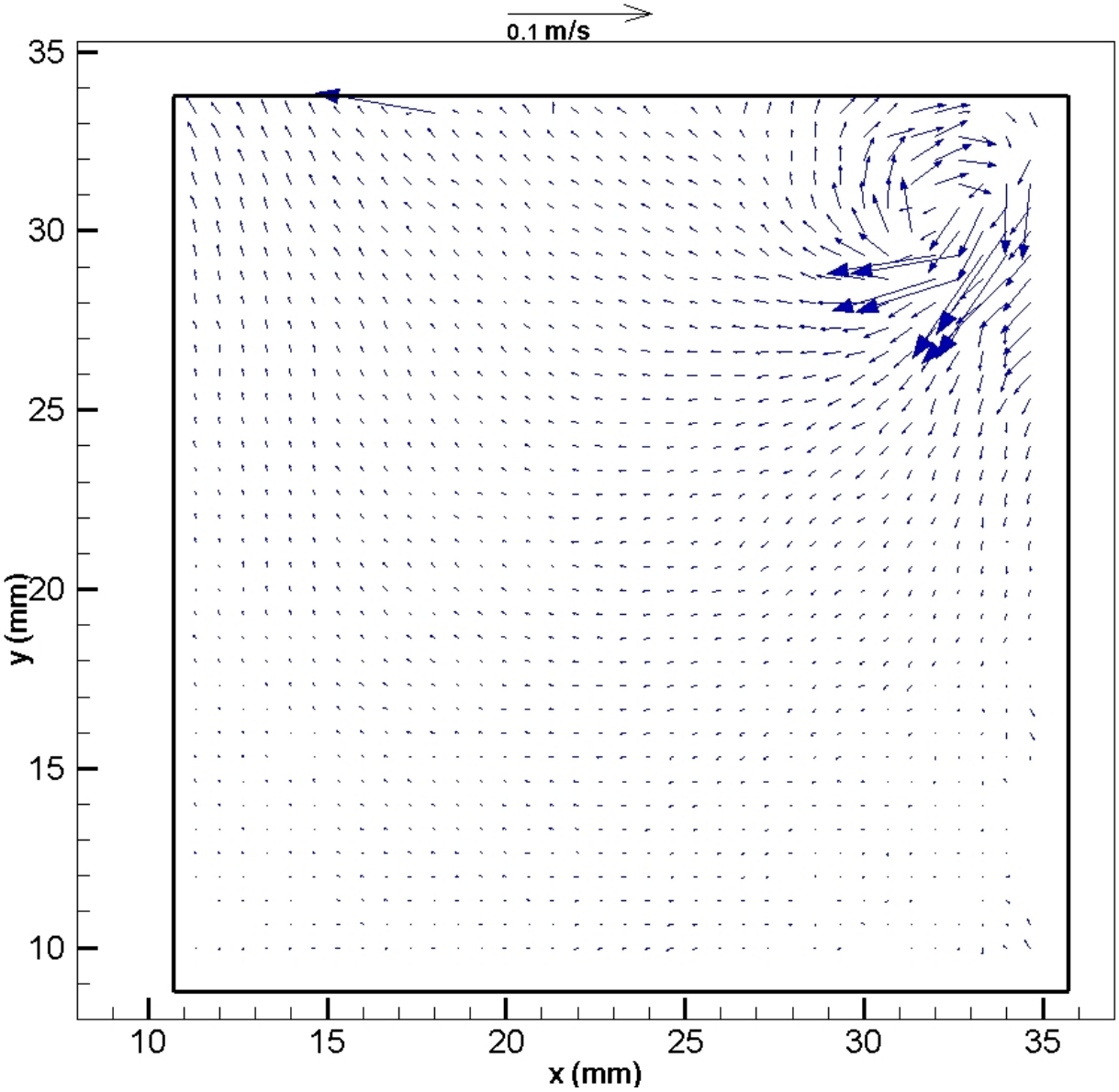

Figure 53- Global Vector Map Experiment 1 Run 5 (Re=1250) at Time t=0.276 Seconds.

In Fig. 53 the movement in the top right corner of the cavity has now become circular as expected.

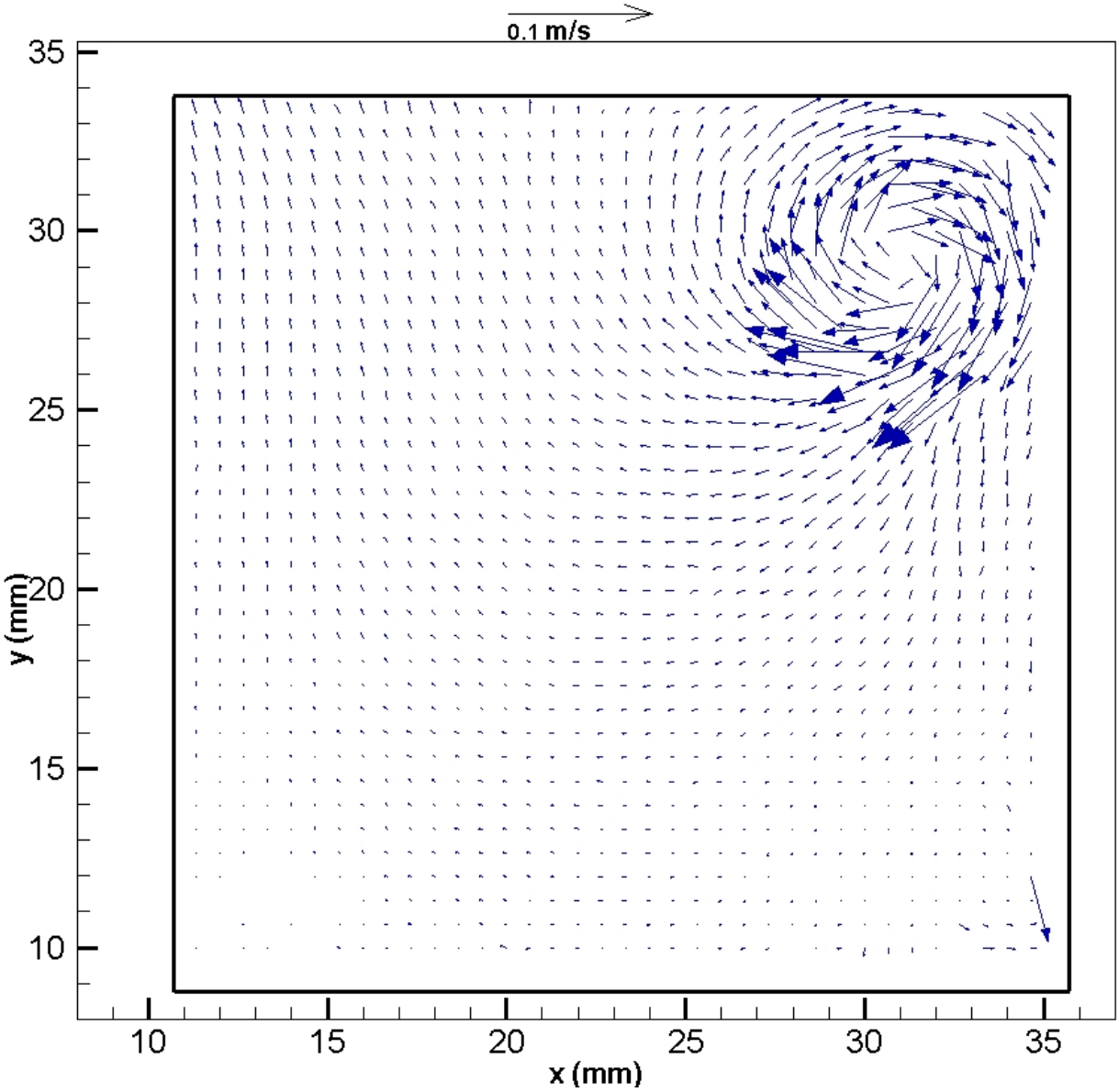

Figure 54- Global Vector Map Experiment 1 Run 5 (Re=1250) at Time t=0.414 Seconds.

In Fig. 54 the circulation has increased in strength and moved left.

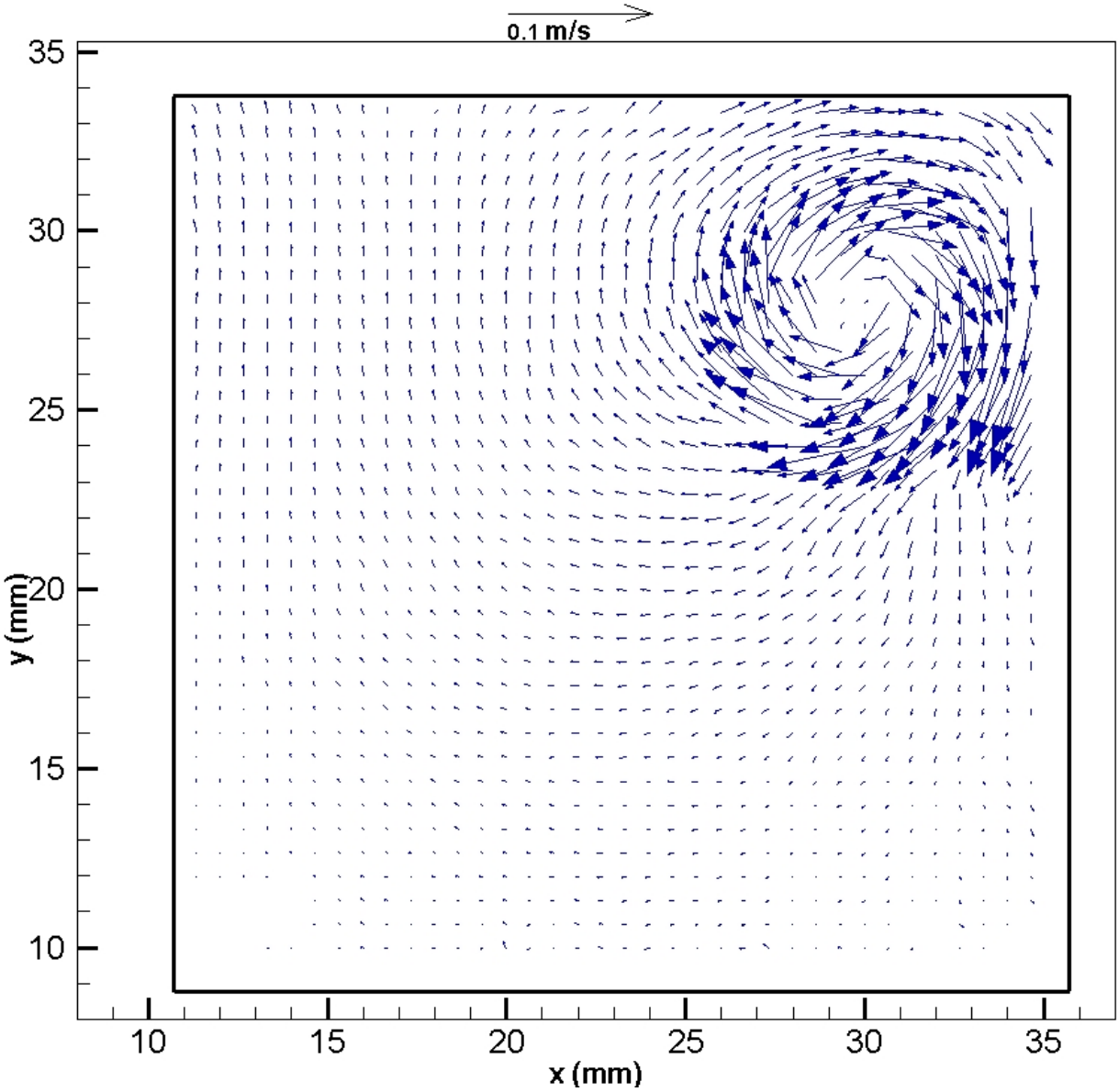

Figure 55- Global Vector Map Experiment 1 Run 5 (Re=1250) at Time t=0.552s Seconds.

In Fig. 55 the circulation continues to increase in strength and movement continues diagonally toward the center of the cavity.

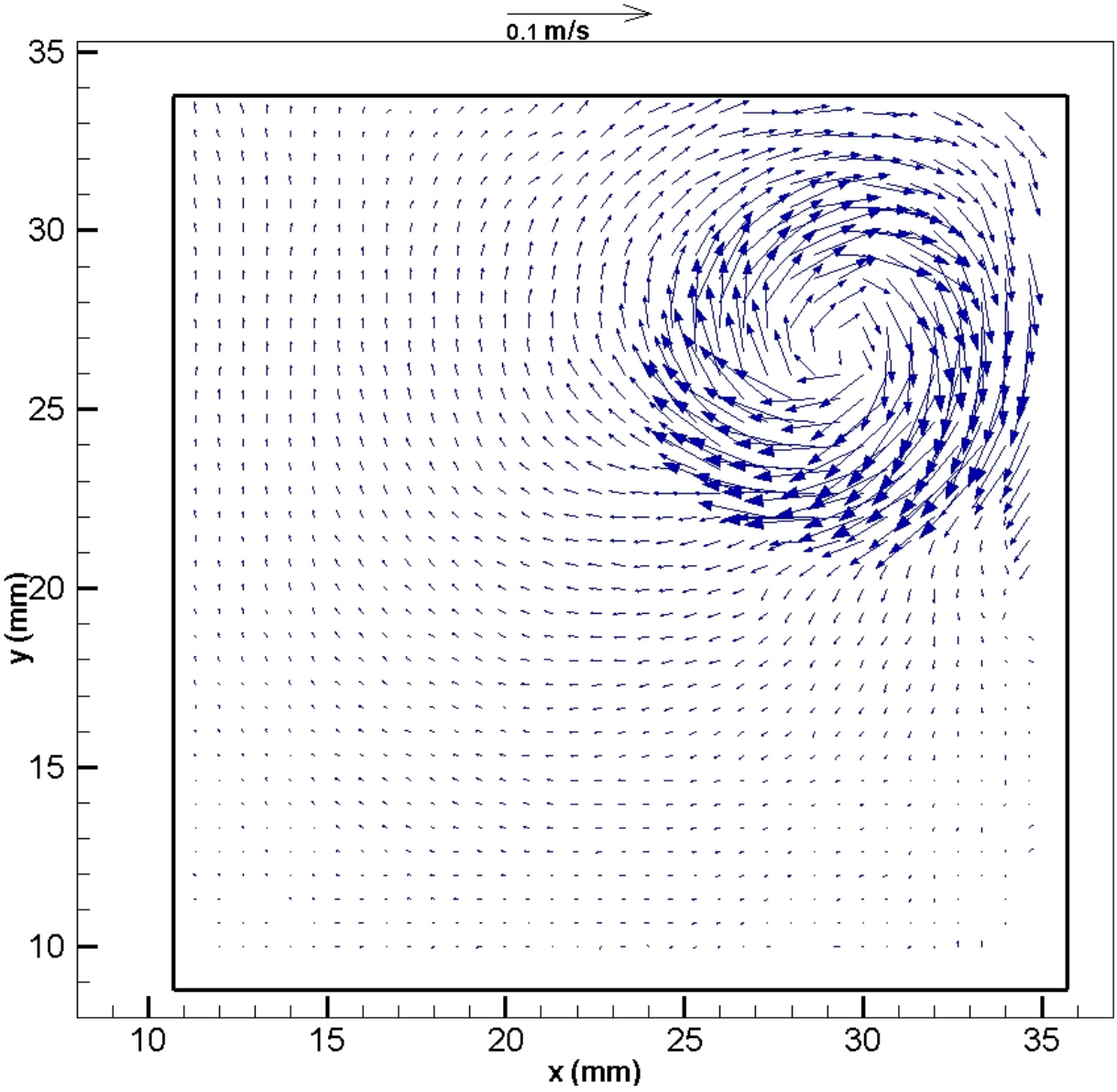

Figure 56- Global Vector Map Experiment 1 Run 5 (Re=1250) at Time t=0.690 Seconds.

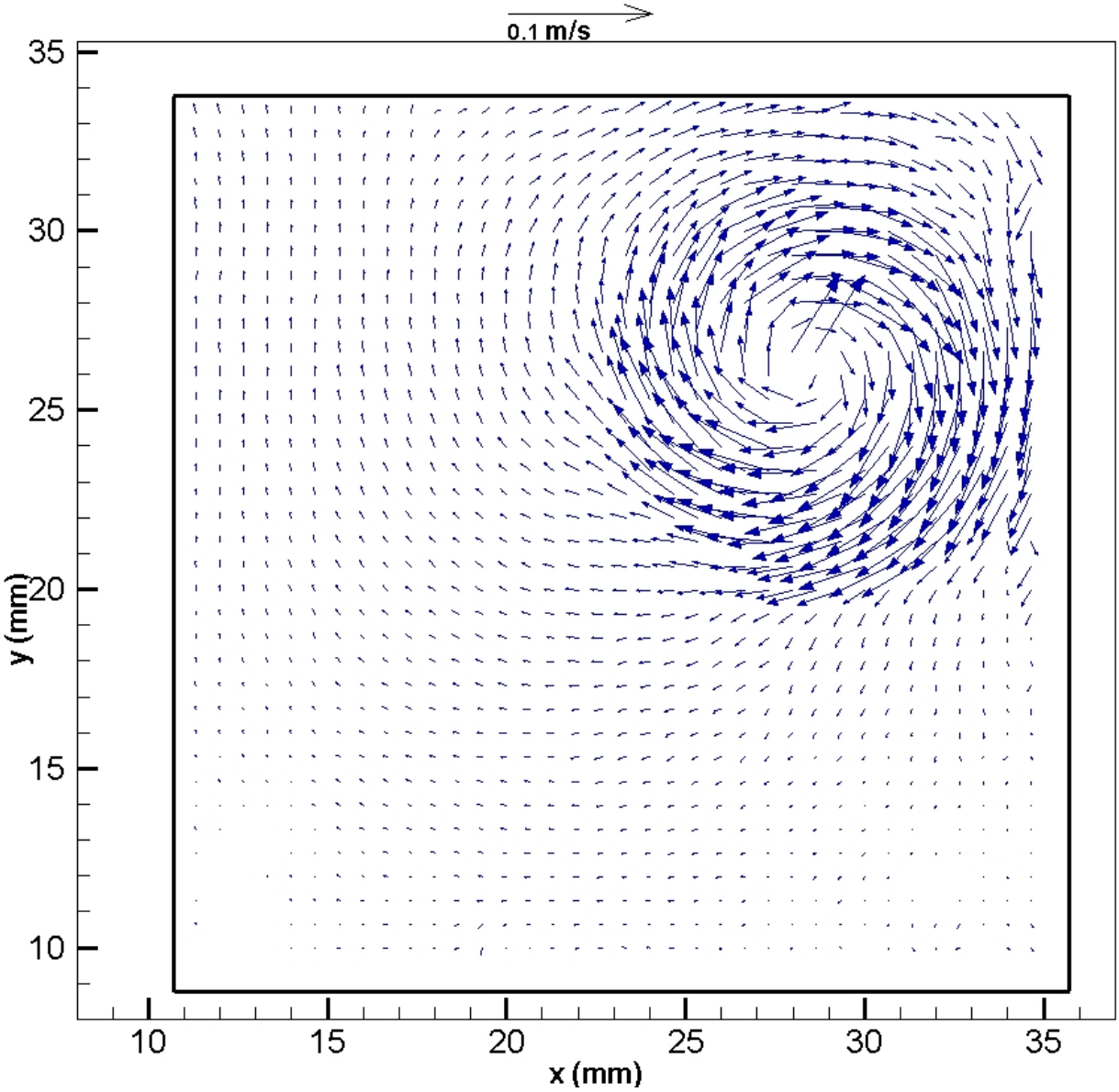

Figure 57- Global Vector Map Experiment 1 Run 5 (Re=1250) at Time t=0.828 Seconds.

.

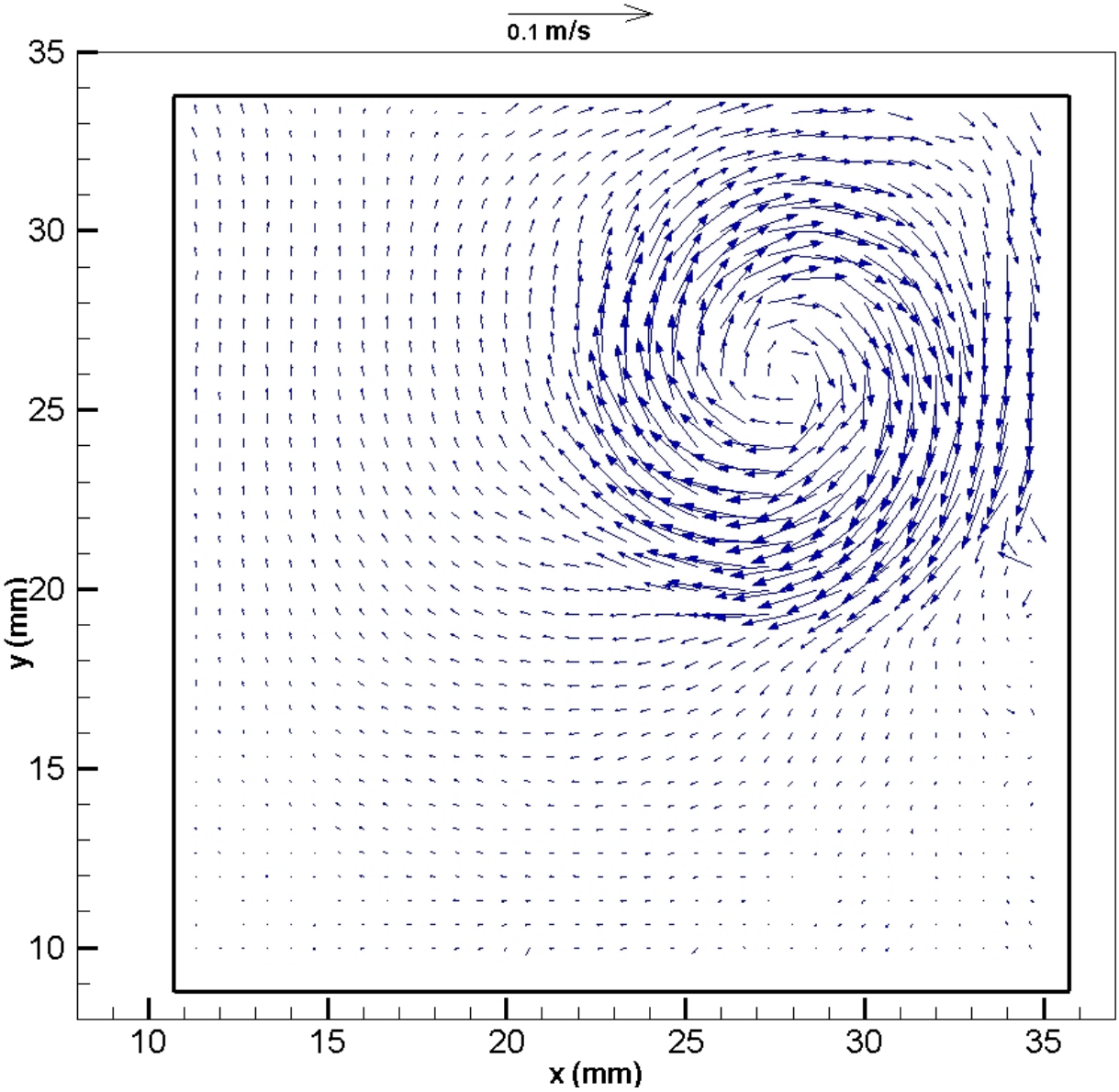

Figure 58- Global Vector Map Experiment 1 Run 5 (Re=1250) at Time t=0.996 Seconds.

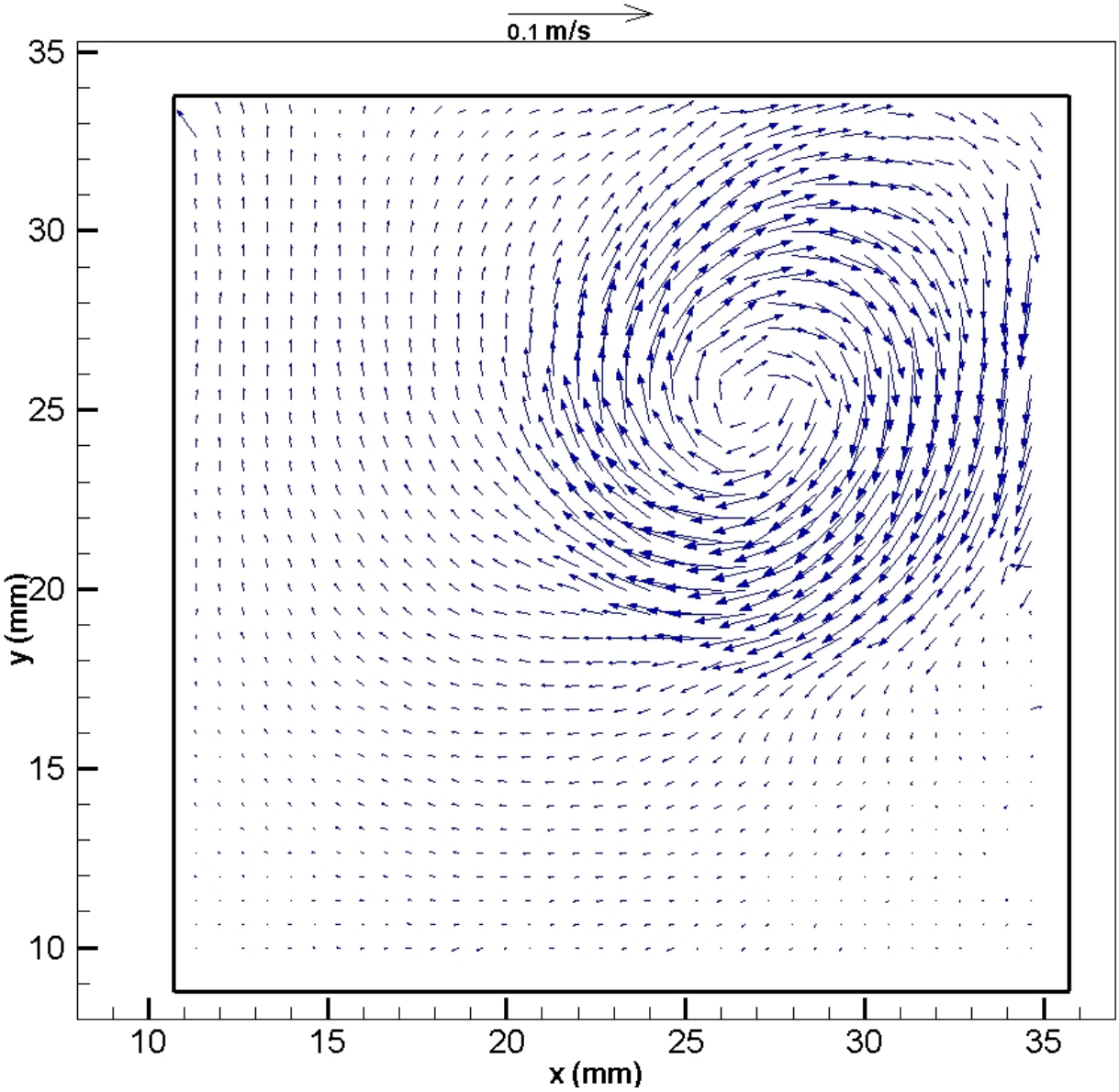

Figure 59- Global Vector Map Experiment 1 Run 5 (Re=1250) at Time t=1.104 Seconds.

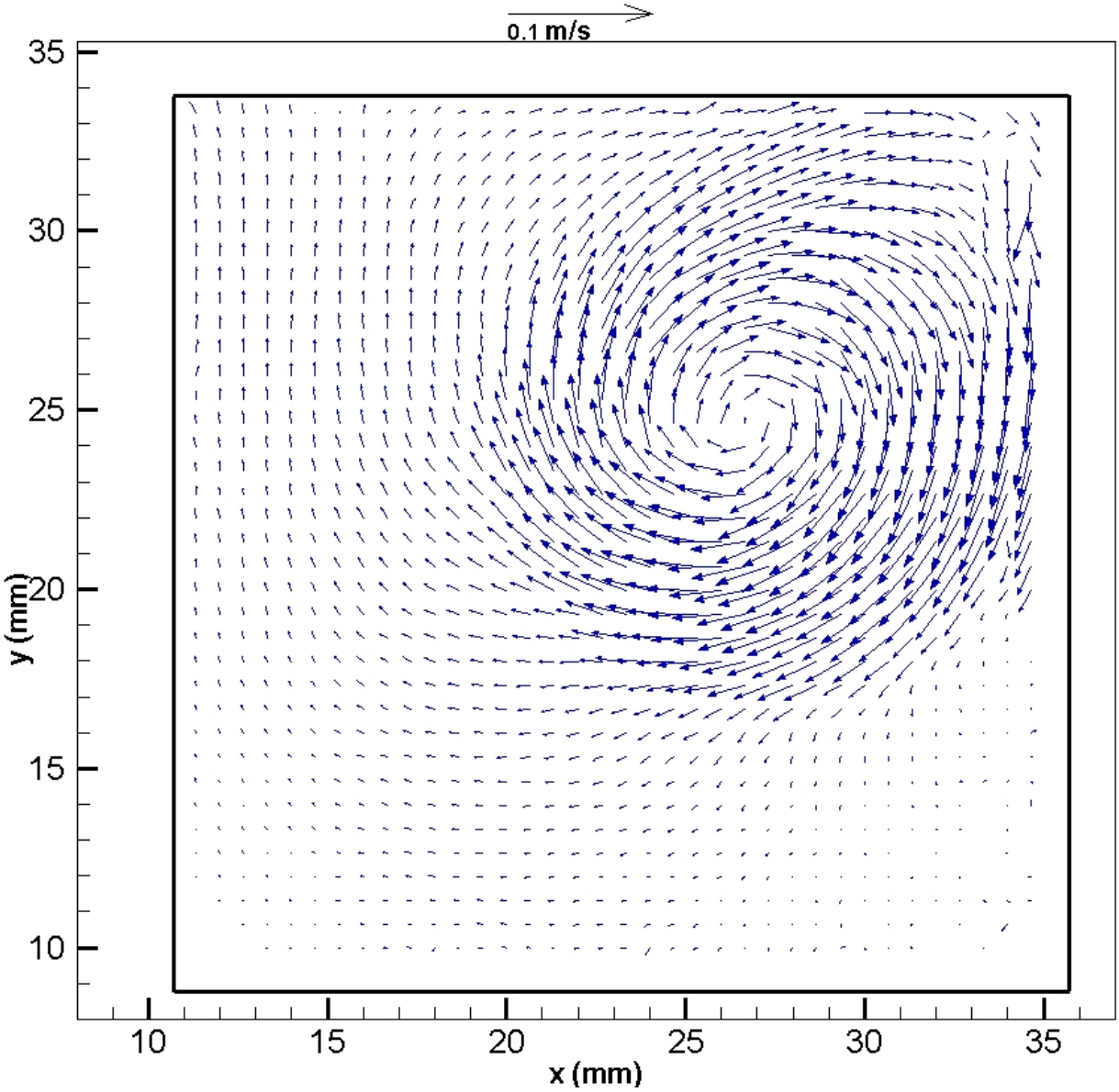

Figure 60- Global Vector Map Experiment 1 Run 5 (Re=1250) at Time t=1.242 Seconds.

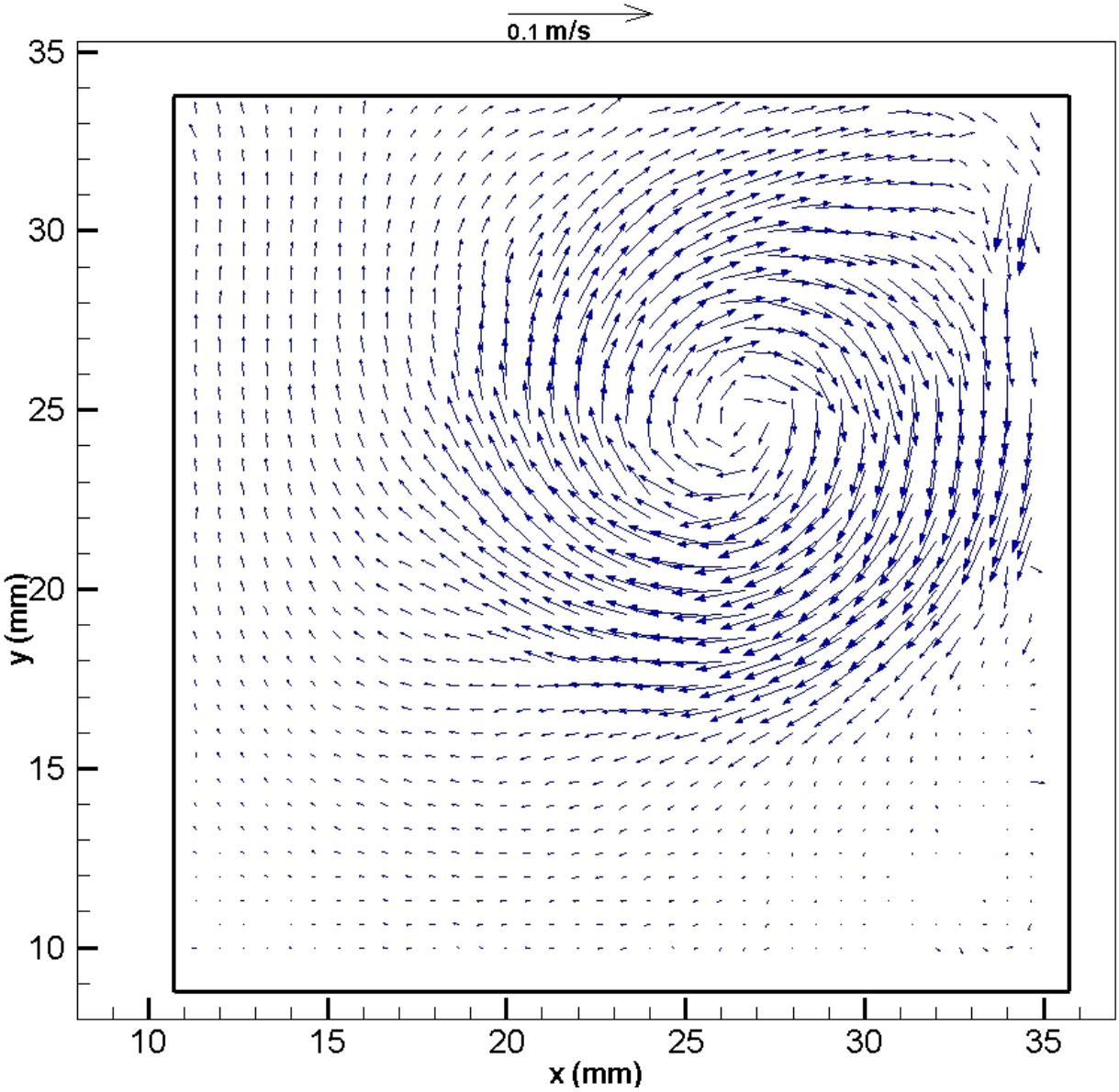

Figure 61- Global Vector Map Experiment 1 Run 5 (Re=1250) at Time t=1.380 Seconds.

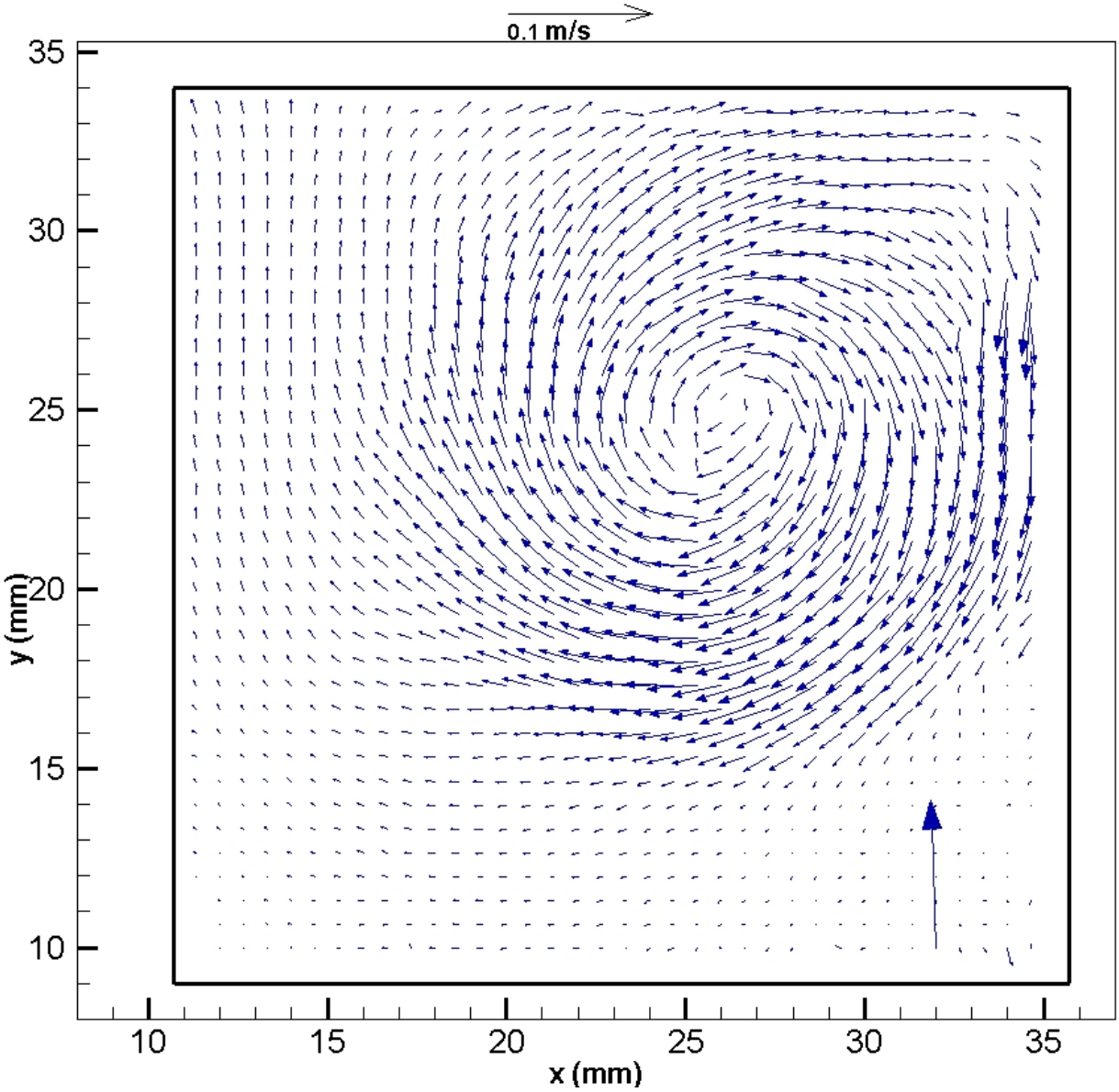

Figure 62- Global Vector Map Experiment 1 Run 5 (Re=1250) at Time t=1.518 Seconds.

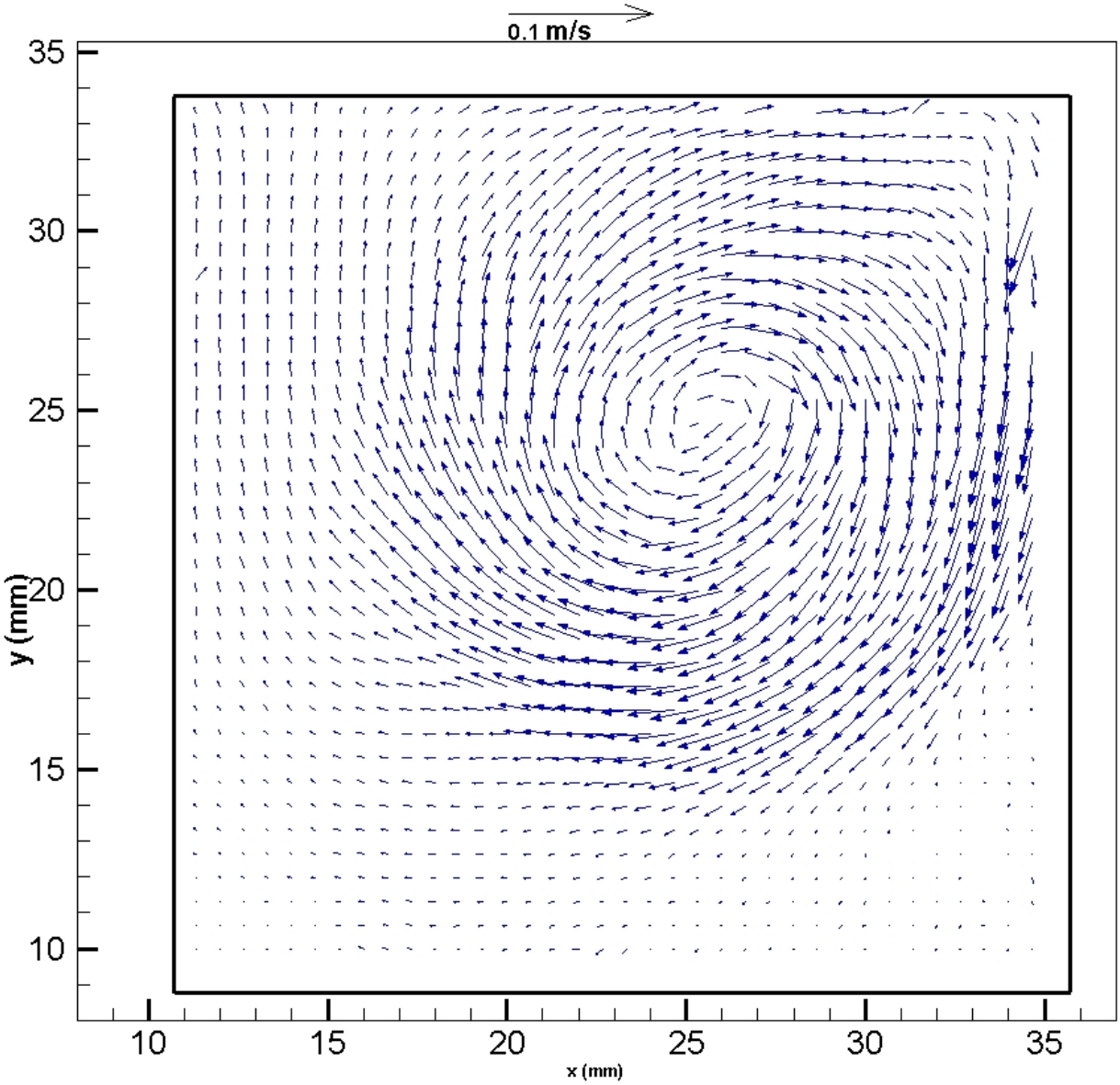

Figure 63- Global Vector Map Experiment 1 Run 5 (Re=1250) at Time t=1.656 Seconds.

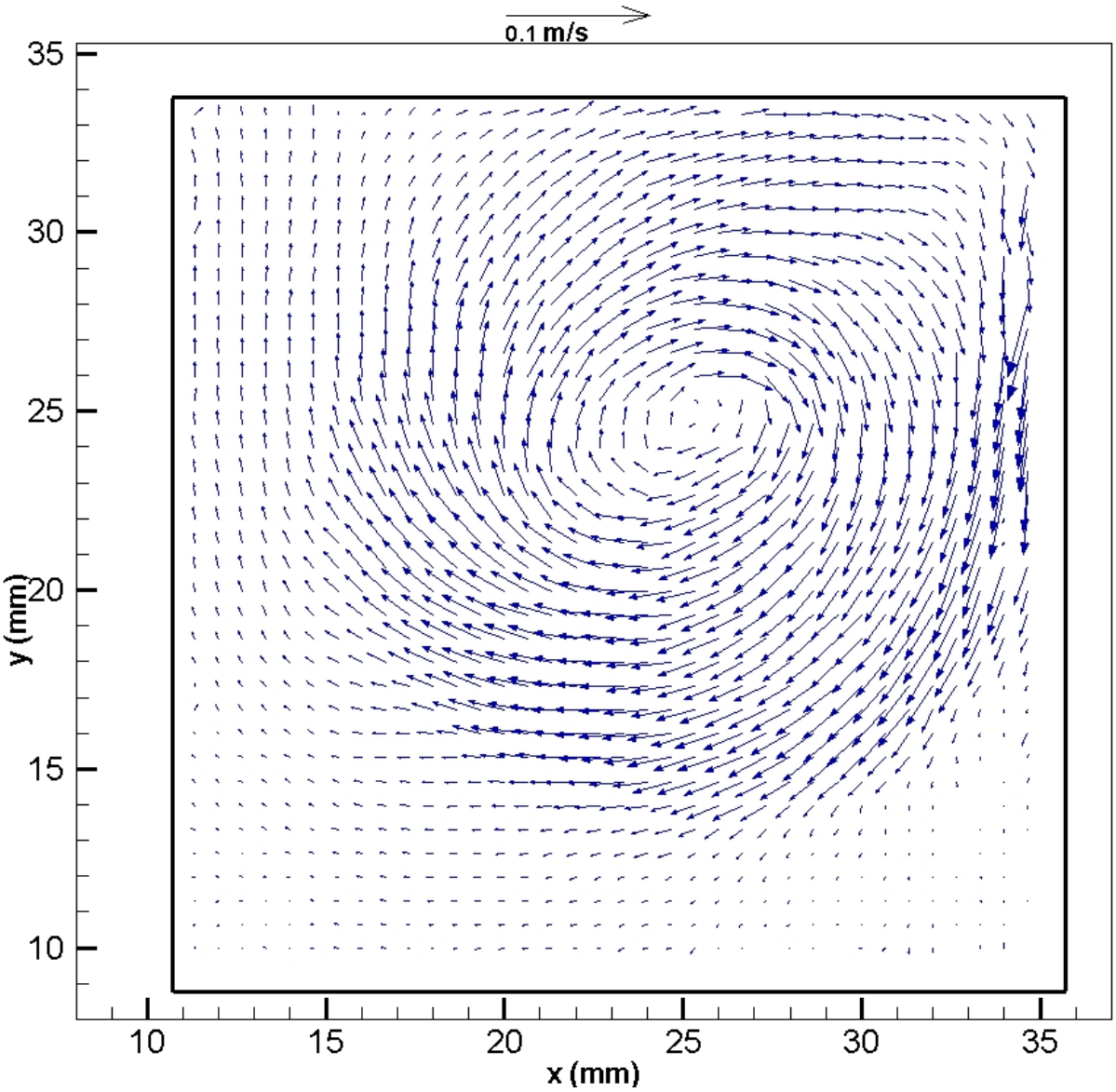

Figure 64- Global Vector Map Experiment 1 Run 5 (Re=1250) at Time t=1.794 Seconds.

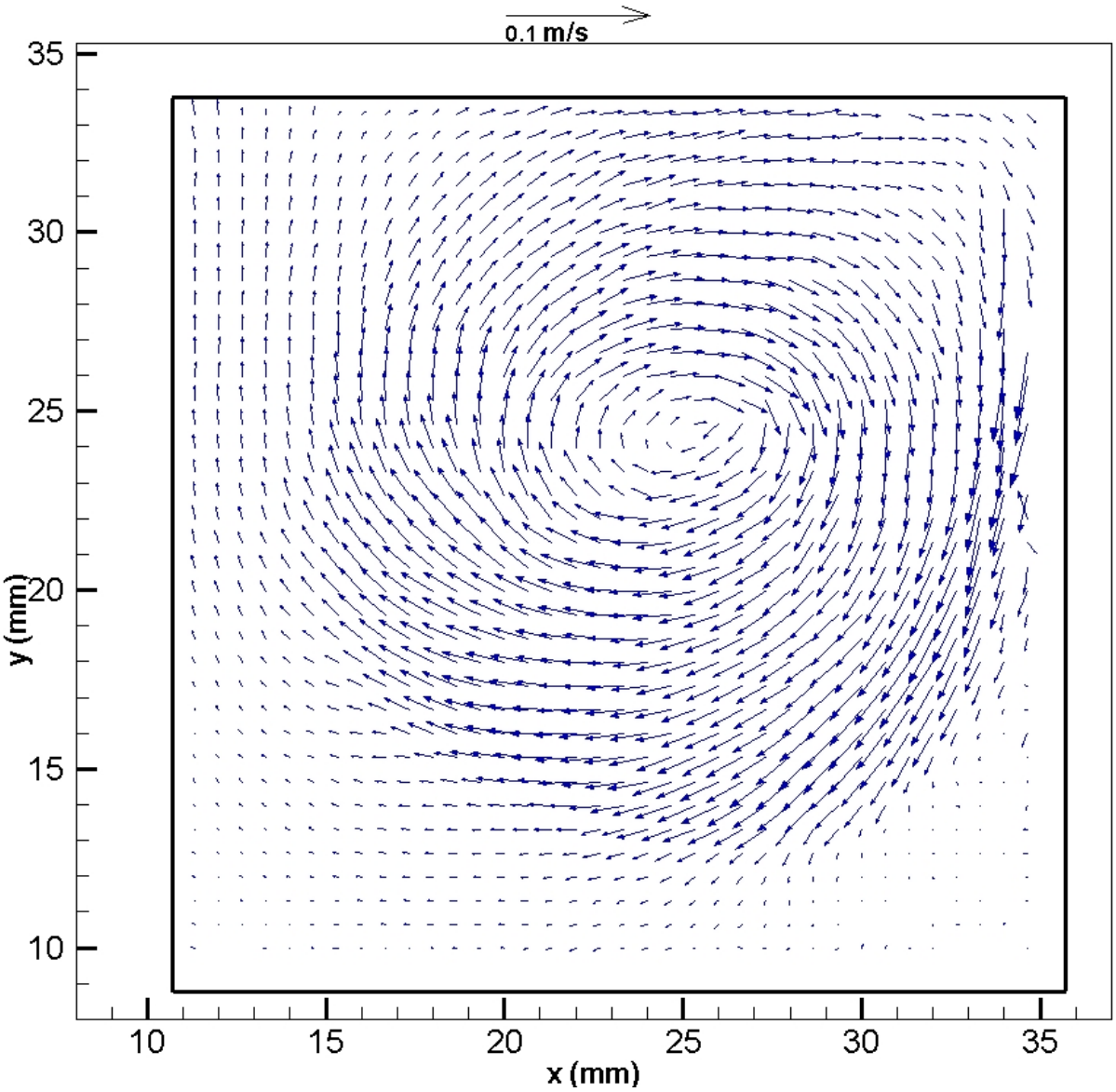

Figure 65- Global Vector Map Experiment 1 Run 5 (Re=1250) at Time t=1.932 Seconds.

In Figs 56-65 the circulation continues to increase in strength. The center of the circulation continues to move toward the center of the cavity as well.

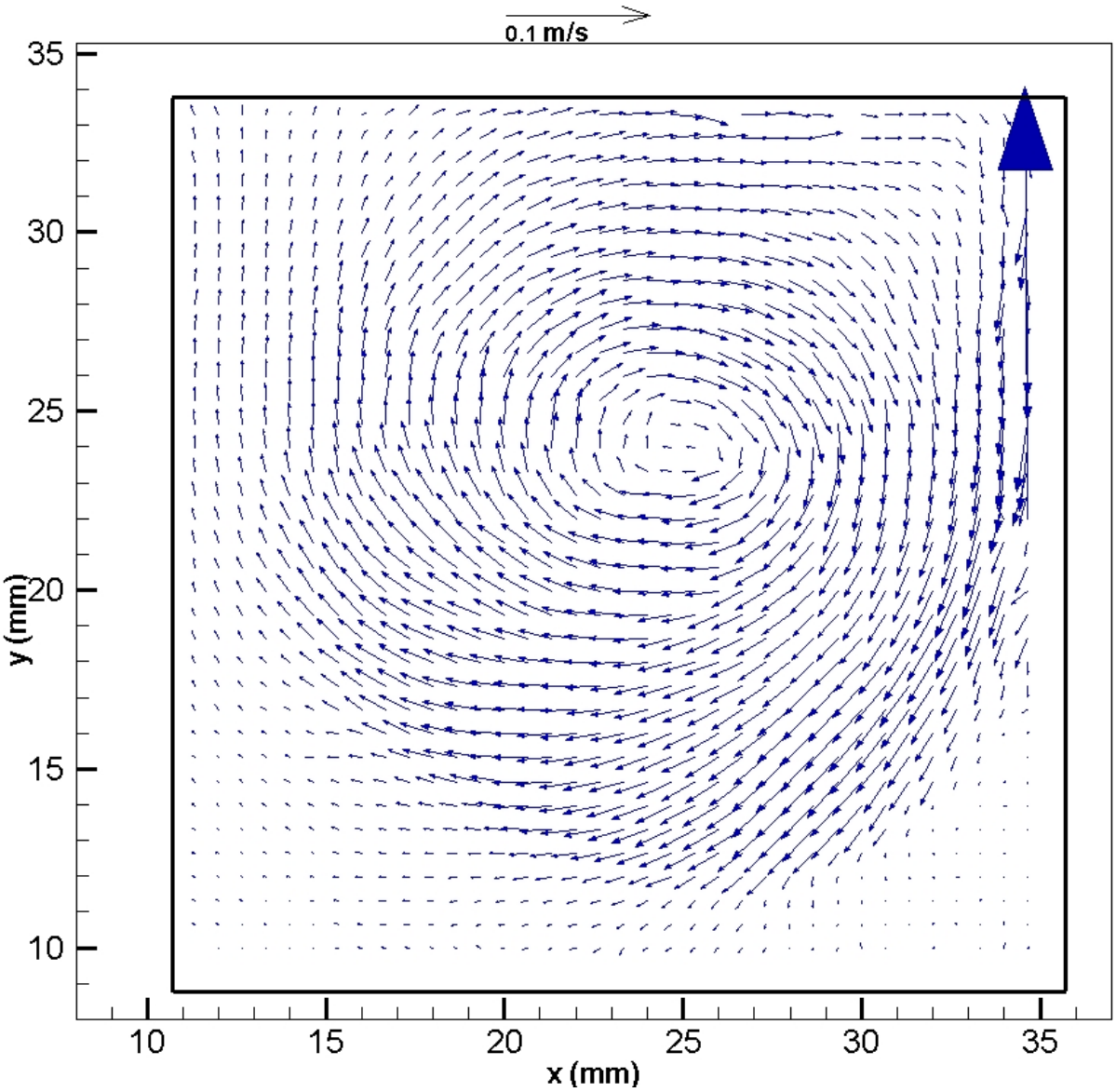

Figure 66- Global Vector Map Experiment 1 Run 5 (Re=1250) at Time t=2.070 Seconds.

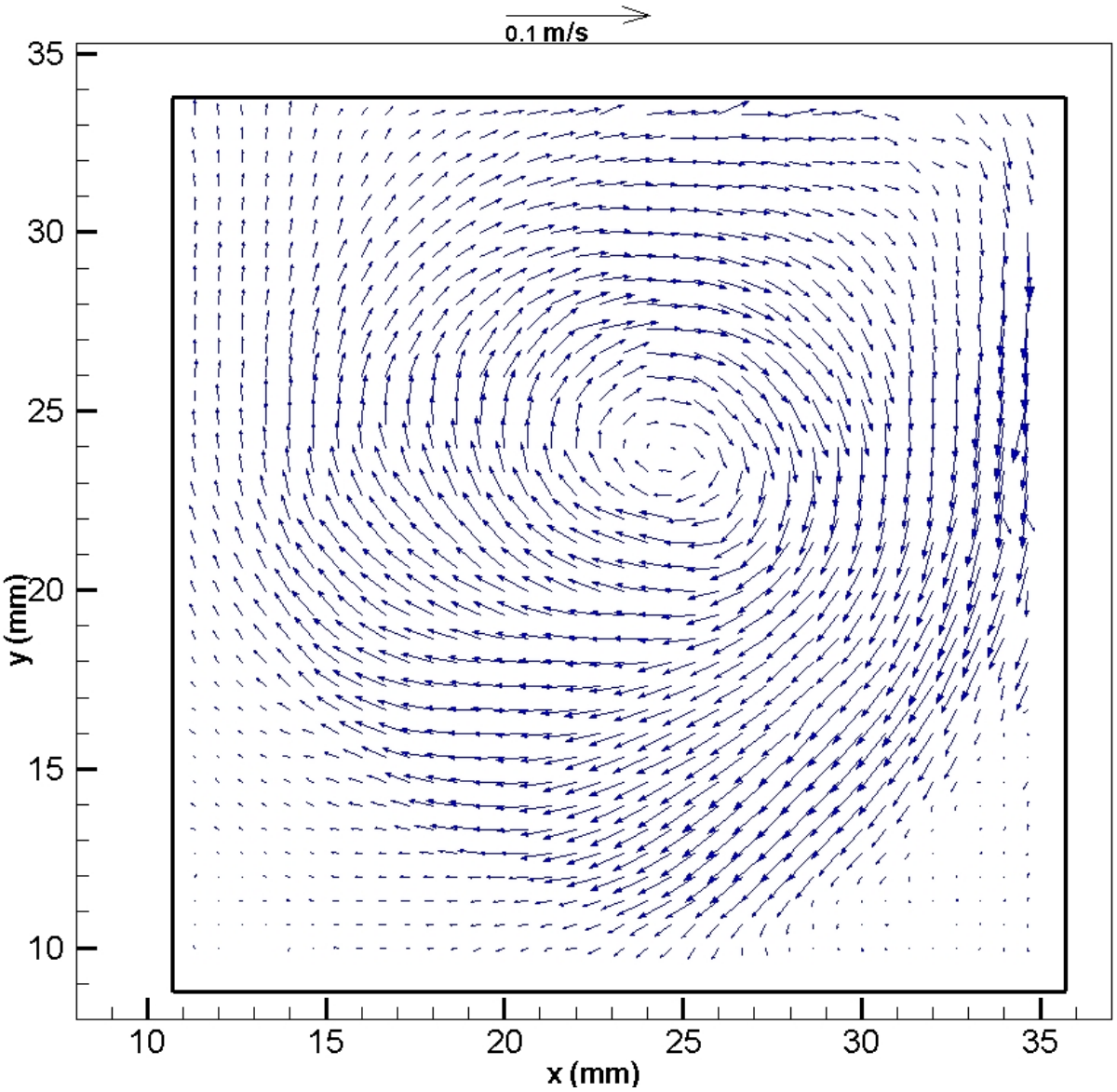

Figure 67- Global Vector Map Experiment 1 Run 5 (Re=1250) at Time t=2.208 Seconds.

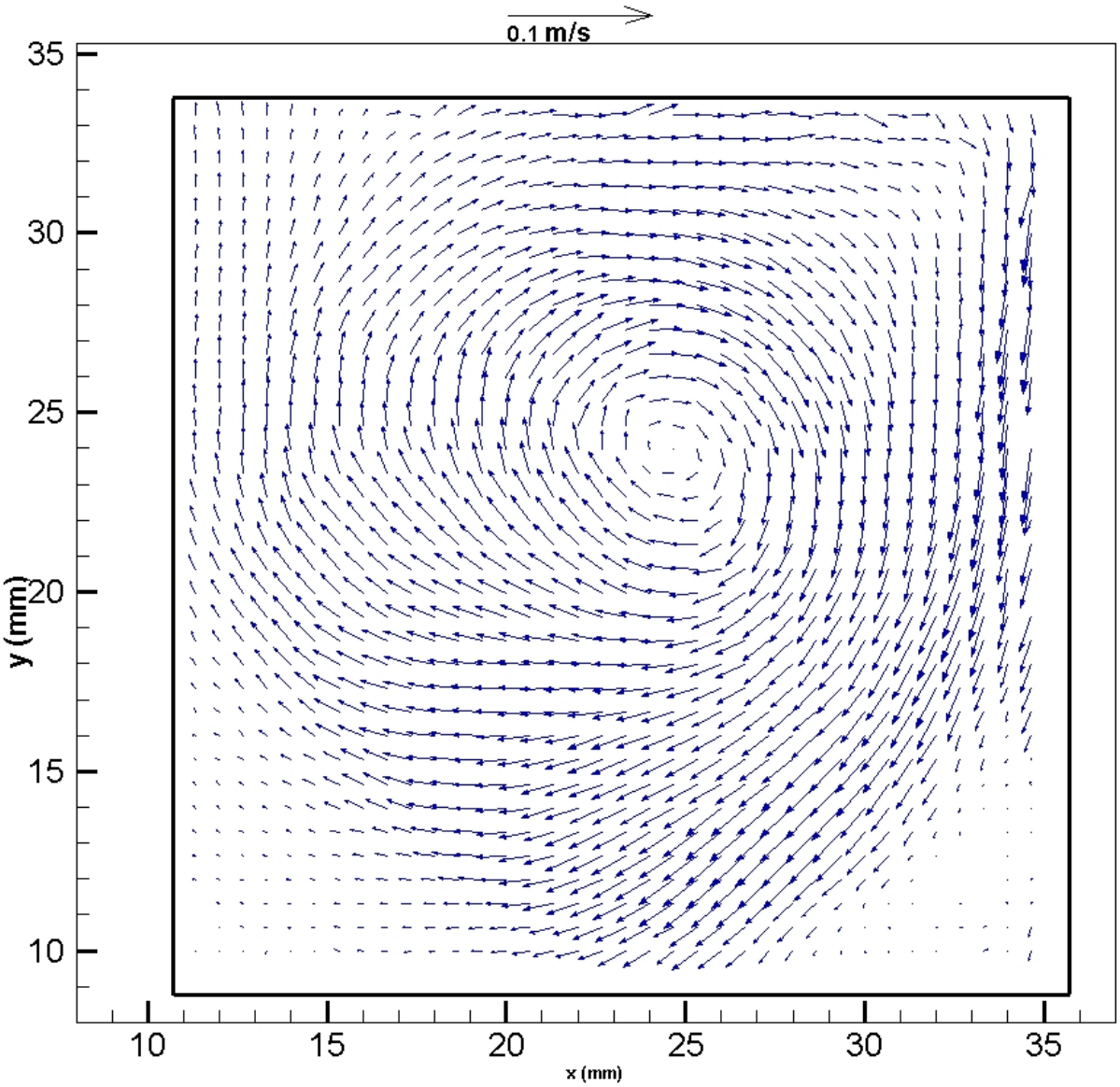

Figure 68- Global Vector Map Experiment 1 Run 5 (Re=1250) at Time t=2.346 Seconds.

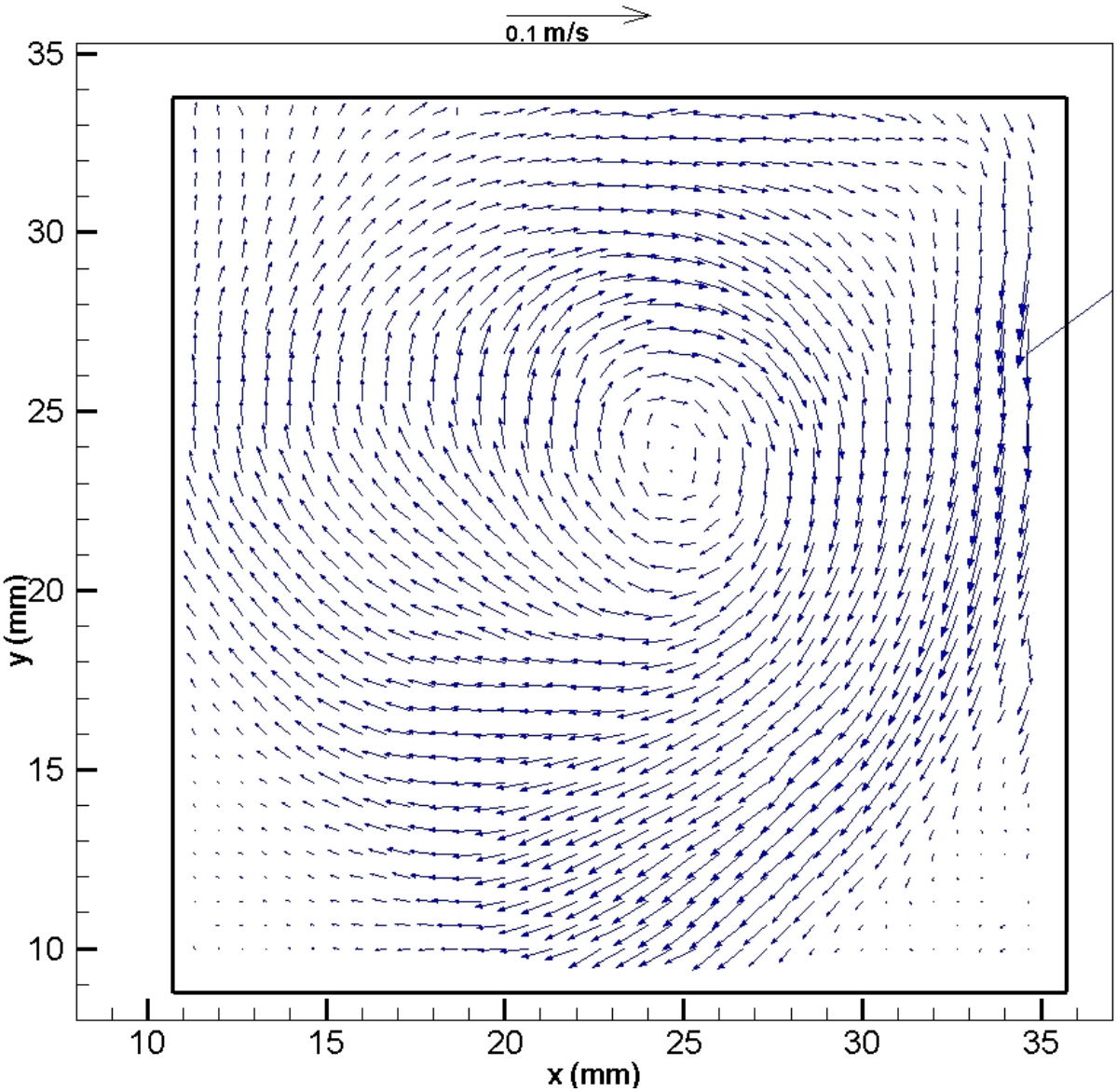

Figure 69- Global Vector Map Experiment 1 Run 5 (Re=1250) at Time t=2.484 Seconds.

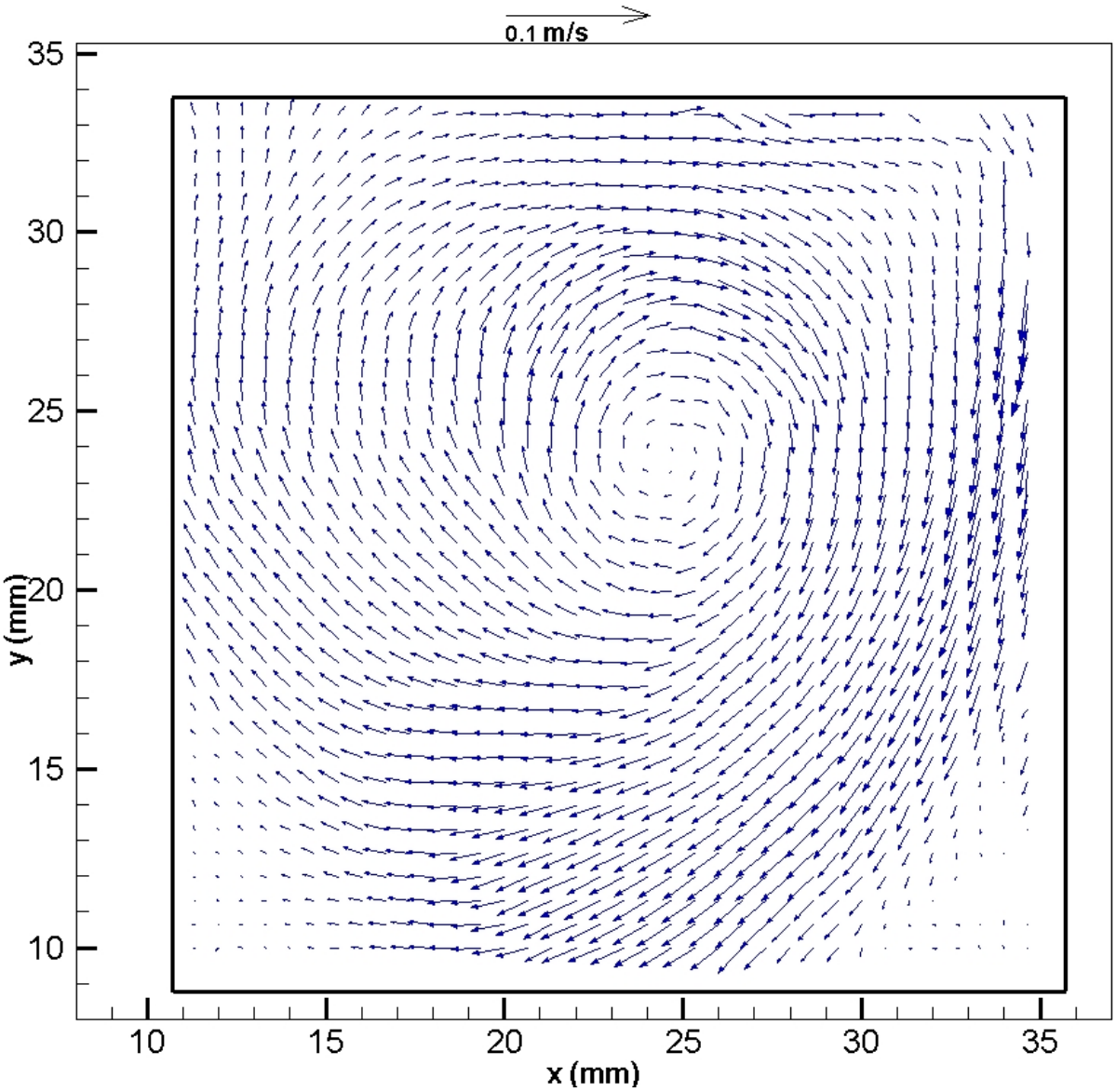

Figure 70- Global Vector Map Experiment 1 Run 5 (Re=1250) at Time t=2.622 Seconds.

In Figs. 67-70 the circulation has achieved steady state. The circulation center does not move from one frame to the next. Steady state has been achieved in less than 3 seconds. The circulation center is shown to be close to, but not exactly at the geometric center of the cavity.

5.3 Parametric Study

A parametric study of three lid speeds was conducted. All experiments were repeated at least three times at the same PIV capture settings and processor settings. The lid speeds and corresponding Reynolds numbers are presented in Table 1. Figures 71- 78 present the second experiment U_2=0.10 m/s Re=2530 from development to steady state.

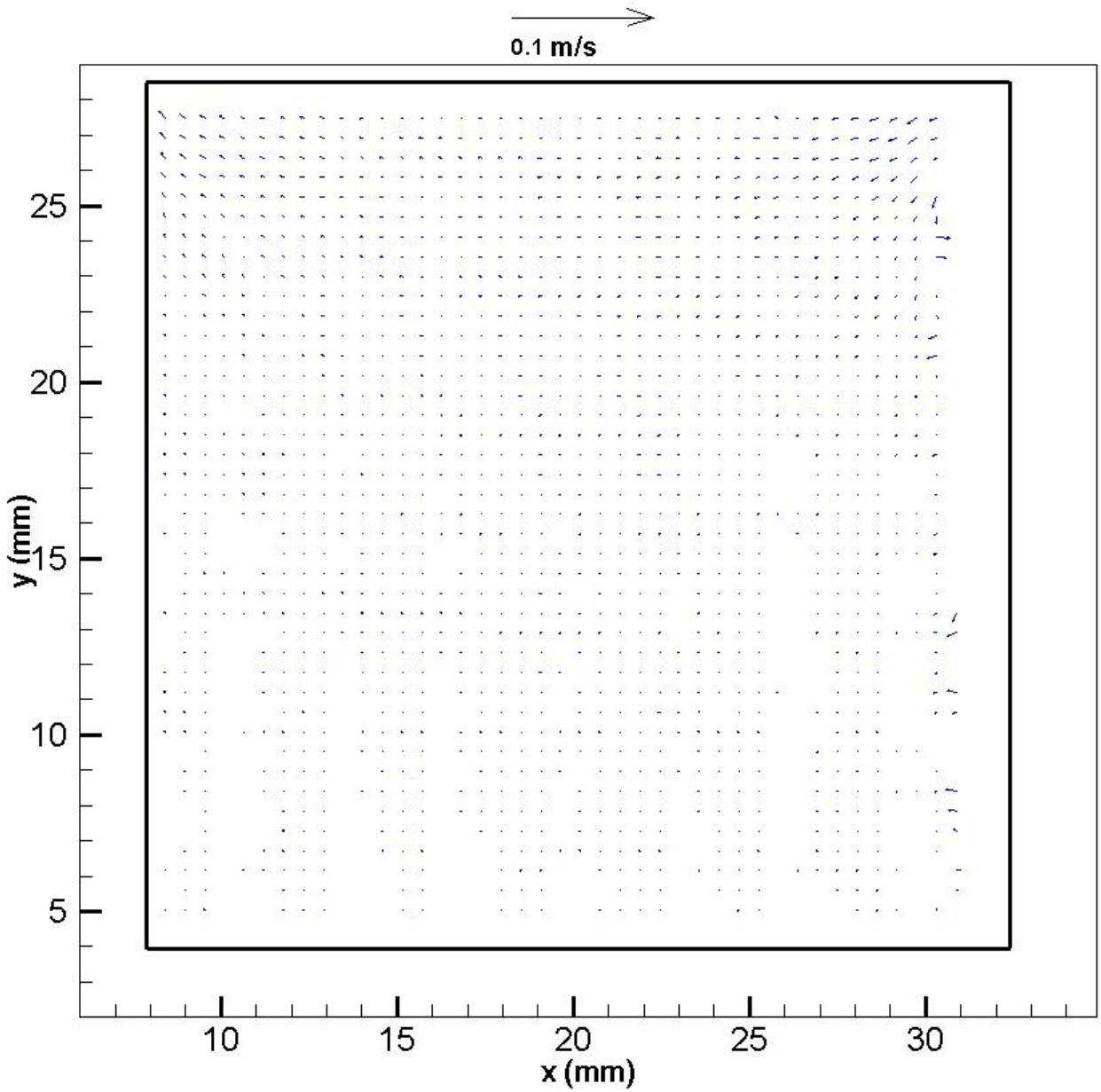

Figure 71- Global Vector Map Experiment 2 Run 3 (Re=2530) at Time t=0.00 Seconds.

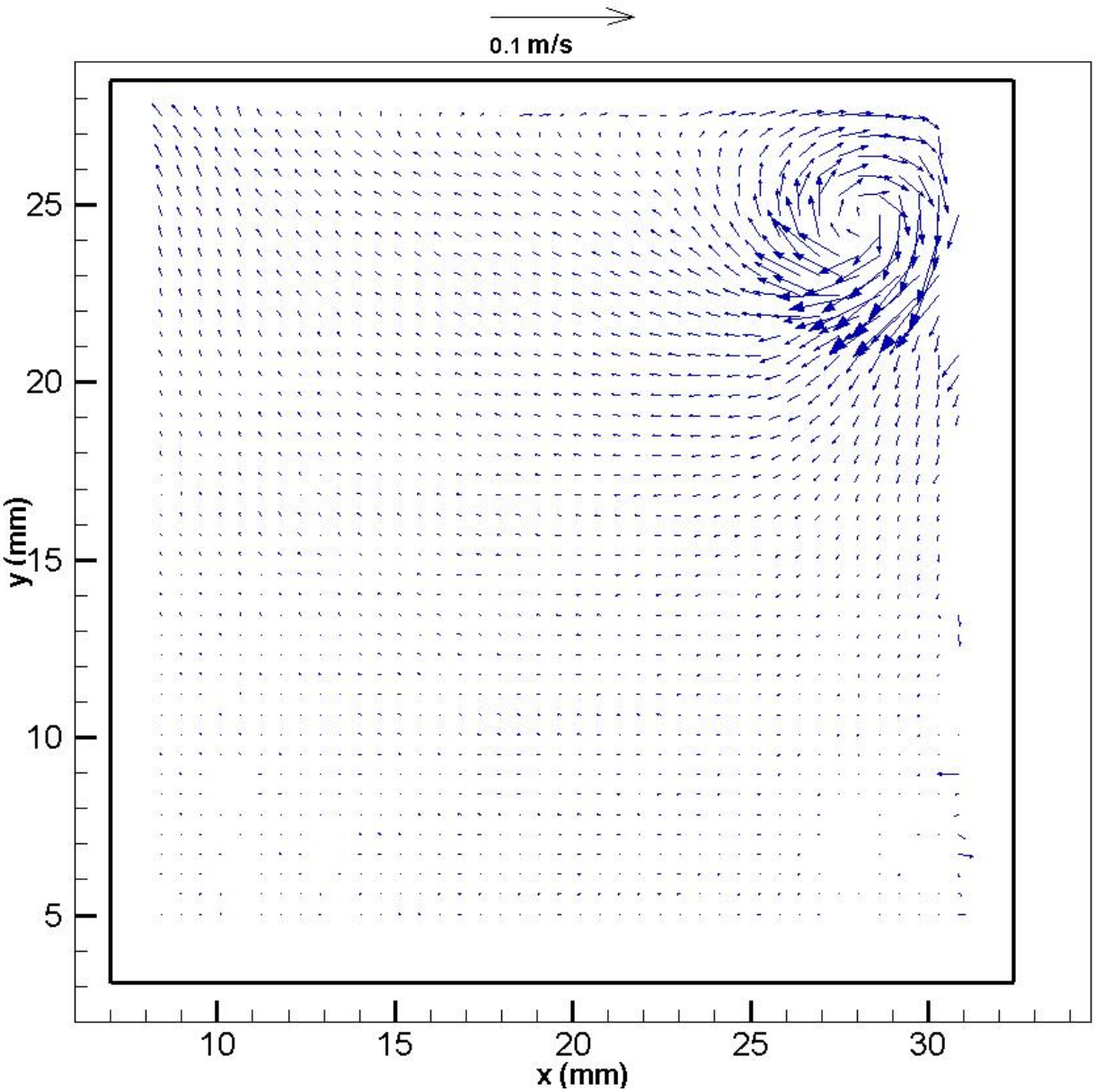

Figure 72- Global Vector Map Experiment 2 Run 3 (Re=2530) at Time t=0.34 Seconds.

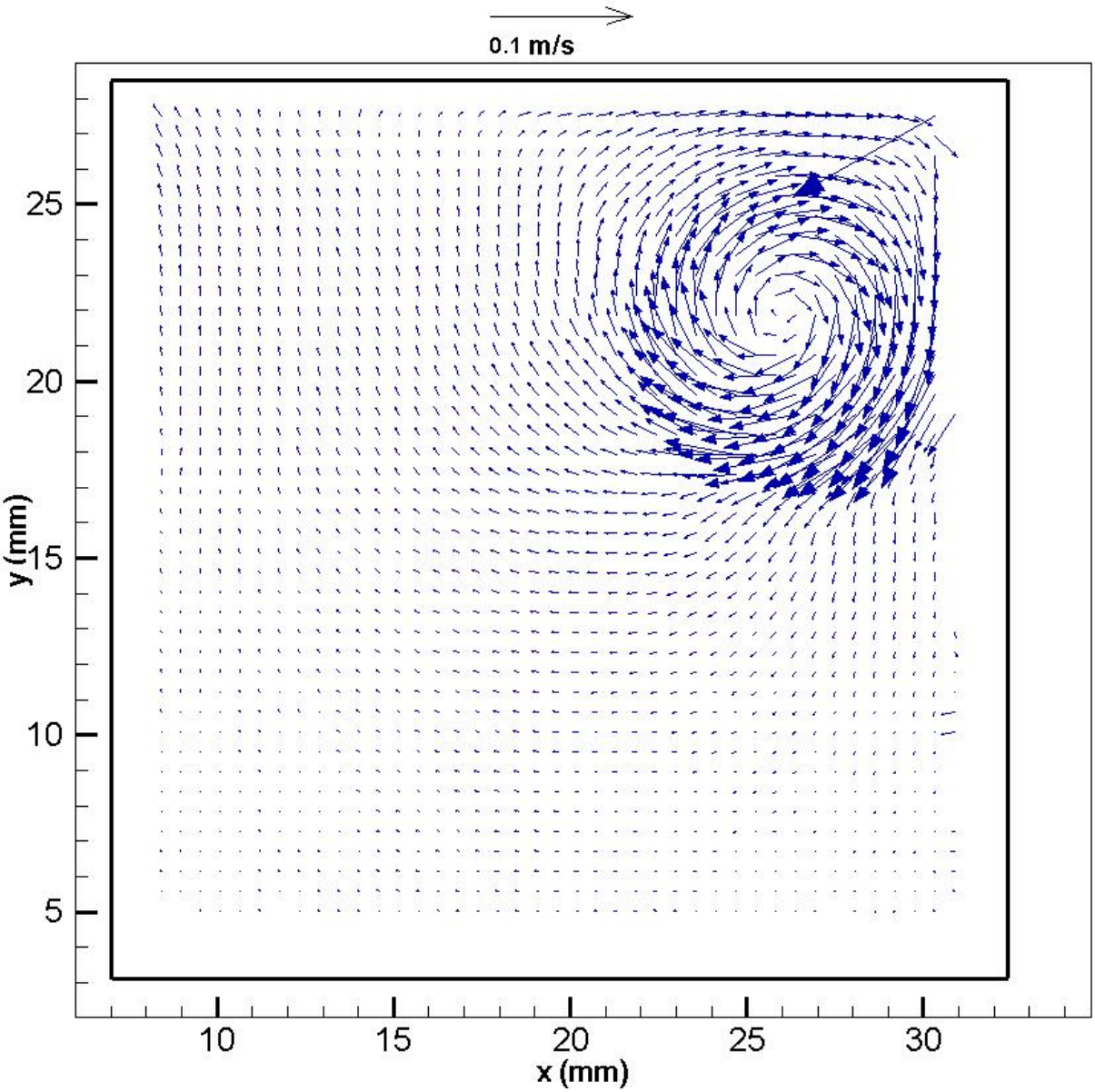

Figure 73- Global Vector Map Experiment 2 Run 3 (Re=2530) at Time t=0.69 Seconds.

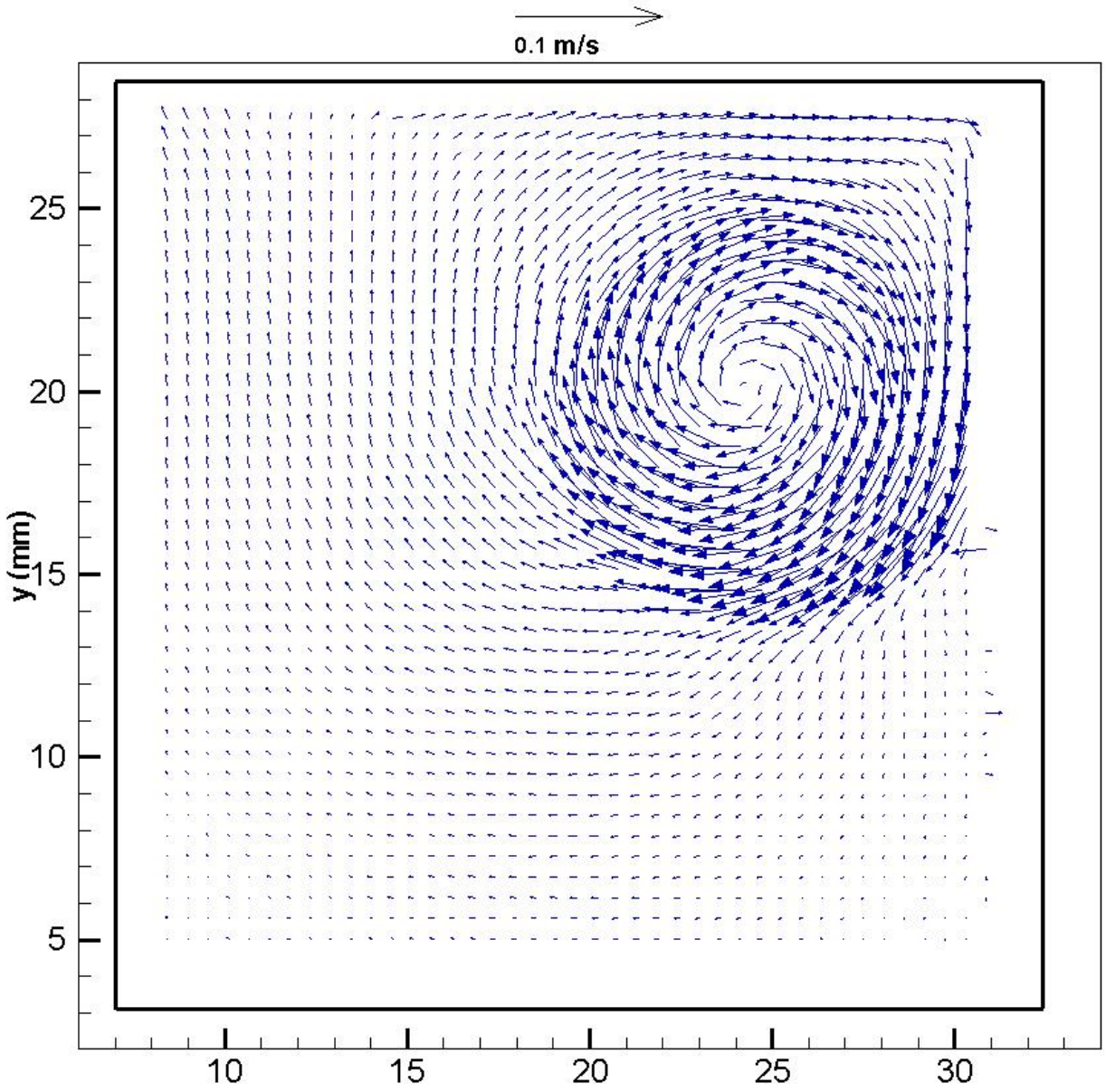

Figure 74- Global Vector Map Experiment 2 Run 3 (Re=2530) at Time t=1.03 Seconds.

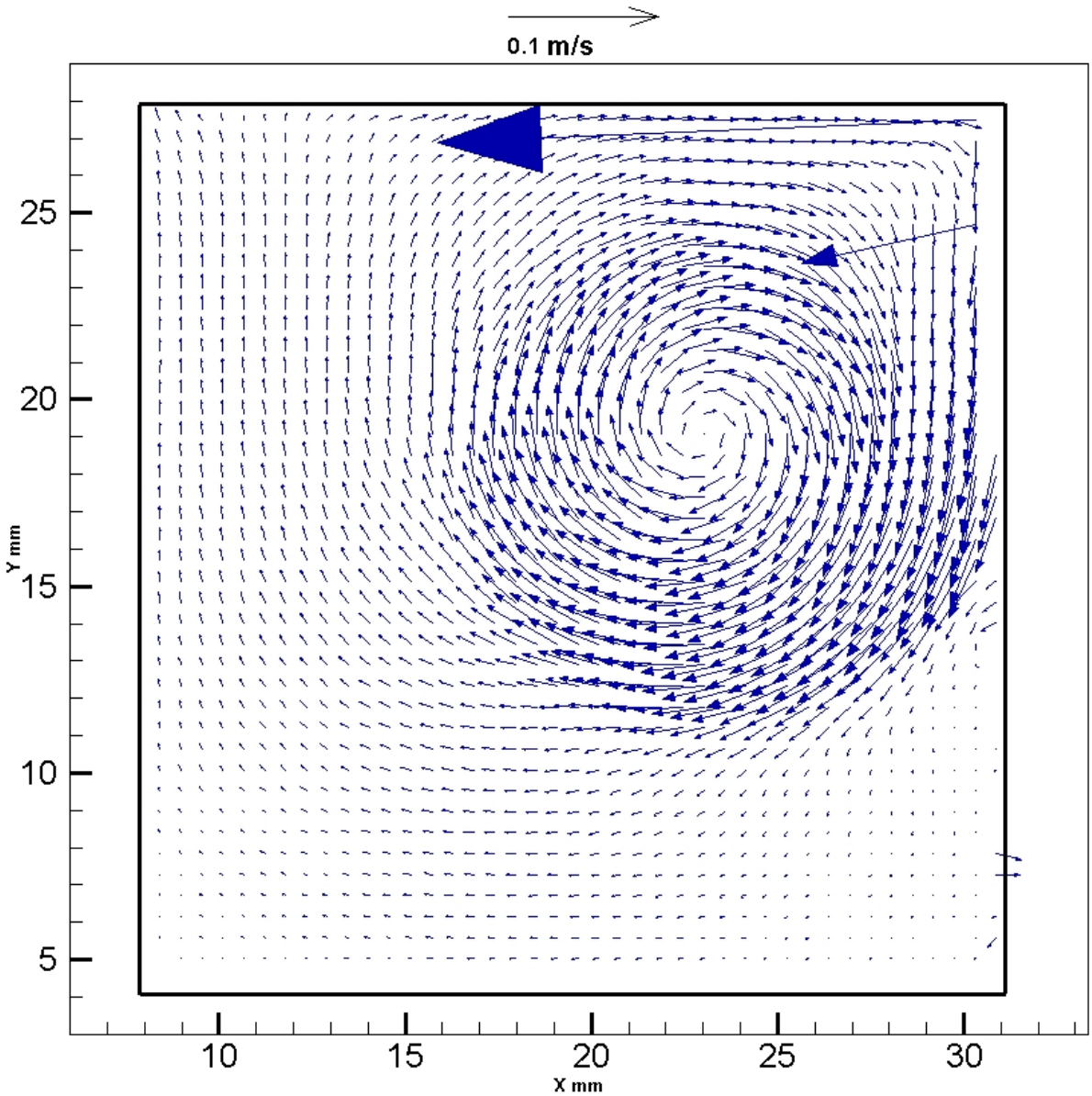

Figure 75- Global Vector Map Experiment 2 Run 3 (Re=2530) at Time t=1.38 Seconds.

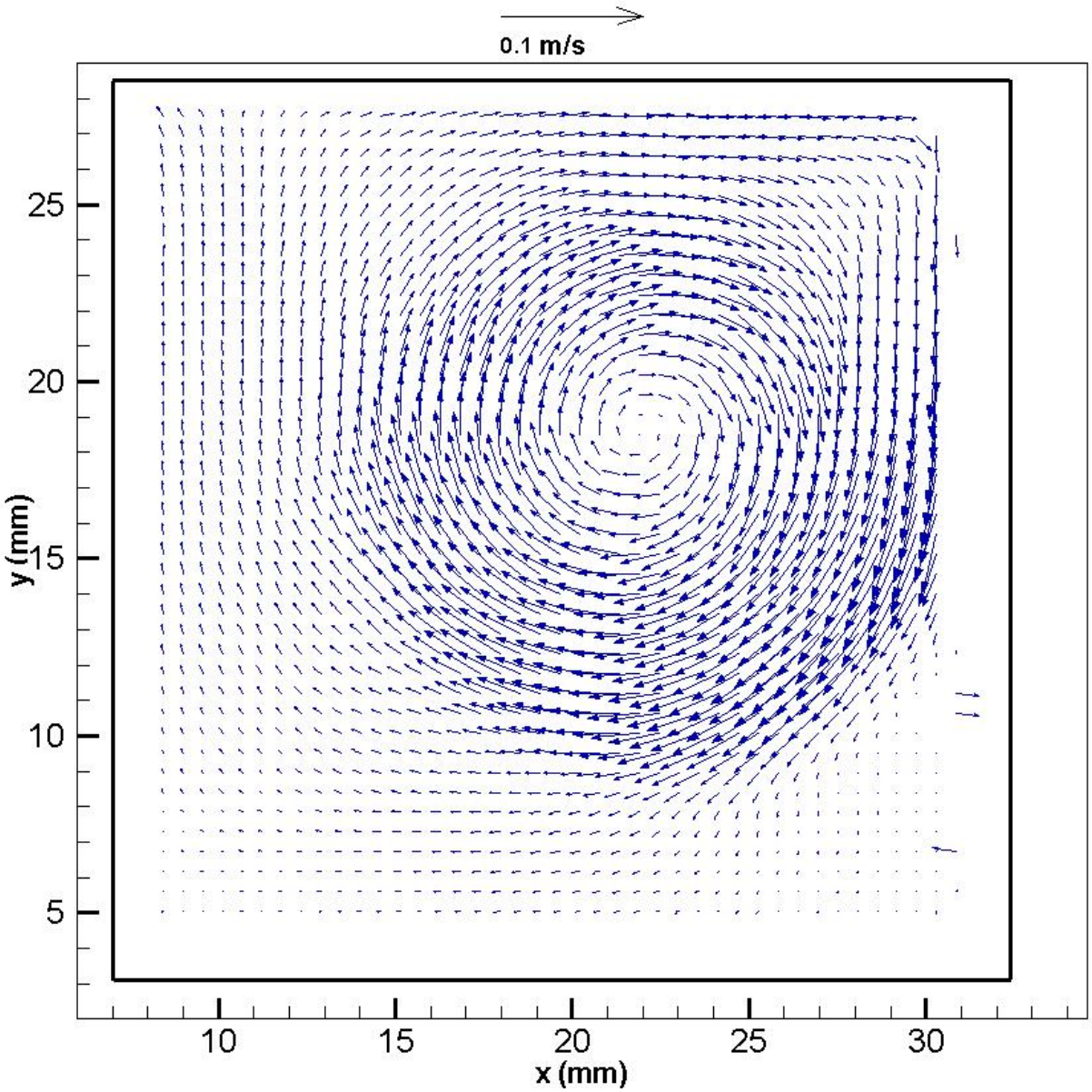

Figure 76- Global Vector Map Experiment 2 Run 3 (Re=2530) at Time t=1.72 Seconds.

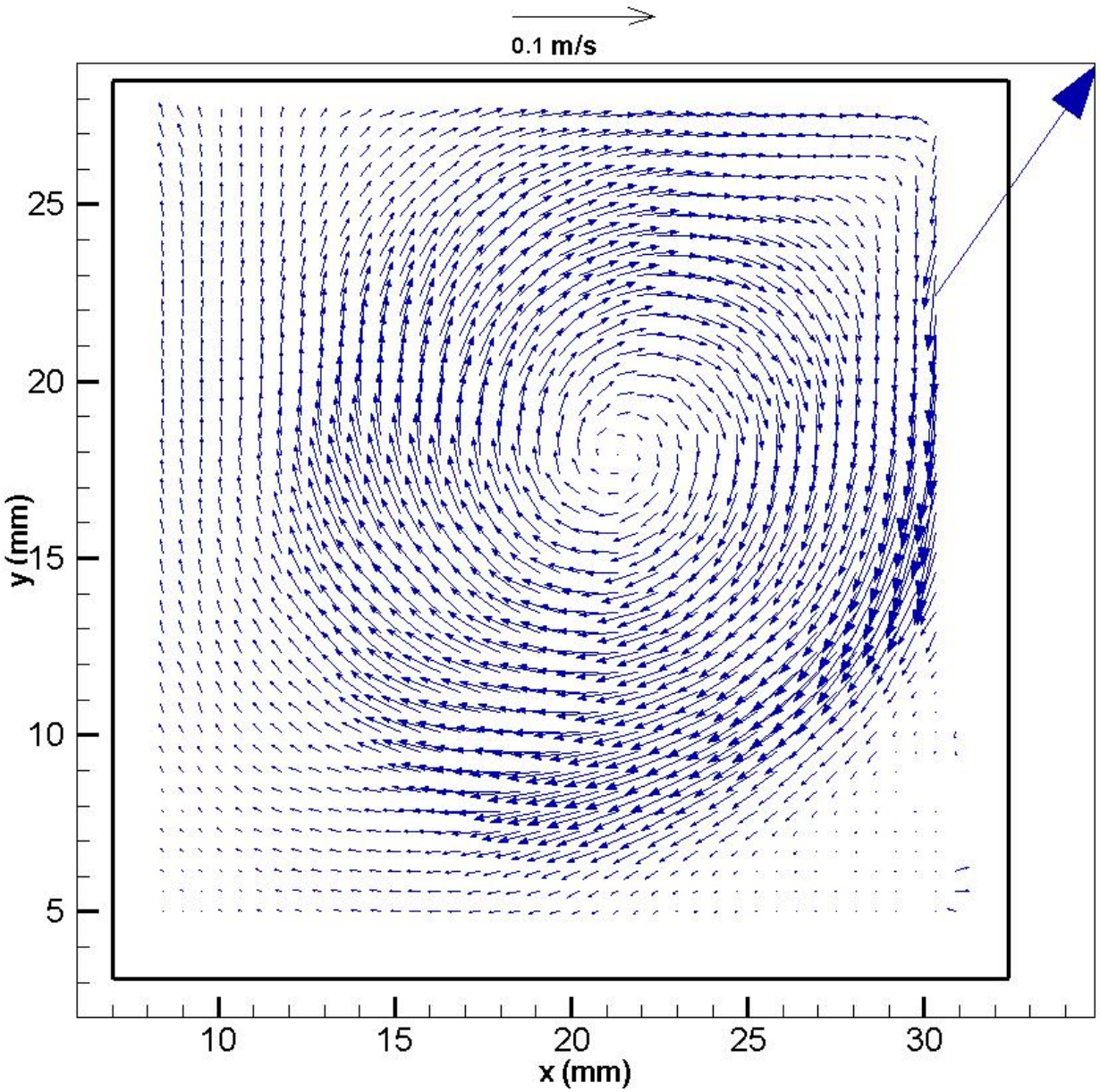

Figure 77- Global Vector Map Experiment 2 Run 3 (Re=2530) at Time t=2.07 Seconds.

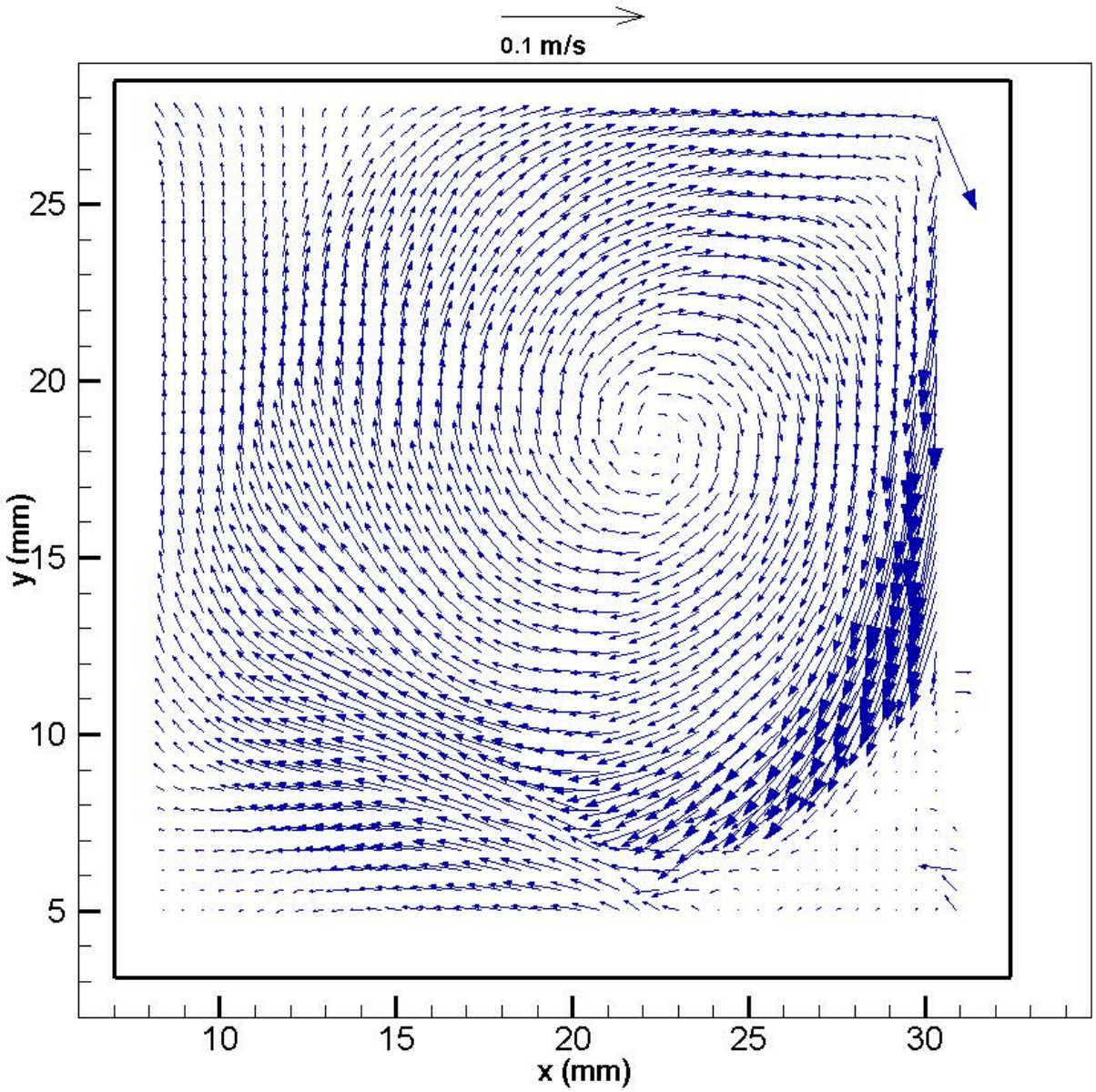

Figure 78- Global Vector Map Experiment 2 Run 3 (Re=2530) at Time t=2.41 Seconds.

Figs. 71-78 show that the circulation development at Re=2530 is consistent with the experiment Re=1250. The circulation develops at the top right corner of the cavity and moves toward the center of the cavity, where it stays after achieving steady state, as expected. Additionally, comparing the diameters of the circulation at the same times shows larger diameters for the higher Reynolds number experiment at the same time.

The third experiment U_3=0.12m/s Re=3030 from development to steady state is presented in figures 79-86.

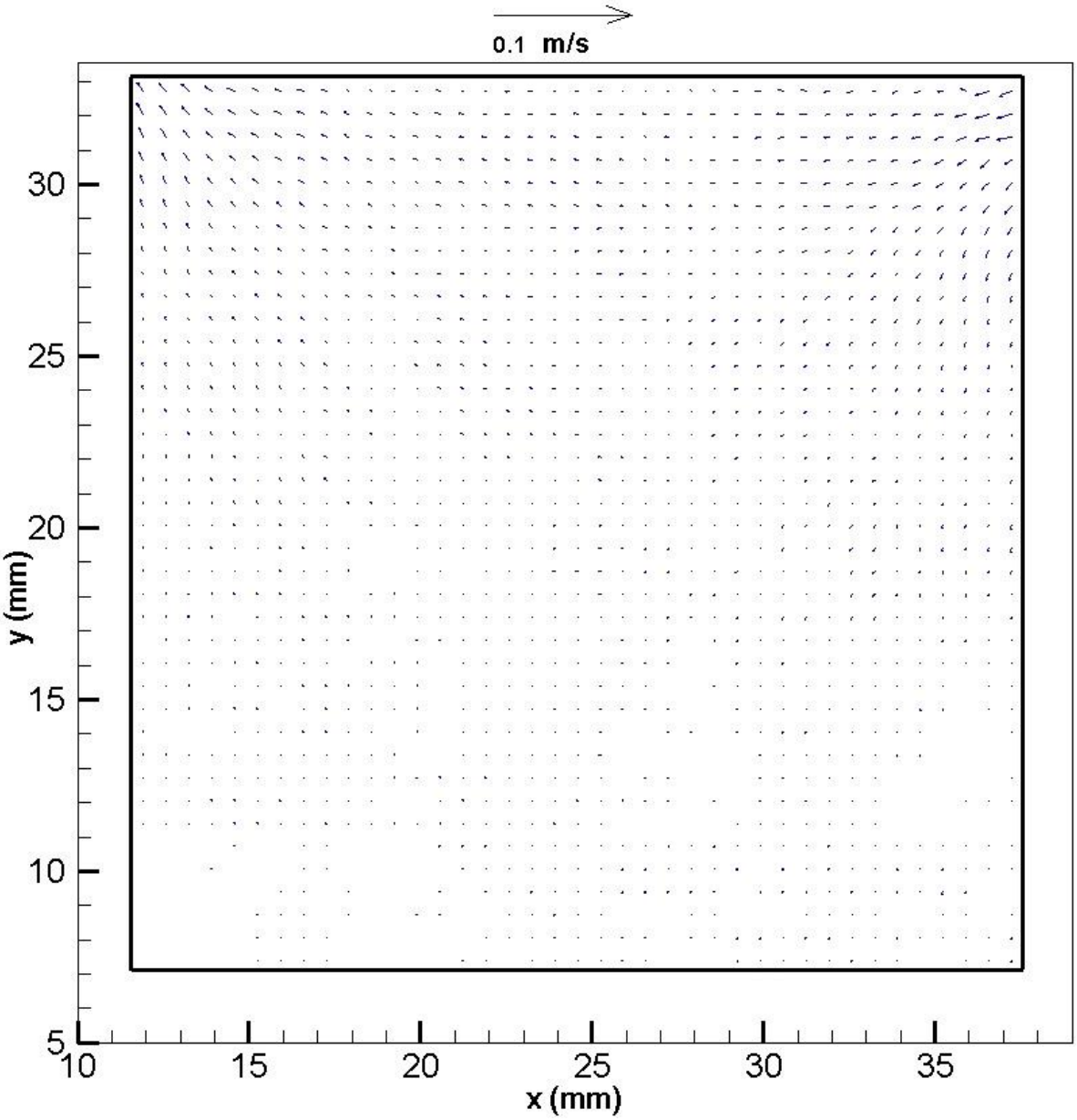

Figure 79- Global Vector Map Experiment 3 Run 4 (Re=3030) at Time t=0.00 Seconds.

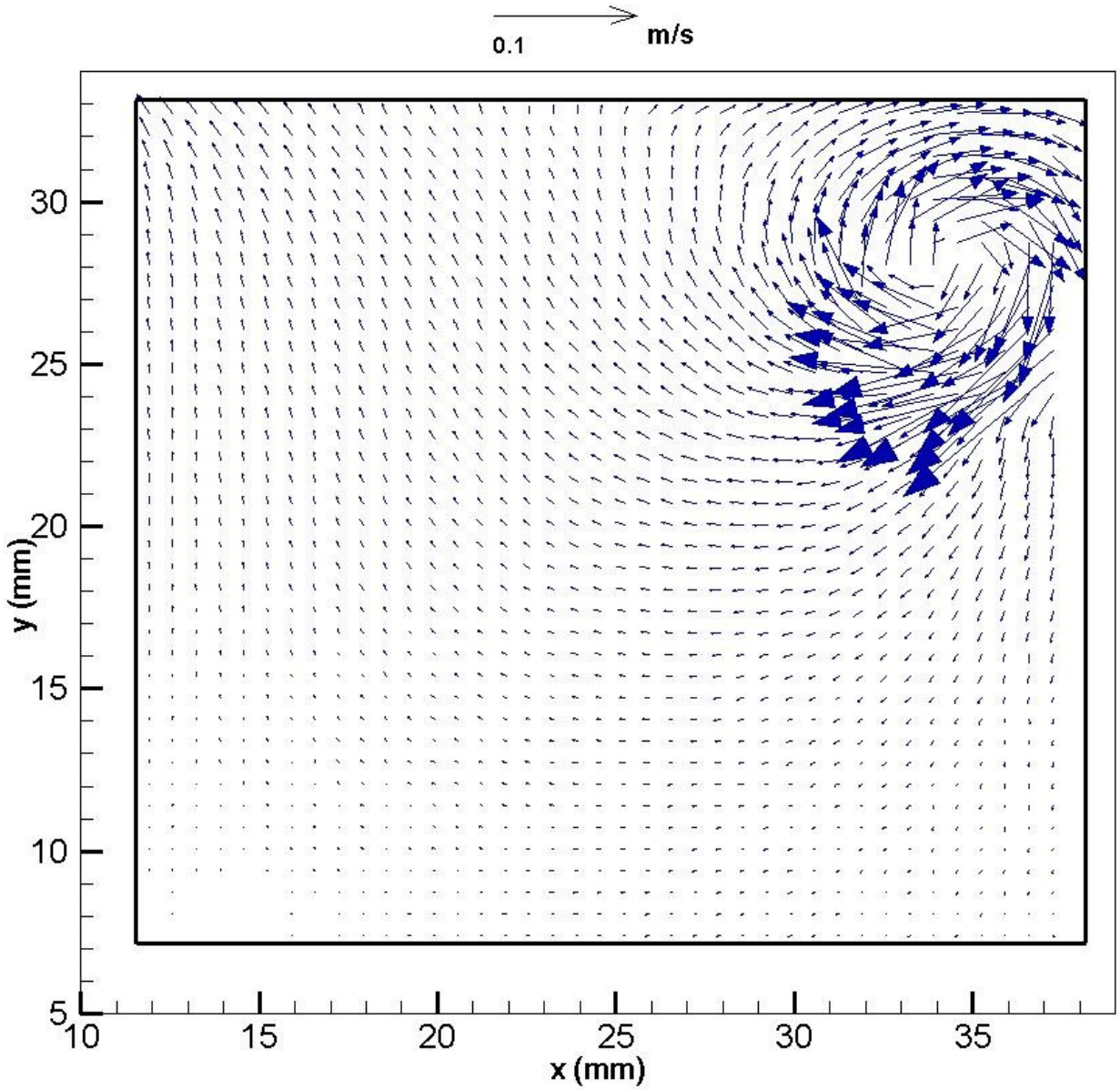

Figure 80- Global Vector Map Experiment 3 Run 4 (Re=3030) at Time t=0.34 Seconds.

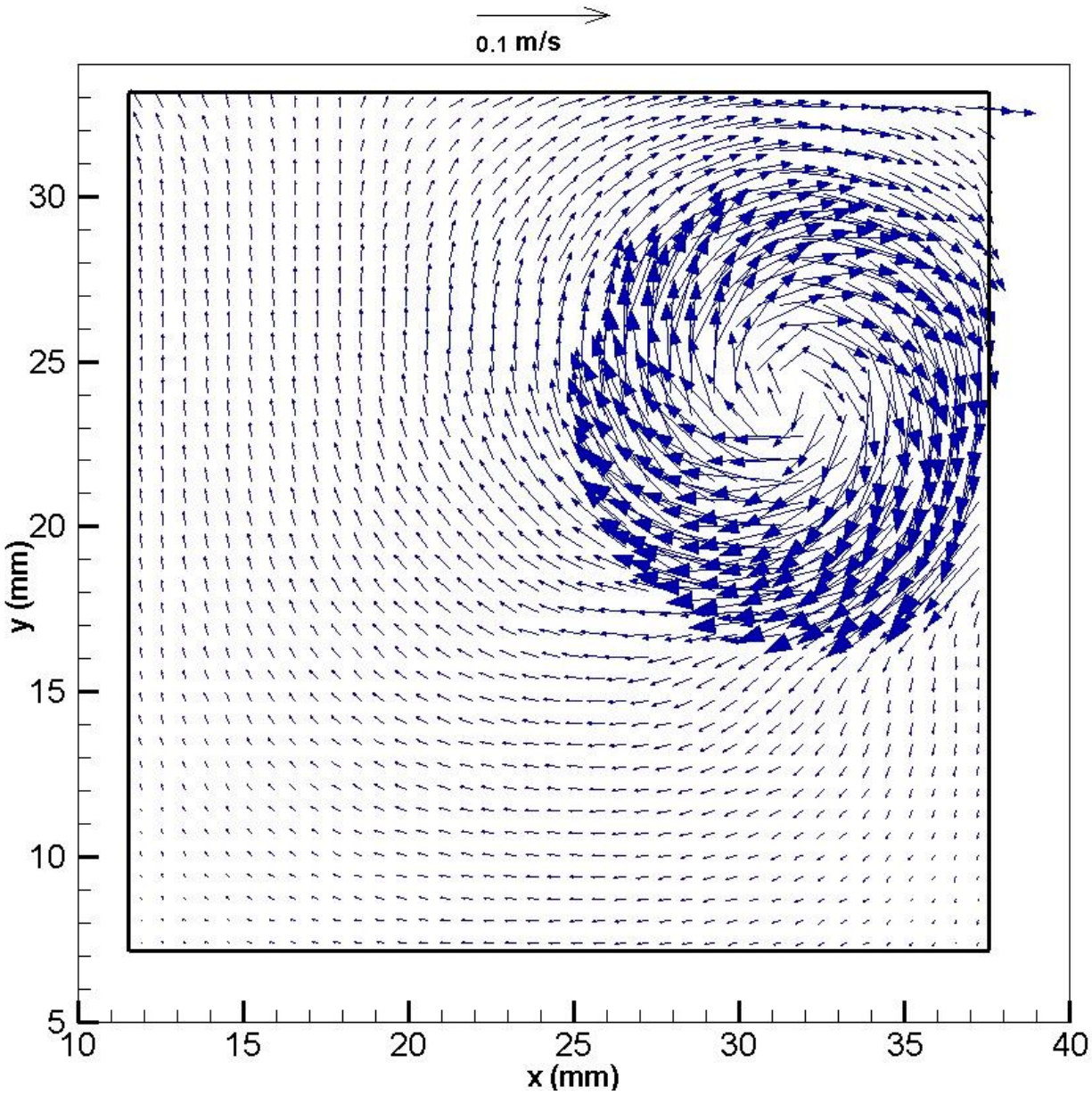

Figure 81- Global Vector Map Experiment 3 Run 4 (Re=3030) at Time t=0.69 Seconds.

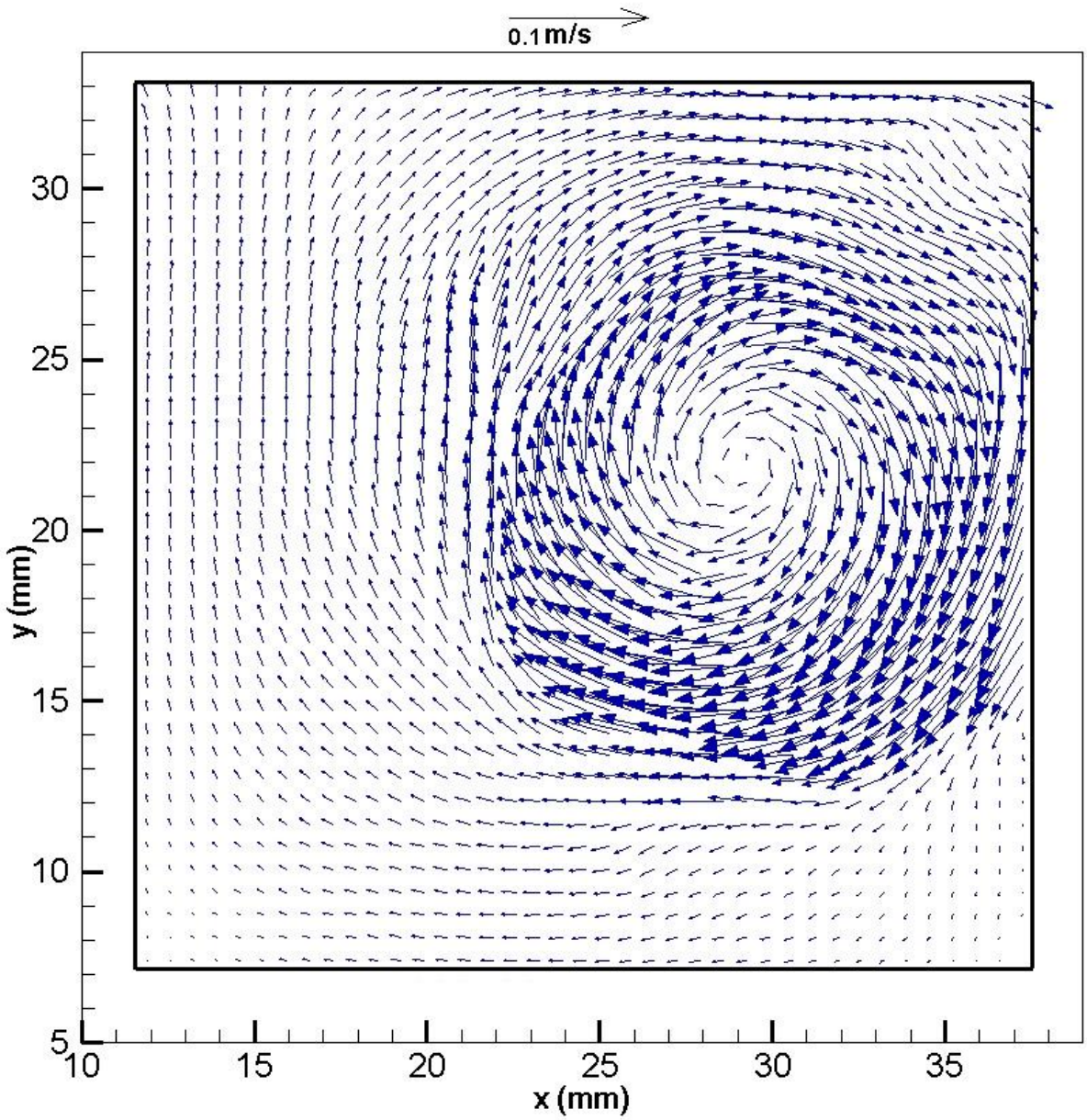

Figure 82- Global Vector Map Experiment 3 Run 4 (Re=3030) at Time t=1.03 Seconds.

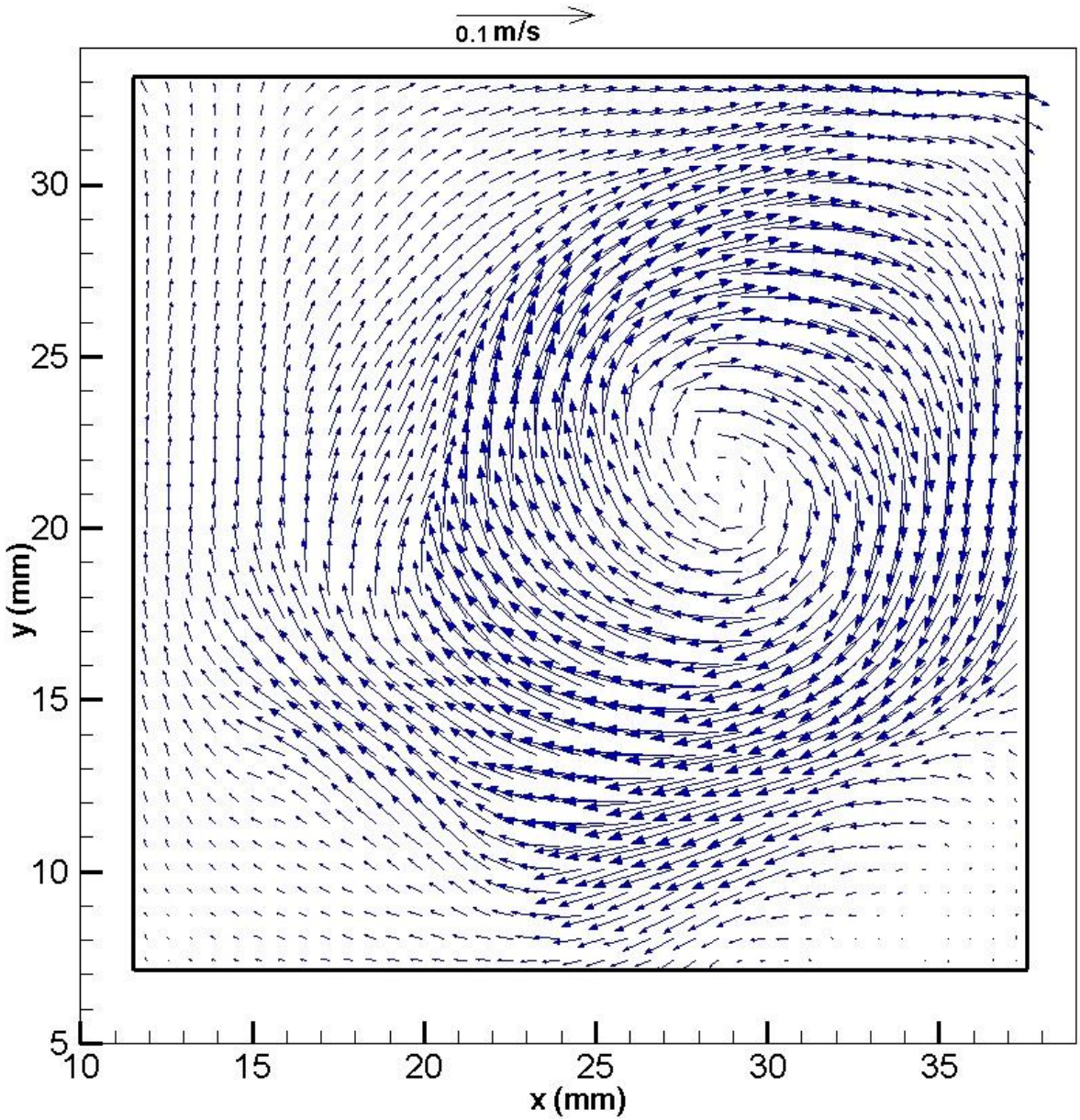

Figure 83- Global Vector Map Experiment 3 Run 4 (Re=3030) at Time t=1.38 Seconds.

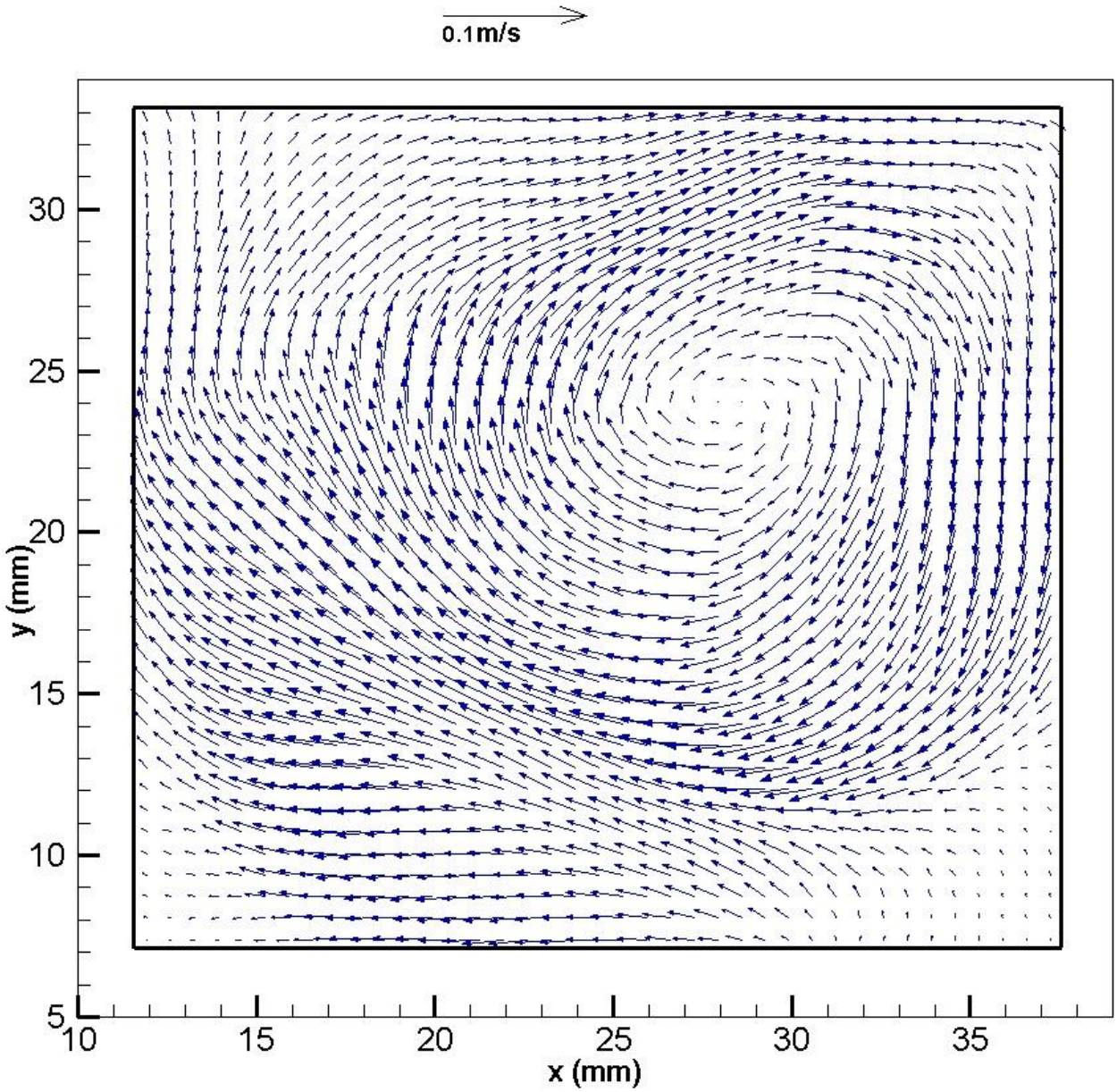

Figure 84- Global Vector Map Experiment 3 Run 4 (Re=3030) at Time t=1.72 Seconds.

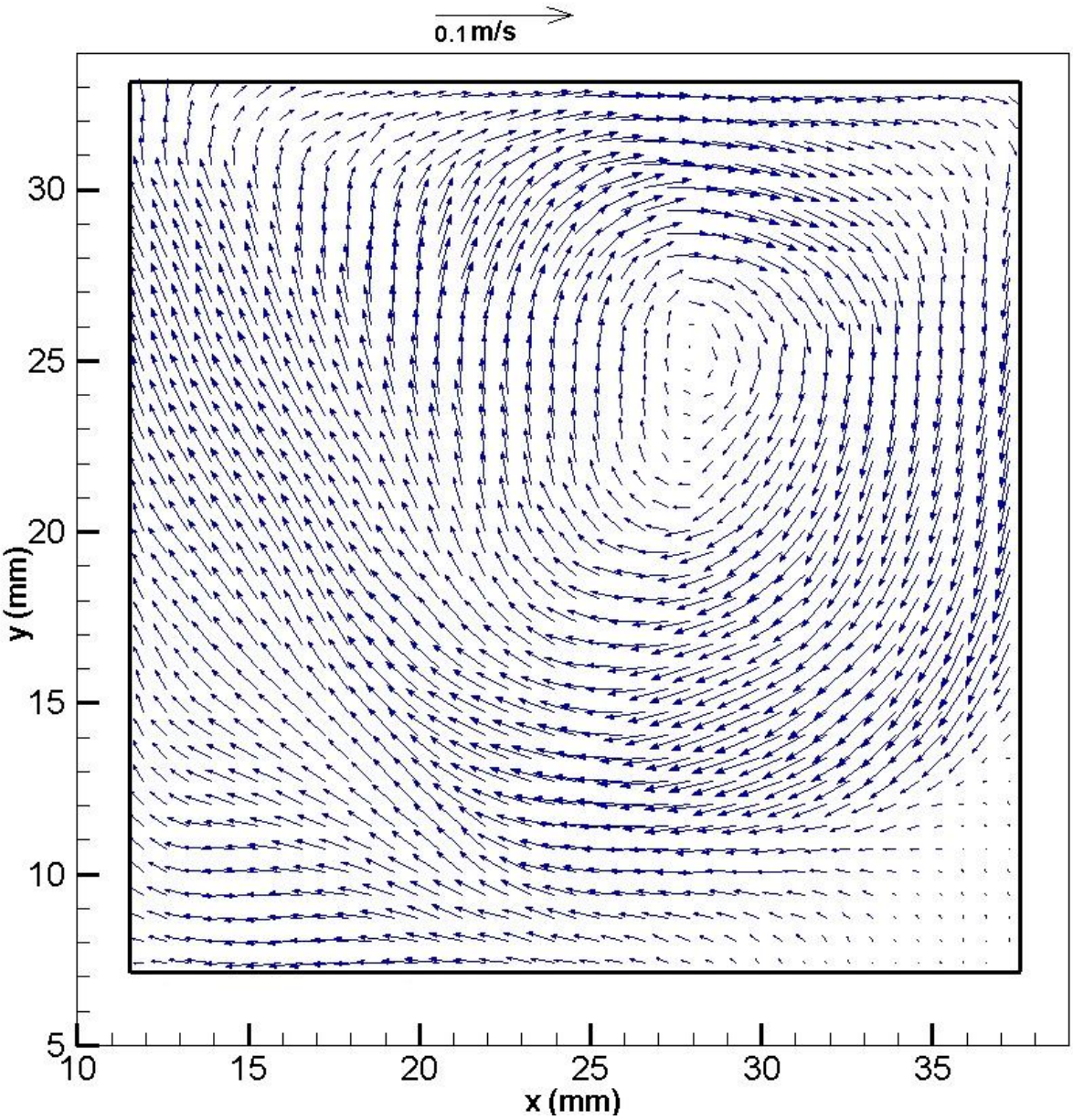

Figure 85- Global Vector Map Experiment 3 Run 4 (Re=3030) at Time t=2.07 Seconds.

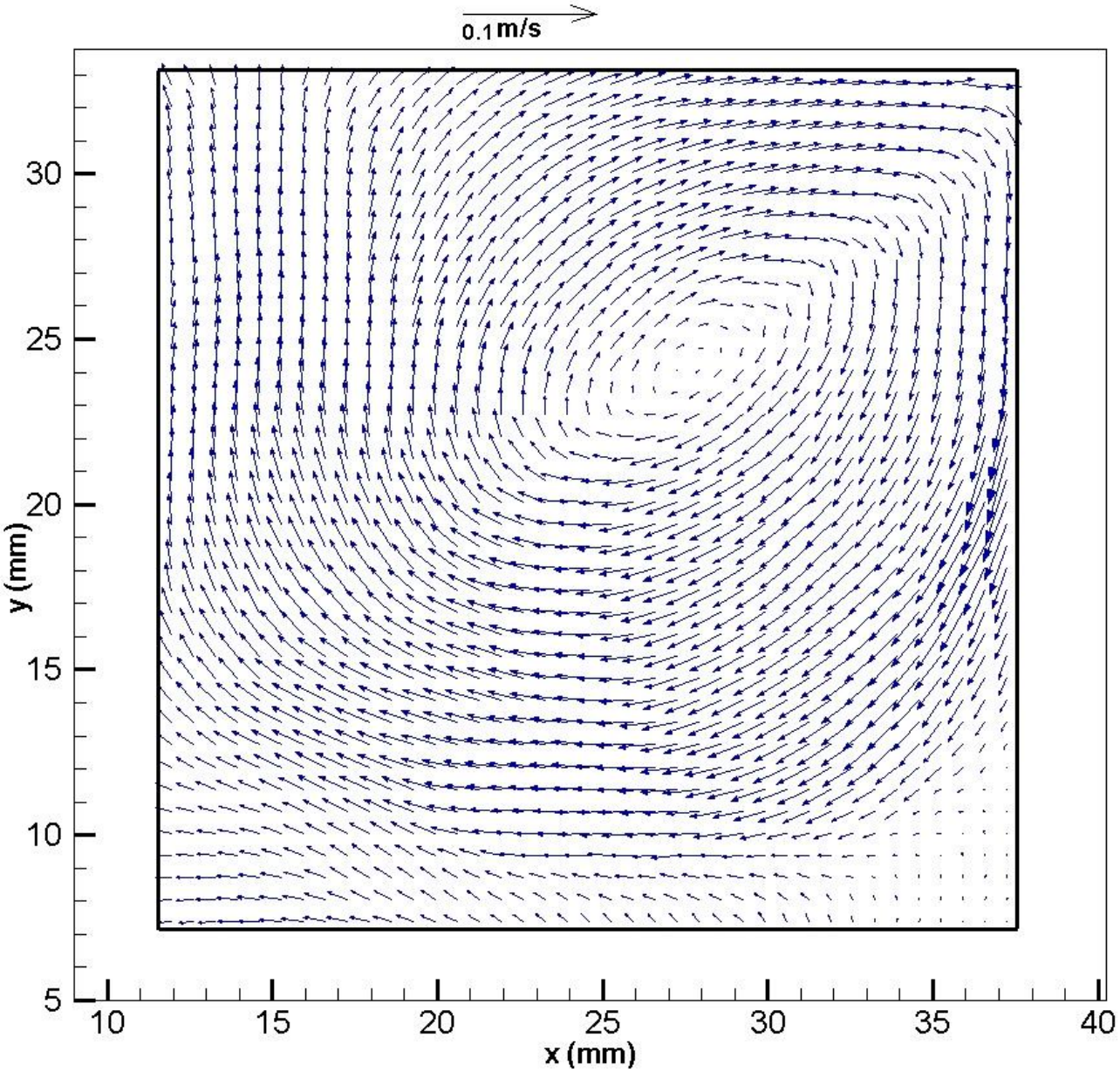

Figure 86- Global Vector Map Experiment 3 Run 4 (Re=3030) at Time t=2.41 Seconds.

Figs. 79-86 show that the circulation development at Re=3030 initially is consistent with the experiments Re=1250 and Re=2030. The circulation develops at the top right corner of the cavity and moves toward the center of the cavity, however it does not achieve a steady location and the center of circulations fluctuates. This was found to occur at Re≥ 3,000, where the flow moves to the transition to turbulent region, and reported in literature by Koseff and Street [5]. Again, comparing the diameters of the circulation at the same times shows larger diameters for the higher Reynolds number experiment at the same time.

The Circulation diameters are then measured and compared. Table 4 shows the diameter of the primary circulation as a function of time for the three experiments. Figure 87 plots the location of the circulation vortex in the cell; this is also shown in Table 5.

Table 4- Circulation Diameter

Time, t (s)	Diameter, d (m) Re=1250	Diameter, d (m) Re=2530	Diameter, d (m) Re=3030
0.00	0.000	0.000	0.000
0.34	0.000	0.005	0.007
0.69	0.007	0.009	0.014
1.03	0.012	0.013	0.018
1.38	0.015	0.016	0.019
1.72	0.017	0.019	0.022
2.07	0.019	0.020	0.028
2.41	0.023	0.024	0.028

Table 4 shows quantitatively what is observed visually, at the same time the circulation diameter is increases as Reynolds number increases.

Table 5- Circulation Center in Relation to Cavity Location by Time.

Time, t (s)	Horizontal vortex center location, x (m) Re=1250	Vertical vortex center location, y (m) Re=1250	Horizontal vortex center location, x (m) Re=2530	Vertical vortex center location, y (m) Re=2530	Horizontal vortex center location, x (m) Re=3030	Vertical vortex center location, y (m) Re=3030
0.00	0.0254	0.0254	0.0254	0.0254	0.0254	0.0254
0.34	0.0254	0.0254	0.02	0.021	0.0225	0.0225
0.69	0.0205	0.019	0.017	0.0185	0.0215	0.018
1.03	0.0175	0.017	0.016	0.017	0.0175	0.017
1.38	0.0155	0.015	0.015	0.0155	0.017	0.015
1.72	0.0145	0.0145	0.0135	0.014	0.0165	0.018
2.07	0.0135	0.014	0.013	0.014	0.016	0.019

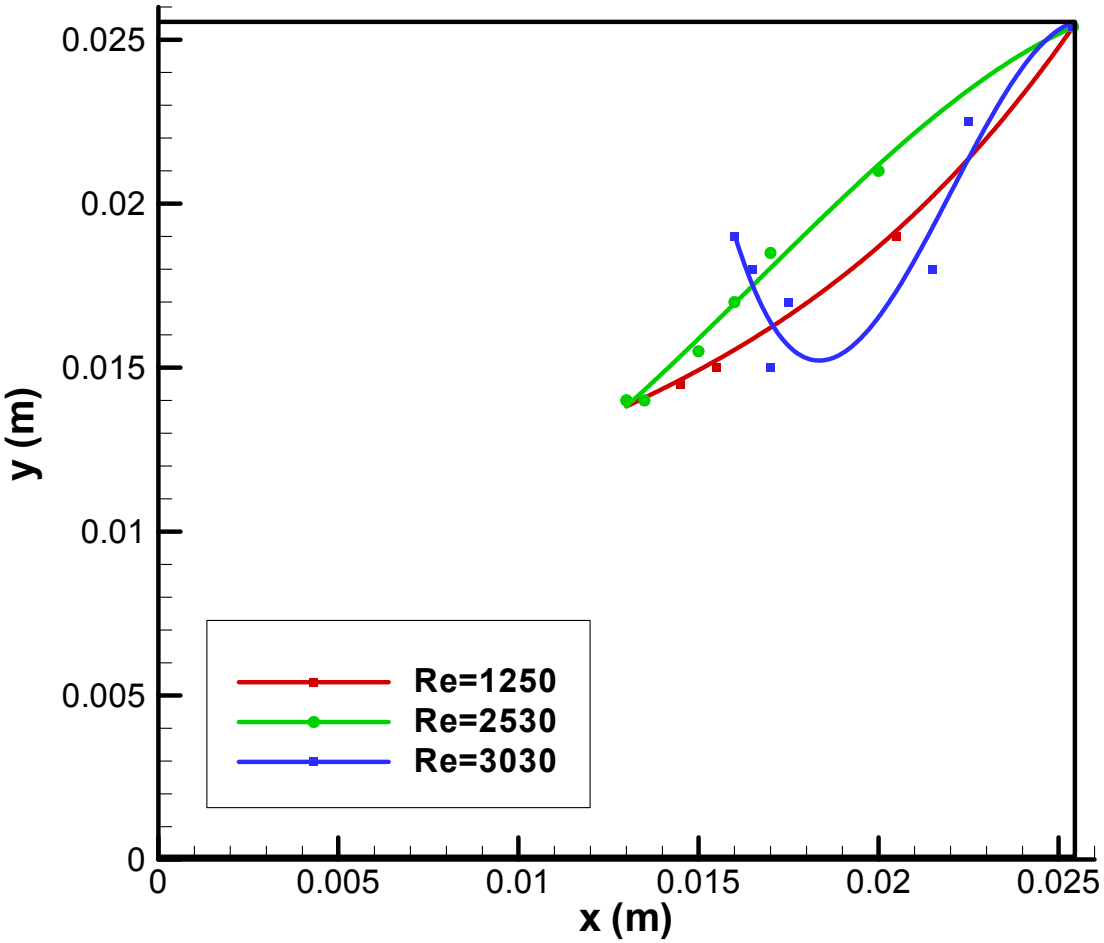

Figure 87- Circulation Center in Relation to Cavity Location.

In Figure 87 the movement of the center circulations is plotted. Here it can be seen, as expected, that for Reynolds numbers the center will move from the top right cavity wall in a straight diagonal line toward the central area of the cavity. For Re≥3000 the center starts to travel in a straight line, but then fluctuates up and down as it gets toward the center of the cavity.

5.4 Error Analysis

Extreme caution was practiced to ensure that experiments were ran accurately and PIV readings were correct. Water loss from the cavity by the lid was present, however it was estimated to be less than 1 %. Measurement of lid velocity was done by averaging multiple readings against a camcorder time stamp. Although accurate some uncertainty in the exact lid velocity is present. The main source of error involves spatial calibration of PIV. The ruler image is placed in path of laser sheet and an image is taken, however the camera lens is refocused after seeded water is introduced to the cavity. This changes the spatial readings slightly, an error of probably less that 5%.

Chapter 6

Conclusions

Evaluation of the experimental data leads to several conclusions. First, it is shown that PIV techniques were successful in capturing the development of circulation and circulation patterns in driven cavity flow. PIV capture settings and processing settings for capture lid driven flow at Reynolds number 3030 and below are determined. The circulation starts in the upper downstream, top right corner, of the cavity. The circulation gains in strength with time as the circulation develops. The growth of circulation strength also increases as the Reynolds number increases. The flow achieves steady state within 1-2.5 seconds. In the laminar region below the critical Reynolds number of 3000 the center of the circulation moves in a straight line from the top right of the cavity to the center of the cavity. When the flow is above the critical Reynolds number of 3000, in the transition region, the center of circulation move from the top right of the cavity towards the center of the cavity but fluctuates unsteadily.

Chapter 7

Recommendations

The experimental setup could be modified to yield readings in the turbulent region. In the current incarnation of the setup the lid velocity of 0.12 m/s, yielding a Reynolds number of 3030, is the highest velocity the lid can move and usable PIV capture can be made. To study the turbulent region the cavity can be double or tripled in size leading to a doubling or tripling of maximum Reynolds number for the same velocity ranges. Automating the lid with a motor controlled roller system would also allow for more velocity possibilities. As the setup currently stands velocities are set by a mass differential limited by mass changes, but with an automated lid a wider range would open up with finer differences allowed. A second parametric study of the effect of Prandtl number could take place in which the experiments could be repeated for the same Reynolds numbers but with different working fluids such as air Prandtl= 0.7 , the most often modeled fluid or mineral oil Prandtl=511.5 . Readings should be verified by a secondary flow velocity measurement system such as a Laser Doppler Anemometer (LDA) system.

List of References

1. C.K. Aidun,. and N.G. Trinatafillopoulos, 1997, “High-speed blade coating,” In Liquid Film Coating (ed. S. F. Kistler and P. M. Schweizer), chap. 12d, p. 637. Chapman and Hall.
2. CH. Blohm and H.C. Kuhlmann, 2000, “ The two-sided lid-driven cavity: experiments on stationary and time-dependent flows,” Journal of Fluid Mechanics, vol. 450, pp. 67-95.
3. V.W.R. Malkus, 1989, “An experimental study of global instabilities due to the tidal (elliptical) distortion of a rotating elastic cylinder. Geophysics Astrophysics Fluid Dynamics, vol. 48, pp. 123-134.
4. P.N. Shankar and M.D. Deshpande, 2000, “Fluid Mechanics in the Driven Cavity,” Annu. Rev. Fluid Mech., vol. 32, pp. 93-136
5. J.R. Koseff and R.L. Street, 1984, “The lid driven cavity: a synthesis of qualitative and quantitative observations, “ Journal of Fluids Eng., vol 106, 21-29
6. J.R. Koseff and R.L. Street, 1984, “On the endwall effects in a lid-driven cavity flow, “ Journal of Fluids Eng., vol 106, 21-29
7. C. Migeon, 2002, “Details on the start-up development of the Taylor-Gortler-like vortices inside a square-section lid –driven cavity for 1,000≤Re≤3,200,” Experiments in Fluid, vol. 33, pp. 594-602.
8. A. Liberzon, 2011, “On the effects of dilute polymers on driven cavity turbulent flows,” Int. J. of Heat and Fluid Flow, doi:10.1016/j.ijheatfluidflow.2011.08.005
9. T.J. O’Hern, J.R. Torczynski, T.K. Blanchat, T.Y. Chu, 1994, “Shear-driven flow in a square cavity: a comparative study using PIV, LDV, and computational simulations” Symposium on Laser Anemometry: Advances and Applications, ASME FED summer meeting, June 1994, Lake Tahoe, NV
10. U. Ghia, K.N. Ghia, C.T. Shin, 1982,“High-Re solutions for incompressible flow using the Navier-Stokes equations and a multigrid method,” Journal of Computational Physics, vol. 48, pp. 387-411
11. E. Eturk, T.C. Corke, C. Gokcol, 2005, “ Numerical Solutions of 2-D steady incompressible driven cavity flow at high Reynolds numbers,” Int. J. Numer. Meth. Fluids, vol. 48, pp 747-774
12. E. Barragy and G.F. Carey, 1993, “Stream function vorticity solution using high-p element by element techniques,” Communications in Numerical Methods in Engineering, vol. 9, 387-397
13. M. Sahin and R.G. Owens, 2003, “A novel fully implicit finite volume method applied to the lid-driven cavity problem-Part I: High Reynolds number flow calculations” Int. J. Numer. Meth. Fluids, vol. 42, pp 57-77
14. TSI Corp., 2006, “ Insight 3g Data Acquisition, Analysis, and Display Software”

Vita

The author earned his B.S. degree in 2004 from Tulane University in the major of Biomedical Engineering. He earned is M.S. degree in 2011 from the university of New Orleans in Mechanical Engineering.